2021

ON THE STRUCTURE AND FUNCTION OF MITOCHONDRIAL UNCOUPLING PROTEINS: THE CASE OF UCP2

Afshan Ardalan
arda6810@mylaurier.ca

ON THE STRUCTURE AND FUNCTION OF MITOCHONDRIAL UNCOUPLING PROTEINS: THE CASE OF UCP2

by

Afshan Ardalan

A Thesis
presented to
Wilfrid Laurier University

In partial fulfilment of requirements
for the degree of
Doctor of Philosophy in
Biological and Chemical Sciences

Waterloo, Ontario, Canada

September 2020

DECLARATION OF CO-AUTHORSHIP

The following people contributed to the works undertaken in the Chapters (and appendices) 3 and 4 of this thesis.

Chapter and Appendix 3
This chapter is in preparation to be submitted to the *Journal of American Chemical Society (JACS).*

Primary Author
Afshan Ardalan planned, prepared, and executed all experiments (unless otherwise noted) and drafted the chapter.

Co-authors
Shahin Sowlati-Hashjin performed all computational simulations and related analyses.
Stephanie O. Uwumarenogie took initial steps for optimization of UCP2 purification.
Michael Fish expressed, purified, reconstituted, and analyzed AAC1.
Mikko Karttunen assisted with planning and interpretation of the computational analyses and editing the document.
Matthew D. Smith assisted with planning and interpretation of the experiments and editing the document.
Masoud Jelokhani-Niaraki assisted with planning and interpretation of the experiments and editing the document.

Chapter and Appendix 4
This chapter is in preparation to a journal that is yet to be determined

Primary Author
Afshan Ardalan planned, prepared, and executed all experiments (unless otherwise noted) and drafted the chapter.

Co-authors
Shahin Sowlati-Hashjin performed all computational simulations and related analyses.
Habib Odowuye assisted in expression and purification of the proteins.
Stephanie O. Uwumarenogie generated four out of eleven UCP2 mutants.
Mikko Karttunen assisted with planning and interpretation of the computational analyses and editing the document.
Matthew D. Smith assisted with planning and interpretation of the experiments and editing the document.
Masoud Jelokhani-Niaraki assisted with planning and interpretation of the experiments and editing the document.

ABSTRACT

ON THE STRUCTURE AND FUNCTION OF MITOCHONDRIAL UNCOUPLING PROTEINS: THE CASE OF UCP2

Afshan Ardalan
Wilfrid Laurier University, 2020

Advisors
Prof. Masoud Jelokhani Niaraki &
Prof. Matthew D. Smith

Uncoupling proteins (UCPs) are regulated proton transporters of the mitochondrial inner membrane. UCP-mediated proton leak negatively impacts the rate of ATP synthesis. Despite the importance of their physiological role(s) in certain tissues, molecular aspects of UCPs' structure-function relationships are not fully understood. The current study explores the tertiary and quaternary structure of UCP2, as well as its proton transport mechanism in lipid membranes. The proteins were expressed in the *E. coli* inner membrane, purified and reconstituted into liposomes. Proteins were characterized by semi-native SDS-PAGE. Circular dichroism spectroscopy (CD) and fluorescence quenching assays were utilized to study the conformation of proteins and evaluate their proton transport function, respectively. Molecular dynamics (MD) simulations were performed in parallel to investigate the protein structure and some details of its proton transport function at atomic and molecular levels.

To study the structure of UCP2, the protein was purified both as monomers and as a mixture of monomers, dimers, and tetramers in detergent micelles. After reconstitution, UCP2 associated into functional tetramers regardless of the original oligomeric/molecular form that was used for reconstitution. Computational analysis suggested that the functional tetramer is in fact a pseudosymmetrical dimer of dimers capable of inducing asymmetry in the membrane structure. Tetrameric UCP2 had a biphasic conformation in which the orientation of cavities of monomers in each dimeric unit was similar but opposite to the monomers of the other dimeric unit. The differences in cavity orientations within a tetramer is consistent with an alternating access mechanism. Based on this mechanism, in order to transport their substrates, the cavity of mitochondrial carrier proteins opens to the matrix and intermembrane space alternately.

Two salt-bridge networks, one close to the matrix (matrix network) and the other close to the intermembrane space (cytoplasmic network) have been previously suggested to play important roles in the alternating access mechanism. The UCP2 matrix network was modified in multiple ways using point mutations of K→Q, D→N, K→D and D→K (resulting in either partial or full disruption or inversion of the network by switching the two ends of salt-bridges) and the consequences of these modifications on proton transport and its inhibition by ATP were analyzed.

The matrix network had a filtering role in proton transport of UCPs and evidence is provided that the network may consist of more salt-bridges than have been previously suggested (five vs. three). A biphasic proton transport model is proposed for tetrameric UCP2 in which the conformation of each functional dimer is either in one or the other mode of transport, acting as an on/off switch. ATP could interact with all positive residues of the matrix network (K38, K141, K239, R88, R185, R279) and thus interfere with the alternating open and close modes of the protein's cavity.

Overall, this thesis provides new insights into the tetrameric structure of UCP2 and the mechanism by which proton transport takes place and is regulated in the tetrameric protein.

ACKNOWLEDGEMENT

I wish to express my deepest gratitude to my supervisor Dr. Masoud Jelokhani-Niaraki; your tireless efforts and dedication in the past four years helped me grow in every aspect of life. Without your efforts I was not able to stand where I am today. When I count my blessings, I count you twice.

I would like to pay my sincere appreciation to Dr. Matthew D. Smith; I was fortunate to have you as my co-supervisor. This thesis could not have been possible without your constant support and inspiration. Your guidance always helped me overcome the ups and downs I was facing throughout the past four years.

I wish to extend my special regards to Dr. Lillian DeBruin; you were extremely helpful from the first moment I contacted you. Your dedication kept me and all of the other graduate students of the department up to date, brought a lively spirit to the department and made science more fun.

I would also like to thank Dr. Geoff Horsman; I really appreciate your valuable contribution to my research. Your constructive suggestions made me think outside the box and strengthened my work. You inspired me with your depth of knowledge and passion for science.

Dr. Leonid Brown; it is a great pleasure to have a knowledgeable membrane protein scientist like you as my external examiner. Thank you for your valuable time and contribution to my journey.

Dr. Mikko Karttunen; I was so lucky to have been able to collaborate with your group. Thanks for bringing up new ideas and helping me to deepen my project. I learned so much from you.

Dr. Shahin Sowlati-Hashjin; thank you for always being there for me. I appreciate your invaluable support, assistance, and love in every situation.

All the past and current Jelokhani and Smith's lab members (Patrick, Stephanie, Mike, Marzi, An, Habib, and Joel); thank you for being a part of my journey, and for your constant friendship and support.

My family, Afkham, Ali and, Ashkan thank you for the great love you gave me, you kept me going, and this work would not have been possible without your constant support.

The contribution of Ontario Government is truly appreciated. Without their funding (Trillium), this project could not have reached its goals.

GLOSSARY OF ABBREVIATIONS

2DN	D138N/D236N mutant
2KQ	K38Q/K239Q mutant
3DN	D35N/D138N/D236N mutant
3KQ	K38Q/K141Q/K239Q mutant
AAC1	Mitochondrial ADP/ATP carrier protein isoform 1
AFM	Atomic force microscopy
AGC	Aspartate/glutamate carrier
AMBER	Assisted model building and energy refinement
ANOVA	Analysis of variance
ANT	Adenine nucleotide translocase
APL	Area per lipid
BKA	Bongkrekic acid
BtAAC	Bovine ADP/ATP carrier
C_8E_4	Tetraethylene glycol monooctyl ether
CATR	Carboxyatractyloside
CHARMM	Chemistry at Harvard molecular mechanics
CL	Cardiolipin
CPA	Cation-proton antiporter
ETC	Electron transport chain
$FADH_2$	Flavin adenine dinucleotide, reduced form
GROMOS	Groningen molecular simulation

HM	Hexamutant, D35K/K141D/D138K/K239D/D236K/K38D
HRP	Horseradish peroxidase
IMM	Inner membrane of mitochondria
IMS	Mitochondrial intermembrane space
ITF	Induced transition fit model
KHE	K^+/H^+ exchanger
LDAO	Lauryldimethylamine oxide
MCF	Mitochondrial carrier superfamily
MCU	Mitochondrial calcium uniporter
MD	Molecular Dynamics
MICOS	Mitochondrial contact site and cristae organizing system
MP	Membrane protein
NADH	Nicotinamide adenine dinucleotide, reduced form
NHE	Na^+/H^+ exchanger
Ni-NTA	Nickel-nitrilotriacetic acid
NPT	Constant pressure and temperature
NVT	Constant volume and temperature
OG	Octyl glucopyranoside
OMM	Mitochondrial outer membrane
OPLS	Optimized Potential for Liquid Simulations
ORC	Mitochondrial ornithine/citrulline exchanger
OXPHOS	Oxidative phosphorylation
PA	Phosphatidic acid

PC	Phosphatidylcholine
PCA	Principal component analysis
PelB	Pectate lyase B
PIC	Phosphate carrier
POPC	1-palmitoyl-2-oleoylphosphatidylcholine
Rg	Radius of gyration
RMSD	Root mean square deviation
ROS	Reactive oxygen species
SASA	Solvent accessible surface area
SBS	Substrate/inhibitor/solute binding site
SDS-PAGE	Sodium dodecyl sulfate–polyacrylamide gel electrophoresis
SLC	Solute carrier proteins
SMALP	Styrene maleic acid lipid particles
SPQ	6-methoxy-N-(3-sulfopropyl) quinolinium
TCA	Tricarboxylic acid
TEA	Tetraethylammonium
TES	N-[tris(hydroxymethyl)methyl]-2-aminoethanesulfonic acid
THP	Tris (hydroxypropyl) phosphine
TM	Transmembrane
TtAAC	*Thermothelomyces thermophila* ADP/ATP carrier
UCP	Uncoupling protein

TABLE OF CONTENTS

LIST OF FIGURES

LIST OF TABLES

CHAPTER 1 - BACKGROUND INFORMATION

1.1 Mitochondria

Mitochondria are organelles surrounded by two membranes, which play multiple vital functions in eukaryotic cell metabolism and beyond [1]. Mitochondria play a pivotal role in cellular bioenergetics by producing ATP via oxidative phosphorylation (OXPHOS). Mitochondria are also involved in the β-oxidation of fatty acids, synthesis of nucleotides, as well as synthesis of heme and iron-sulfur clusters [1]. Beyond metabolism, mitochondria regulate propagation of signals for a diverse set of biological outcomes such as calcium (Ca^{2+}) homeostasis, gene expression, cellular differentiation and cell death [1].

1.2 Mitochondrial membrane compartments

Inner and outer membranes of mitochondria separate this organelle from the cytosol [2]. The outer membrane of mitochondria (OMM) is porous; small molecules and ions can pass through OMM porins, and as a result of this permeability no membrane potential/voltage can be formed across the OMM [2]. In contrast to the OMM, only specific ions and molecules can be transported across the inner membrane of mitochondria (IMM) through membrane protein (MP) channels and transporters [2]. The selectivity of transporters and channels generates an electrochemical potential across the IMM (discussed below in detail) [2].

Three distinct aqueous zones can be distinguished in a mitochondrion: (i) matrix, the innermost aqueous mitochondrial zone which is characterized by a low proton concentration (pH = 7.9-8) [3]; (ii) intermembrane space (IMS), a ~200 Å wide aqueous space between the IMM and OMM (pH = 7.2-7.4) [2]; and (iii) cristae, which are the tubular, lamellar or bag-like invaginations of the IMM that extend into the matrix (Figure 1-1, A) [2]. The higher pH of the matrix compared

to IMS drives the ATP synthesis [3]. The IMM can be subdivided into two domains with distinct function and protein composition: (i) the boundary membrane, which is parallel (and close) to the OMM, and (ii) the cristae membrane (Figure 1-1, A) [4]. The boundary and cristae membranes are continuous; the transition between the two domains of the IMM occur at the site of cristae junctions (narrow slits at the entrance of the cristae [4]).

Cristae are the main site of cellular respiration in all eukaryotes, as the complexes of the electron transport chain (ETC) and ATP synthase are present in cristae membrane (Figure 1-1, A-B), and cytochrome c (the small soluble protein that carries electrons) is present in cristae lumen (the region of the IMS that is constrained within an IMM cristae) [2]. Cristae are anchored to the OMM through mitochondrial contact sites and cristae organizing system (MICOS) [5]. MICOS is an assembly of six (one soluble and five membrane) proteins. It has been proposed that MICOS provides a barrier for lateral diffusion of the proteins between cristae and the boundary membranes and restricts the movement of protons [2, 6]. The observation that individual cristae have different membrane potentials could be the result of restricted movement of protons out of the cristae lumen [6].

1.3 Mitochondria are referred to as the powerhouse of the cell

In order to produce consumable energy molecules (ATP) that can be used to drive metabolic processes in the cell, the tricarboxylic acid (TCA) cycle [7] (also known as the citric acid cycle or Krebs cycle) and OXPHOS take place in mitochondria [8]. The final product of lipid, sugar, or amino acid catabolism, acetyl-coA, enters the Krebs cycle upon interaction with oxaloacetate (a four-carbon molecule) in the mitochondria matrix to form a six-carbon citrate molecule. After seven subsequent enzymatic steps, oxaloacetate will be regenerated and can then re-enter the cycle to receive another molecule of acetyl-CoA [9]. During the Krebs cycle, the two

carbons from the acetyl group of acetyl-coA are released in the form of two CO_2 molecules, and the extra electrons are passed to nicotinamide adenine dinucleotide (NADH) and flavin adenine dinucleotide ($FADH_2$) to be carried to the ETC, a series of protein complexes located in the IMM (Figure 1-1, C) [8].

The passage of electrons from NADH and $FADH_2$ molecules to the ETC components triggers the efflux of protons from the matrix to the IMS, thus generating an electrochemical gradient across the IMM widely known as the proton motive force [10] that eventually results in formation of ATP by the aid of ATP synthase complex [10].

Complex I of the ETC, NADH dehydrogenase, is a 1 MDa protein complex with a binding site for NADH in the matrix [11]. Donation of two electrons from NADH to complex I leads to a series of oxidation-reduction reactions throughout the iron-sulfur clusters within the protein which result in transfer of the electrons to coenzyme Q, a lipophilic redox carrier [8]. A consequence of the passage of electrons through complex I is a conformational change which ultimately causes pumping of four protons from the matrix to the IMS [8]. The other electron carrier generated during the Krebs cycle, $FADH_2$, carries two electrons to the complex II of the ETC, called succinate dehydrogenase [8]. Similar to complex I, complex II passes the electrons to coenzyme Q through iron-sulfur clusters. However, unlike complex I, complex II does not pump protons to the IMS [8] (Figure 1-1, C).

After accepting electrons from complex I or II, Coenzyme Q transfers the electrons to complex III, cytochrome c reductase [8]. Cytochrome c reductase oxidizes coenzyme Q and passes the two accepted electrons to two cytochrome c molecules (one electron per cytochrome c) (Figure 1-1, C) [8]. Two protons are liberated to the IMS as a result of oxidation of Coenzyme Q and two additional protons are pumped from the matrix to the IMS upon reduction of cytochrome c.

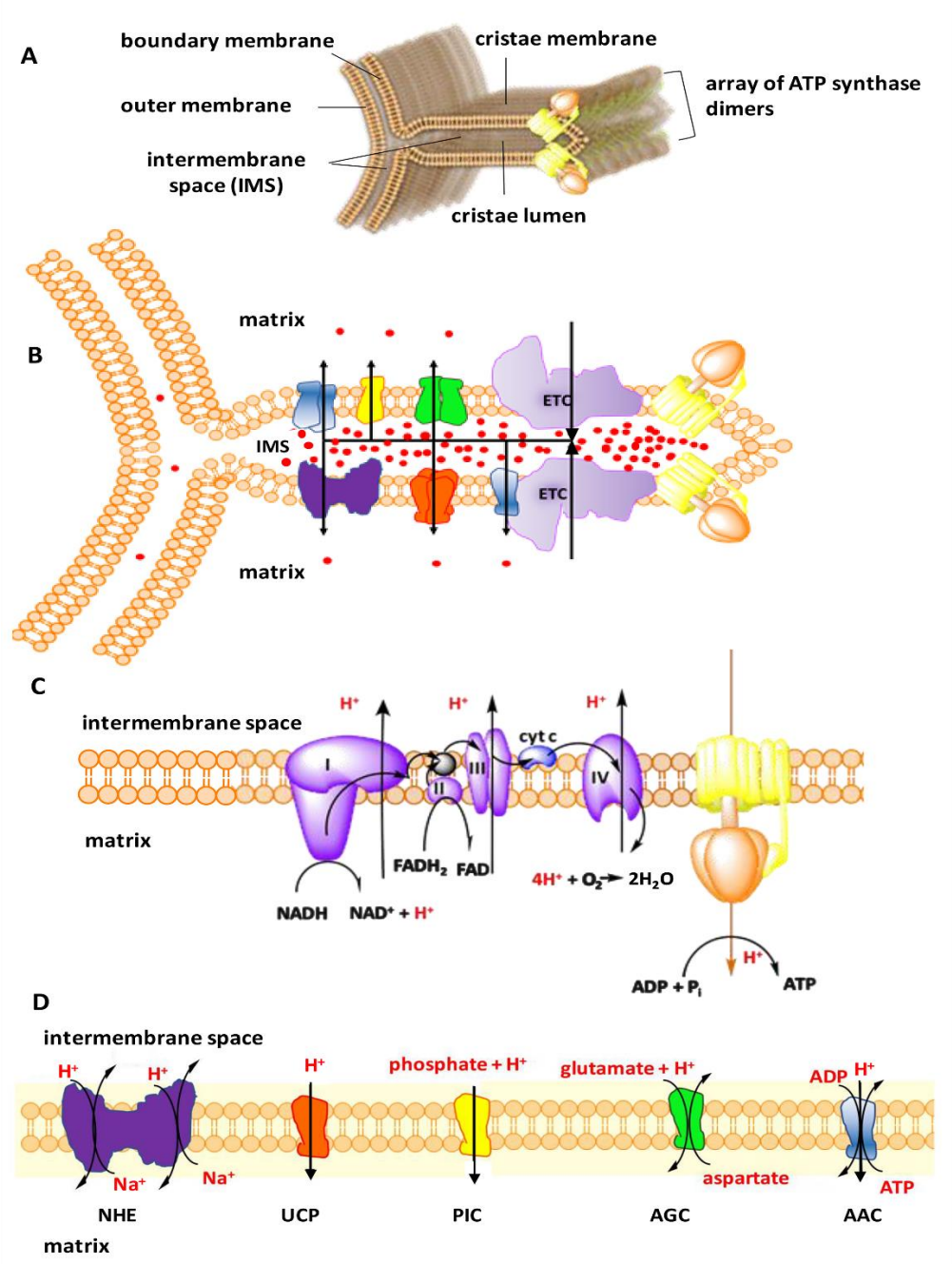

Figure 1-1 Structural and functional elements of cristae. A) Three-dimensional representation of cristae shows the presence of an array of ATP synthase dimers (yellow and orange). B) Movement of protons into and out of the IMS by the aid of protein complexes. ETC complexes (light purple) pump protons (red circle) from the matrix into the IMS. Some other proteins in the IMM such as uncoupling protein (UCP, orange), phosphate carrier (PIC, yellow), aspartate/glutamate carrier (AGC, green), ADP/ATP carrier (AAC, blue) and Na^+/H^+ transporter (NHE, dark purple) relocate protons back to the matrix. Black arrows show the direction of movement of protons. C) Complexes of the ETC pass the electrons forward (black arrows) and pump the protons up to the IMS resulting in formation of proton motive force and synthesis of ATP by ATP synthase. D) Function of selected proton transporters of the IMM. AAC, UCP, PIC, AGC are not necessarily monomers, the monomeric form is shown for simplicity. Figure generated by ChemBioDraw Ultra 14.0.

Each cytochrome c molecule donates one electron to complex IV, cytochrome c oxidase. Four cytochrome c enzymes transfer four electrons to complex IV, where the last step of the ETC takes place [8]. Complex IV passes the four electrons to one molecule of oxygen (O_2) to produce two molecules of H_2O (Figure 1-1, C). Parallel to this reduction, four protons are pumped across the IMM to the IMS from the matrix (Figure 1-1, C) [8].

Complexes of the ETC can oligomerize in different arrangements and stoichiometries [12]. For example, a copy of complex I, two copies of complex III and a copy of complex IV can come together in the IMM to form a 1.7 MDa supercomplex called the respirasome [13]. It has been recently shown that the oxidoreductase activity of complex I increases up to three times upon formation of respirasomes [14]. As a result of this finding, researchers suggest that formation and dissociation of supercomplexes such as respirasomes can be a cellular response to ATP demand and to control reactive oxygen species (ROS) formation [14]. At low concentrations of ATP, respirasomes are formed to increase the enzymatic efficiency of complex I, and thereby increase electron and proton flux. Conversely, at high ATP concentrations respirasomes dissociate to decrease electron transport, and thus decrease the risk of ROS formation [14].

The consequence of translocation of protons from the matrix to the IMS in different steps of the ETC is the generation of a ~200 mV electric potential across the IMM [8]. After the Krebs cycle and ETC, the resulting electrochemical gradient across the IMM is transformed into a more readily consumable form of energy for the cell through a "coupling" process. Coupling of the electrochemical gradient to ATP synthesis was first proposed by Peter Mitchell in 1961 [10], who won the Nobel Prize in chemistry for the discovery 17 years later. ATP synthase (also known as complex V and F_0F_1 ATPase) provides a route for protons to flow in accordance with their

concentration gradient from the IMS to the matrix. The outcome of this passage is conformational changes in ATP Synthase that result in ATP synthesis from ADP and P_i [8]. The mechanism of ATP synthesis was hypothesized and developed by Paul Boyer and John Walker from 1964 to 1994, for which they were awarded the Nobel Prize in chemistry in 1997 [15]. It is estimated that the transport of between 2-5 protons are needed for the synthesis of one molecule of ATP. However, relating these numbers to the number of required NADH or $FADH_2$ is not straightforward as protons can leak across the IMM through routes other than the ATP synthase complex. Three ATP per one NADH or two ATP molecules per one $FADH_2$ are common estimations [8]. Eukaryotic ATP synthase macromolecules are arranged as linear arrays of dimeric complexes found in narrow cristae ridgelines or near tight tubular cristae [16]. (Figure 1-1, A-B)

Not only protons, but also electrons can leak across the IMM. Leakage of electrons from different complexes of the ETC, other than complex IV, can lead to reduction of O_2 to superoxide radical anions [8]. Most intracellular ROS are formed from superoxide [17]. Even though low levels of ROS are important for cell function, high levels of ROS can cause oxidative stress [17]. Oxidative stress is a condition where ROS production is uncontrollable by the antioxidant defense system of a cell [18]. Oxidative stress has multiple deleterious effects in cells, including causing chemical damage to proteins, lipids and nucleic acids, as well as apoptosis [18].

1.4 Uncoupling of oxidative phosphorylation

Translocation of protons that are pumped into the IMS during the electron transport process back to the matrix results in dissipation of the electrochemical gradient across the IMM, and thus uncouples electron transport from ATP synthesis [19].

Proton leak across the IMM is the outcome of two leakage processes: basal and inducible proton leak [20]. Basal proton leak is non-regulated leakage of protons across the IMM, which

depends on the fatty acyl composition of the membrane and the presence of mitochondrial carriers that are able to translocate protons [such as ADP/ATP carrier (AAC), also known as adenine nucleotide translocase (ANT)]. (Figure 1-1, B and D) [20, 21]. Inducible proton leak is controlled by a specific family within the mitochondrial carrier superfamily (MCF) known as "**Uncoupling Proteins**" (UCPs) (Figure 1-1, B and D) and can be regulated by fatty acids, superoxides, lipid peroxidation products and adenine nucleotides [21].

UCP1 (thermogenin, the prototypic member of the UCP family), was discovered in 1978 by Heaton *et al.* in hamster [22], and was purified from brown adipose tissue of rat and hamster mitochondria in high yields by Lin and Klingenberg within two years of its discovery [23]. Almost 20 years after the discovery of UCP1, four other homologues of UCPs were discovered: UCP2 (1997) [24, 25], UCP3 (1997) [26, 27], UCP4 (1999) [28], and UCP5 (1998) [29].

UCPs have different expression patterns in the human body. UCP1 is mainly found in brown fat adipose tissue [19]. UCP2 is expressed in several tissues such as skeletal muscles, heart, liver, kidney, lung, pancreas, spleen, and macrophages [19]. UCP3 is mostly expressed in brown adipose tissue and muscles [19]. UCPs 4 and 5 are specifically neuronal and mainly expressed in brain tissues [19]. UCPs 2, 4 and 5 are considered as neuronal UCPs, as they are predominantly found in the central nervous system (CNS) [30].

In addition to protons, UCPs transport a wide spectrum of ions including (but not limited to) monovalent anions such as chloride, bromide, nitrate [31, 32] and alkyl sulfonates [33]. It is reported that UCP2 is able to transport anionic C_4 metabolites such as aspartate, malate and oxaloacetate [34].

1.4.1 ROS regulation at mitochondrial level

Mitochondria contribute significantly to the production of cellular ROS [35]. Approximately 1 to 2% of the oxygen utilized by mitochondria results in the productions of superoxide anion ($O_2^{\bullet -}$) [35]. In cases where excess ROS generation leads to oxidative stress, mitochondria overexpress UCPs [36]. The evidence for the preventive role of UCPs against oxidative stress has been discussed in many studies [36-38]. UCPs activity may also decrease the rate of apoptosis (programmed cell death) induced by ROS species [36]. These proteins can be activated by superoxide anions, resulting in the dissipation of the electrochemical gradient across the IMM [35]. Overall, UCPs are considered to contribute in a feedback loop which is activated by ROS, and leads to decrease in superoxide concentration [35, 36].

1.4.2 Thermoregulation at the neuronal level

Among UCPs, UCP1 is known to have a thermogenic physiological function in brown adipose tissues. It has also been shown that neuronal UCPs can increase the temperature in neuronal microenvironments during uncoupling activity [39]. As neuronal UCPs mostly accumulate in axon terminals, their thermogenesis can lead to changes in neurotransmission mechanisms [39]. It has been suggested that temperature differences between neuronal cells in the absence and presence of UCPs result in a temperature gradient that facilitates the diffusion of neurochemicals toward their postsynaptic targets [40]. Furthermore, although UCPs decrease the amount of synthesized ATP per mitochondrion, these proteins trigger mitochondria biogenesis, thereby raising overall cellular ATP levels. Higher cellular ATP concentrations in presynaptic nerve terminals, where UCP is present, assist active processes (such as formation, transportation and exocytosis of vesicles), and consequently facilitates neurotransmission [39, 40].

1.4.3 Calcium uptake regulation

Mitochondria can modulate the Ca^{2+} content of intact cells via uptake and release mechanisms, which are carried out separately. Mitochondrial ATP production and metabolism can be regulated by Ca^{2+} uptake activity in the IMM, which is mostly performed by the mitochondrial Ca^{2+} uniporter (MCU) [41]. The fundamental role of UCPs in regulating MCU activity has been reported in intact cells and in isolated liver mitochondria [42]. However, the involvement of UCPs in regulation of Ca^{2+} transporters remains controversial [43, 44]. Using gene silencing in human and mice cell lines, Trenker et al. [43] showed that UCPs 2 and 3 could affect both the amount and the rate of Ca^{2+} uptake [43]. Additionally, it has been proposed that UCPs can act as conductive ion channels for Ca^{2+} [41, 43].

1.5 Mitochondrial carrier family

Solute carrier proteins (SLCs) are integral MPs, responsible for transport of solutes across intracellular membranes [45]. The largest family of SLCs in the human body is the MCF or SLC25 with 53 members [46]. MCF proteins are mostly antiporters, transporting different solutes across the IMM in opposite directions. Some MCF proteins are uniporters, transporting solute molecules in one direction, whereas others are thought to be substrate-proton symporters [46]. Because of amino acid sequence similarities among the MCF members it has been suggested that these proteins have comparable secondary and tertiary structures [47, 48].

1.5.1 Structural features of the MCF members

Most of what is known about the structure of MCF members is based on knowledge of AAC, which is the most characterized member of the MCF. AAC is the only member of the MCF for which high resolution x-ray structures are available [49, 50] (Figure 1-2, A-F). The first AAC x-

ray structure was of bovine AAC1 (BtAAC) (2003) (PDB ID: 1OKC) [49]. AAC imports ADP from the IMS into the matrix and exports ATP from the matrix to the IMS [50].

The structure of AAC reveals a trilateral pseudosymmetric structure that includes 3 tandem repeats. Each repeat is composed of ~100 amino acids distributed into two transmembrane (TM) α-helices that are connected by a hydrophilic short helix parallel to the membrane on the matrix side [49] (Figure 1-2, A and D).

1.5.1.1 Matrix and cytoplasmic gates

Two conserved signature motifs are present at the water-membrane interface of mitochondrial carrier proteins. The first signature motif, PX[DE]XX[RK], is located on odd numbered helices (helices 1, 3 and 5) close to the matrix side [49, 51]. The **matrix salt-bridge network** (or matrix network) is formed as a result of electrostatic interactions between positive and negative residues of the matrix side signature motifs [49, 51] (Figure 1-2). Conserved glutamine residues, known as the **Q-brace/glutamine-brace,** located in close proximity to the matrix signature motif (Px[DE]xx[KR]xxxQ) on helices 1 and/or 3 and/or 5 provide extra structural support by forming hydrogen bonds with the salt-bridge network residues [46] (Figure 1-2).

The second signature motif, [FY][DE]XX[RK], is located on even numbered helices (helices 2, 4 and 6) close to the IMS. Just like the matrix network, an intramolecular salt-bridge network is also formed from electrostatic interactions of positively and negatively charged residues of the signature motifs close to the IMS, known as the **cytoplasmic salt-bridge network** (cytoplasmic network) [51]. The cytoplasmic network is supported by hydrogen bond formation between tyrosine residues that are in the motif with the residues of the cytoplasmic network (**Y brace/tyrosine-brace**). MCF members have one to three of each brace (Q or Y) [46] (Figure 1-2).

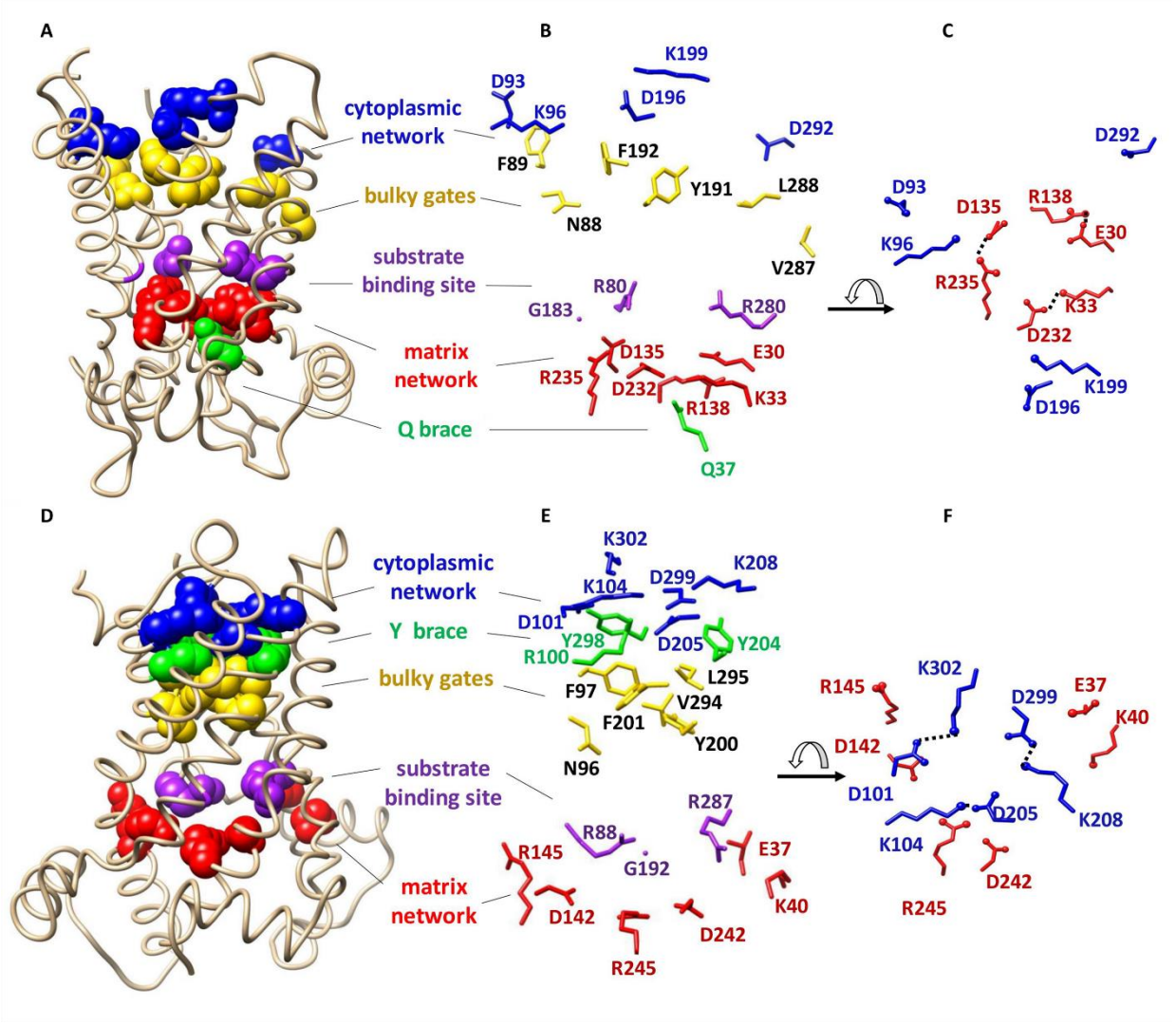

Figure 1-2 Overall structure and conserved functional residues of AAC. A) X-ray structure of bovine AAC in the cytoplasmic state (1OKC). The conserved functional residues are shown as spheres. B) Detailed representation of the side chains and directions of conserved residues of bovine AAC. C) Top view of broken cytoplasmic and formed matrix networks of bovine AAC in the cytoplasmic state. D) X-ray structure of TtAAC in the matrix state (6GCI). The conserved functional residues are shown in spherical format. E) Detailed representation of the side chains of TtAAC. F) Top view of the broken matrix and formed cytoplasmic networks of Tt AAC in the matrix state. Figure generated by USCF Chimera 1.13rc

1.5.1.2 Single Binding site

Based on the structure of AAC1 it has been proposed that a single conserved common substrate/inhibitor/solute binding site (SBS) is present at the center of the transporter cavity in all MCF members (Figure 1-2) [48]. This binding site resides at the bottom of a solvent accessible

cavity and includes three protein-substrate specific contact points at even numbered helices [52, 53]. It has been suggested that contact points I (located on helix 2) and II (located on helix 4) can confer substrate specificity to the carrier; however, it seems that the positively charged contact point III (located on helix 6) does not contribute to substrate specificity [46] (Figure 1-2).

1.5.1.3 πGπXπG and πXXXπ motifs

Besides signature motifs, there are other sequences that are conserved between the members of MCF, such as the πGπXπG motif on helices 1, 3 and 5 and the πXXXπ motif on helices 2, 4 and 6 [50]. The symbol π refers to amino acids with short side chains; however, occasionally amino acids with bulky side chains might be found at the π positions [46]. These two motifs contribute to the function of the protein which will be discussed in the next section [50].

1.5.2 Functioning via a comparable alternating mechanism

Comparable amino acid sequences and the presence of conserved motifs led some researchers to suggest that all members of the MCF transport their respective solutes (substrates) via an alternating access mechanism [46, 54]. In this hypothesized mechanism, mitochondrial anion carriers can adopt two different conformational states: a cytoplasmic state (V), in which the solvent accessible cavity of the carrier is open towards the IMS (like the letter "V"); and the matrix state (Λ), in which the solvent accessible cavity of the carrier is open towards the matrix side (like the symbol "Λ") [52]. Members of the MCF can alternate between matrix and cytoplasmic states by movement of the helices towards or away from the central Z axis (normal to the bilayer) as a consequence of substrate binding [50] (Figure 1-3).

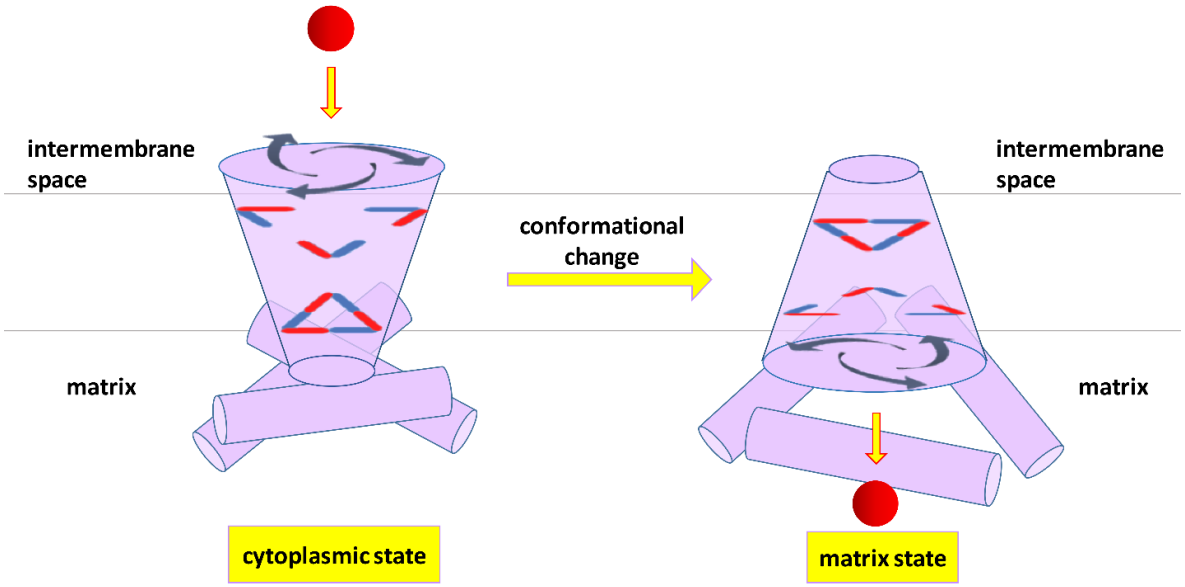

Figure 1-3 Alternating access mechanism is proposed to be a common mechanism for substrate translocation by members of the MCF. In this model the protein's cavity opens alternately towards the cytoplasmic and matrix sides alternatively. Figure generated in PowerPoint 365.

Matrix and cytoplasmic salt-bridge networks and Q and Y braces are important structural features that contribute to stabilizing the protein conformation in each state [55]. It has been hypothesized that in the cytoplasmic state (V) all three salt-bridges of the matrix network are formed, thereby narrowing the matrix-facing side of the cavity, while the salt-bridges of the cytoplasmic network are all broken; this state is in contrast to the matrix state (Λ) during which it has been hypothesized that the cytoplasmic salt-bridge network is fully formed and the matrix salt-bridge network is broken [51]. Until 2019, the reported structures of different isoforms of AAC (AAC1-4) in different organisms were all locked in the cytsoplasmic state [49, 55] (Figure 1-2, A-C). In 2019, Ruprecht et al. (50) published a structure of yeast (*Thermothelomyces thermophila*) AAC (TtAAC) locked in the matrix state (Figure 1-2, D-F). Availability AAC structure (from different sources) locked in matrix and cytoplasmic states further supports the alternating access hypothesis. The small size of the residues of the conserved motifs πGπXπG and πXXXπ allows

the helices to come close to one another in the matrix state (Λ), assisting the cytoplasmic network to form [50]. Furthermore, the aromatic residues of the signature motif, plus aromatic and bulky residues in the vicinity of the IMS in the cytoplasmic state, provide a ~15 Å shield to oppose uncontrolled proton leak through the protein in the cytoplasmic state [56]. The amino acids that are believed to participate in the formation of these proton gates are conserved among all MCF members [46].

1.6 Proton transport/leak across the IMM by MCF proteins

Among members of the MCF, a few are known to transport protons across the IMM. Other than UCPs, of which proton transport is the common regulated function [21], most other transporters of protons are in fact anion carriers, which use the proton (gradient) as a driving force to co-transport other substrates across the IMM [57]. Substrate-proton co-transport by some MCF proteins is accomplished mainly by symport or antiport mechanisms [52, 57]. Section 1.6 provides structural and mechanistic information about the regulated proton leak by UCPs and non-regulated proton leak by other members of MCF. Due to similarity of the proposed mechanisms of MCF members, one example of each transport mode (symport and antiport) will be discussed in detail. The list of human MCF proton leakers of the IMM, along with their respective amino acid sequences and transport modes (symport or antiport), can be found in Figure A-1-1. The sequence alignments were generated using Jalview [58]. The conserved elements involved in the alternating access mechanism are marked at the top of the respective columns.

1.6.1 Regulated proton transporters of IMM: Uncoupling proteins

As mentioned above, UCPs are the only subfamily of the MCF known to be responsible for regulated proton leak across the IMM [21]. Because of low purification yield and numerous preparation steps (such as extraction from membrane, purification in native form and reconstitution

in a bilayer mimicking environment) analyses of structure and function of MPs have always been difficult and controversial [59]. UCPs are good examples of such controversies. Researchers disagree on UCPs' mechanism of function and inhibition [60-63], as well as their tertiary [59, 64] and quaternary structures [65-68]. Even though there is no available x-ray structure for UCP homologues, structures of UCP1 [69] and UCP2 (PDB ID: 2LCK) (Figure 1-4) [70] have been obtained by NMR spectroscopy. The reported structures of UCPs 1 and 2 possess the common structural features of MCF proteins; however, the internal cavity in UCP monomers is higher compared to what is commonly observed in other members of the MCF [59]. Despite disagreements on structure and function, activation of UCPs by fatty acids and their inhibition by purine nucleotides are generally accepted [60, 71].

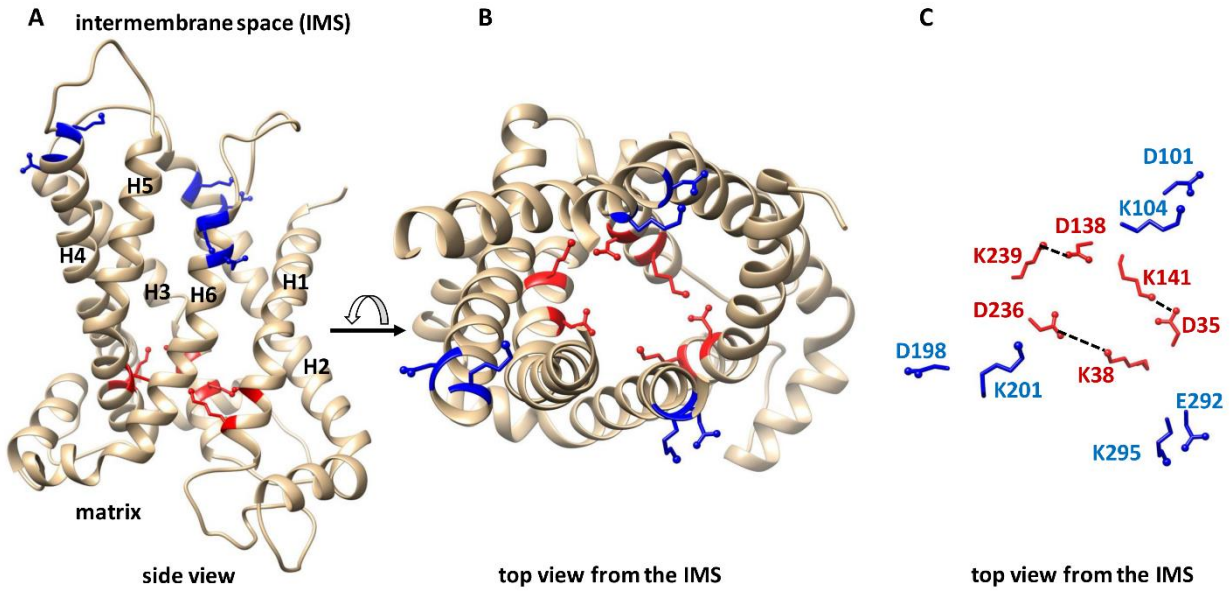

Figure 1-4 Structure of UCP2 in cytoplasmic state. A) sideview, B and C) top view, residues involved in the cytoplasmic and matrix salt-bridge networks are shown in blue and red, respectively. Figure generated by USCF Chimera 1.13rc.

Proton flux by UCPs is activated by fatty acids [30, 71]. Evaluation of the effect of fatty acid features (length, structural rigidity, hydrophobicity) on proton transport rate of neuronal UCPs

reveals that unsaturated and long chain fatty acids are generally more potent proton transport activators [30, 32]. Alterations of circular dichroism (CD) spectra of neuronal UCPs reconstituted in phosphatidylcholine (PC) vesicles upon addition of fatty acids imply that fatty acids are able to induce conformational changes in UCPs [30]. NMR spectroscopy of UCP1 and 2 suggests that there is a groove between helices 1 and 6, which might be a fatty acid binding site; the hydrophobic chain of the fatty acid lays in the groove and its headgroup faces the matrix side [63, 69]. Hoang et al. [32] also proposed the presence of a specific geometrically optimized binding site for fatty acids in UCPs 2, 4 and 5. Furthermore, mutagenetic and functional analysis of UCPs by different researchers and different methods provide important insights about fatty acid-UCP interactions, as well as residues that are involved in UCP-mediated transport. Table 1-1 shows the residues that are involved in proton transport regulation along with the major findings of related studies [30, 32, 48, 63, 69, 70, 72-76].

Three models have been proposed to describe the role of fatty acids in activation of proton transport of UCP/UCP1: (i) fatty acid cycling model [61]; (ii) buffering/cofactor model [62]; and (iii) proton shuttling model [73] (Figure 1-5). In the fatty acid cycling model, a (protonated) fatty acid that resides in the IMS is transferred to the matrix through a “flip-flop” process across the lipid bilayer and releases its proton to the matrix. Transport of the fatty acid anion back from the matrix to the IMS is then facilitated by UCP (Figure 1-5) [61]. NMR results from Zhao et al. [69] are compatible with the cycling model. In the buffering model, fatty acid anions bind to UCP and accept/donate protons via their carboxylate group from and to titratable amino acids of the translocon channel (the central channel of the carrier), all the way to the matrix side, where the proton is released (Figure 1-5) [60, 62]. The shuttling model proposes that the proton transport mechanism depends on the length of the fatty acid; short chain protonated fatty acids can be

transported from the IMS to the matrix (where they release their proton) via UCPs' translocon channel, whereas long chain fatty acids remain in the translocation channel. Long chain fatty acids

Table 1-1 Residues involved in proton transport regulation and the major findings of related studies.

protein	H^+ transport (activated by fatty acids)	inhibition (by purine nucleotides)	methods	Findings related to H^+ transport mechanism	Ref.
UCP2	R279 R60 R241 R88 K141 K16 K271	R185 K141 R88	-NMR -mutagenesis -fluorescence	**1**-The fatty acid chain probably partitions into a groove between helices 1 and 6 which is likely its binding site and the carboxylate head group interacts with R60 and K271. **2**- Fatty acid flipping is required for H^+ transport activity of UCP2. **3**-GDP can allosterically dislocate fatty acid from its binding.	[63, 70]
UCP1	K269 K56		-NMR -mutagenesis -fluorescence -MD simul.	There is a specific binding site between helices 1 and 6 close to the matrix for fatty acid.	[69]
UCP1	D28 R84 R183 R277		-patch clamp of whole mitoplast	1- Proposed induced fit mechanism (shuttling model + alternating access) **2**-Long chain low pKa fatty acid anions can inhibit proton transport thus transport of proton and fatty acid is from the same translocation path.	[72, 73]
UCP1		R84 R183 R277	-mutagenesis -fluorescence	Single point mutations of R84Q, R183T and R277L resulted in more than 93% decrease in inhibition.	[75]
UCP1	D210 D28 H146 H148	R84 R183 R277	-mutagenesis -fluorescence	E168Q, R84I and R92T inhibited Cl^- transport but did not affect proton transport.	[76]
UCP2	R96 k104		-mutagenesis -fluorescence	**1**-Longer fatty acids showed better transport rate: PA>MA>LA **2**-Sensitivity of mutants to fatty acid length was different: K104Q>R96Q>>UCP2 **3**-R76Q and R88Q decreased the chloride transport rate up to 82-83%. **4**-Succinic acid (C4) did not activate proton transport of UCP2.	[32]
UCP2			-fluorescence	Addition of fatty acid inhibited UCP2 inherent chloride transport up to ~50%, suggesting that fatty acids and chloride ions (anions) share the same path.	[30]
UCP1	Single binding site: D28, R84, R183, S184, I187, S230, R277 (Found based on sequence alignment with AAC)				[52]

remain bound to the protein while their head group moves back and forth across the IMM (getting protonated in the IMS and releasing the proton into the matrix) (Figure 1-5) [73].

In addition to the three "UCP specific" mechanisms of proton transport, as a member of the MCF, UCPs also share the structural features necessary for an alternating access mechanism (Figure 1-2). Consequently, alternating access could be considered a fourth potential model for the mechanism of proton transport by UCPs. Even though the three arginine residues of the proposed single binding site (in the alternating access mechanism) cannot be the binding site for long chain fatty acids (as they are polar and have symmetrical arrangement compared to the asymmetric structure of fatty acids) [51], these arginine residues could attract the fatty acid from the IMS [51]. In 2017, an updated version of the shuttling model [induced transition fit model (ITF)] was proposed by Bertholet et al. [72]. In this model, the elements of alternating access have been combined with the shuttling mechanism. Based on this ITF model, the arginine residues of the single binding site (R84, R13, R277) of UCP1 attract long chain anionic fatty acids towards the cavity of the protein where D28 is present [72]. Proximity of the anionic fatty acid's head and D28 will result in increasing the pKa of both fatty acid and aspartate residue leading to attraction of a proton from the IMS. Co-presence of fatty acid and proton in the cavity will lead to further conformational changes from the cytoplasmic to matrix state at which point the proton gets released into the matrix [72] (Figure 1-5).

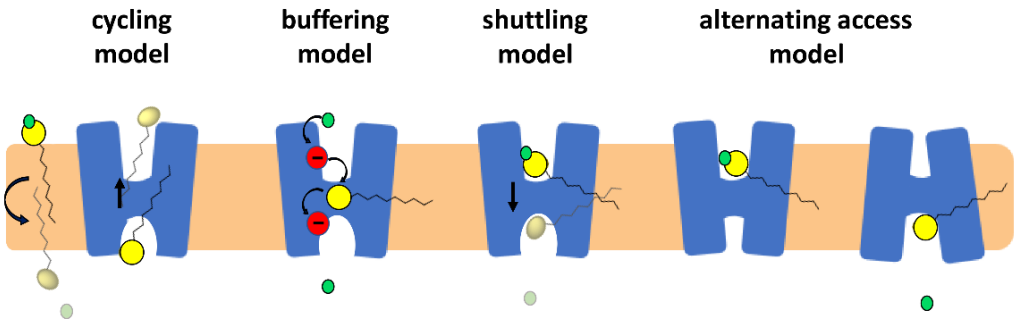

Figure 1-5 Proposed mechanisms of proton transport by UCPs. In the fatty acid cycling model, protonated fatty acid (yellow head group and a black tail) flip-flops across the lipid bilayer, releases its proton (green circle) and is transported from to the IMS as an anion by UCP. In the buffering model, fatty acid anion binds to UCP and accepts/donates protons via its carboxylate group from and to titratable amino acids of the translocon channel. In the shuttling model long chain fatty acids remain bound to the protein while their head moves back and forth across the IMM (getting protonated in the IMS and releasing the proton into the matrix). In the alternating access model (or ITF), UCP changes conformation from cytoplasmic to matrix state and vice versa upon movement of fatty acid across the translocon channel. Figure generated by PowerPoint 365.

None of these models are universally accepted and there are arguments in support and against all of them [60]. Fatty acids are not the only compounds that are able to activate UCPs; superoxides and alkenals (lipid peroxidation products) such as HNE (4-hydroxy 2-nonenal) can also activate UCPs [77]. It has been demonstrated that superoxides activate UCPs from the matrix side and that they are also sufficient for UCP activation [78].

Di- and tri-phosphate purine nucleotides (ADP, ATP, GDP, and GTP) inhibit UCPs' proton flux activity [79]. The degree of inhibition of UCPs by purine nucleotides is different; for example, UCP2 is more inhibited by ATP compared to ADP [80]. The mechanism of inhibition by purine nucleotides is not fully known yet; but the current working model for inhibition is based on mutational studies on UCP1. These studies indicated that three arginine residues are essential in binding of GDP by UCP1: R84, R183, and R277 [74]. Single mutations of R183T and R277L resulted in loss of more than 90% of proton transport inhibition without any changes in the uninhibited rate of transport. A single mutation of R88Q caused 99% loss of inhibition, while the proton transport rate doubled [74]. The three R residues are conserved among all human UCPs and

also make up part of the single SBS [based on homology/sequence alignment with other members of MCF (Table 1-1)] [52]. It has been demonstrated that addition of purine nucleotides to UCPs reconstituted in lipid vesicles induces minor changes in the protein's overall conformation [80, 81]. One NMR study of UCP2 showed that GDP could broaden NMR resonances on helices 1, 2, 3 and 4 [70], which means that GDP interacts with these helices [82]. This study suggested that R185 and K141 of UCP2 can interact with GDP [70]. A complementary study by the same group added R88 to the list of GDP-interacting residues [63]. Interestingly, two out of the three amino acids were among those that have been shown to interact with fatty acid as well (Table 1-1) [63]. One suggested inhibitory mechanism of GDP is that it can bind inside the translocation channel of the protein and allosterically displace fatty acid from its binding site [63].

There are different reports about the stoichiometry of UCP inhibition by purine nucleotides; some have concluded that inhibition is achieved by one nucleotide per monomer [83], while others suggest the stoichiometry is one nucleotide per dimer [84].

In addition to protons, all UCP homologues are able to transport chloride [80]. However, the rate at which UCPs transport chloride ions is lower compared to that of protons, also no fatty acid is needed to initiate chloride transport [80, 30]. In fact, fatty acids inhibit UCPs chloride transport activity, suggesting that both species are sharing the same path [30].

1.6.2 Non-regulated proton leak

1.6.2.1 ADP/ATP carrier

AAC is an antiporter of ADP and ATP across the IMM. As a result of the conversion between the cytoplasmic and matrix states, AAC transports around a human body weight of ADP and ATP per day [50]. Two inhibitors of AAC, carboxyatractyloside (CATR) [85] and bongkrekic acid (BKA) [86, 87], are able to lock the structure in cytoplasmic and matrix states, respectively.

The structural elements that are involved in the alternative access mechanism can all be seen in the crystal structures of the carrier [46, 50] (Figures 1-2 and A-1-1).

i) Matrix network three salt-bridges (K33-D232, R235-D135 and R235-E30) and the Q-brace (Q37) from BtAAC, V;

ii) The cytoplasmic network salt-bridges (D299-K208, D205-K104 and D101-Q302) and the Y brace Y298, Y204 (and R100) from TtAAC, Λ;

iii) The SBS residues R88, G192 and R287 for TtAAC and R80, G183 and R 280 for BtAAC.

After the matrix state structure was reported by Ruprecht et al. (Figure 1-2) [50], the same researchers proposed a detailed mechanism of transport, which is in agreement with the previously proposed alternating access mechanism [50]. In this mechanism, matrix and cytoplasmic conformational states can be interconverted as a result of interconnected movement of the helices (between 12-17 Å) towards the central z-axis of the carrier or away from it [56]. It has also been proposed that the SBS has minimal movement during the conversion of the two conformational states and is accessible from either side [56]. In fact, the contact points appear to act as a fulcrum during conformational changes [50, 56].

A comparison of CATR-locked (V) and BKA-locked (Λ) structures reveals that only 20% of the carrier structure changes during the interconversion of the two conformational states. [50]. One notable change is the movement of cytoplasmic ends of the even numbered helices resulting in formation or disruption of the cytoplasmic network [50]. Surface analyses of the cytoplasmic and matrix states are in agreement with the two-state alternating access mechanism, as in each state the exposed site provides a positively charged accessible surface available for ATP or ADP binding; conversely, the opposite side is closed at the same time with no/very low positively charged surface available for interaction [50].

The proposed transport mechanism of AAC is very thorough and detailed [50], however, it suggests that non-solvent accessible gates in both cytoplasmic and matrix states prevent the proton leak across the protein. However, AAC has long been known to be able to transport protons from the IMS to the matrix [21, 88, 89]. A recent patch-clamp study of mouse AAC in mitoplasts (mitochondria with the OMM removed) provides valuable insights into this carrier's proton transport mechanism [90], which is consistent with, yet complementary to, the mechanism proposed by Ruprecht et al. [50]. In this patch-clamp study, AAC was shown to be capable of transporting protons only in the presence of micromolar concentrations of fatty acids on the cytosolic/IMS side [90]. In the proposed mechanism, fatty acid functions as a co-factor bound to the carrier, and its carboxylate head moves through the translocation pathway. Therefore, inhibitors of the translocation pathway (CATR and BKA) inhibit the AAC mediated proton transport [90]. Fatty acid can bind to the carrier regardless of its initial conformational state (matrix state or cytoplasmic state), and proton transport cannot induce any changes in the carriers' conformational state [90]. Furthermore, translocation of ADP and ATP by AAC decreases the proton transport activity. Based on these studies it has been hypothesized that AAC functions via

two transport modes both sharing the same translocation path: (i) ADP/ATP antiporter mode based on the alternating access mechanism (cytoplasmic state and matrix state interconversions [46]), and (ii) proton transport mode, which relies on presence of/ activation by fatty acids [90].

1.6.2.2 Proton driven symporters: phosphate carrier

One example of a proton-driven symporter among MCF members is the mitochondrial phosphate carrier (PIC) [91]. PIC is responsible for stoichiometric symport of phosphate and protons from the IMS into the matrix; as a result of this symport, inorganic phosphate will be available for ATP synthesis in the matrix [92]. Like many other members of the MCF, no high-resolution structure is available for PICs and there is no consensus on the mechanisms of transport. Symport of proton and phosphate [92], antiport of OH and phosphate [92], fatty acid cycling model for the proton transport function [93] and MCF alternating access mechanism [57] are among the proposed mechanisms of PIC function.

As shown in Figure 1-6, A, three amino acids (Q227, R226 and D177) are present in the binding site of human PIC (SLC25A3) and play a role in the co-transport of protons and phosphate molecules [57]. It has been shown that the carriers which are thought to symport substrate and protons across the IMM, all possess a negatively charged residue in close proximity to positive residues in their contact points [57]. In the case of human PIC, the positively charged R226 can provide a potential binding site for the anionic phosphate; however, aspartic acid residue

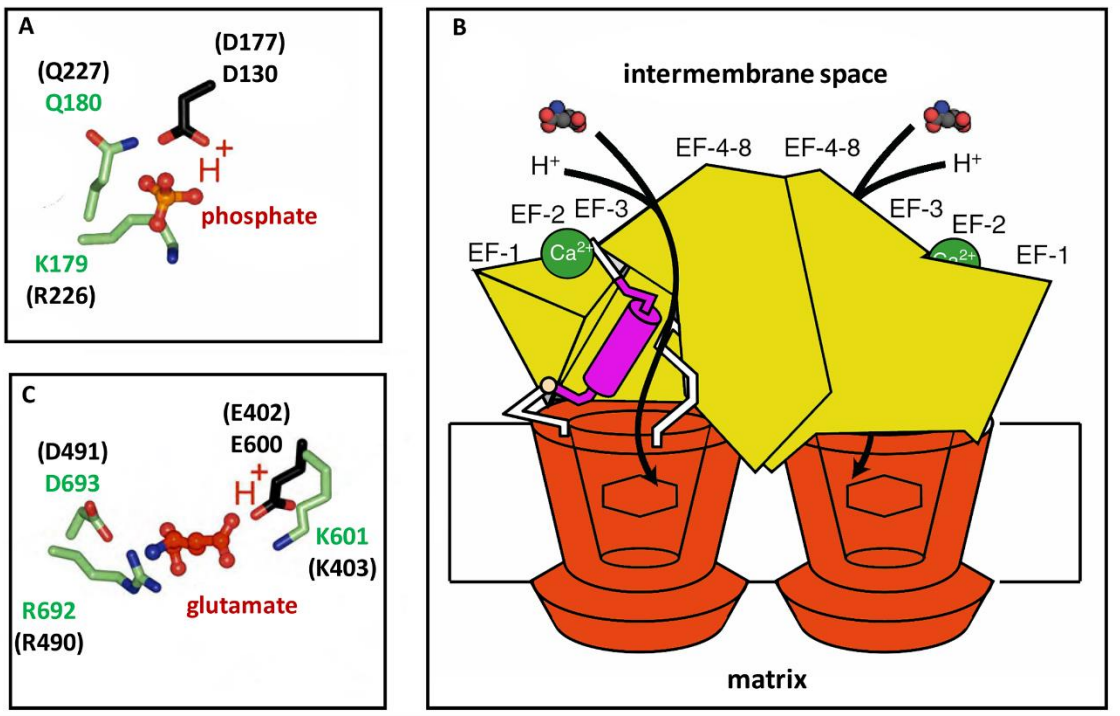

Figure 1-6 Mechanism of nonregulated proton co-transport across PIC and AGC. A) residues involved in substrate co-transport of PIC (the residues in the parentheses are human counterparts of the studied *Candida albicans* residues) B) schematic structure of active (calcium bound) dimeric AGC1. Ca^{2+} binding results in formation of a hydrophobic groove for binding of C-terminal α-helix (purple). This movement results in activation of glutamate and proton transport. C) residues involved in substrate co-transport of AGC1 (the residues in the parentheses are human counterparts of the studied *Saccharomyces cerevisiae* residues). This figure is copied from refs. [57] and [94] with permission, minor changes applied.

at position 177 could prevent this substrate binding in two ways: (i) by electrostatically pushing back the phosphate group, or (ii) by interacting with Q180 and R179, thereby decreasing the affinity of the cationic contact site to bind to the negative substrate (Figure 1-6, A) [57]. Co-transport of a proton with phosphate neutralizes D177, and not only cancels the two preventive roles of aspartate but can also assist the transport of the substrate against its gradient using the proton motive force [57]. When the PIC is in the cytoplasmic state the contact points are available/exposed for interacting with the substrate. Nonetheless, the aspartate residue of PIC cannot be protonated in the absence of phosphate even in high proton concentrations of the IMS, as the Arginine residue will keep Aspartate's pKa low (~4) [57]. While the phosphate group

interacts with R226 and Q227 the negative charges of phosphate and aspartate will drive the proton towards the binding site by electrostatic attraction. Furthermore, the additional electrostatic interactions resulting from co-transport of a proton provides the energy needed to disrupt the matrix network [57]. Consequently, the carrier can change its conformation and opens towards the matrix side (cytoplasmic to matrix state conformational change) and the phosphate and proton can be released into the matrix [57].

1.6.2.3 Proton driven antiporters: aspartate/glutamate transporter

Aspartate/glutamate carriers 1 and 2 (AGC1 and AGC2) are examples of MCF antiporters with the ability to co-transport protons across the IMM [95]. Human AGC1 and AGC2 are encoded by SLC25A12 and SLC25A13 genes, respectively [95]. These carriers transport the aspartate which is synthesized in the mitochondrial matrix to the IMS in exchange for glutamate which is co-transported with a proton [95]. AGCs have ~675 amino acid residues which are divided into 8 N-terminal EF-hands in the IMS (~330 amino-acids) [94] plus a C-terminal domain of ~340 amino-acids [96]. The C-terminal domain is composed of a TM domain structurally similar to other MCF members [52] and a further ~40 amino acid soluble domain in the IMS (Figure 1-6, B) [94]. AGCs are believed to be dimeric [94]. Upon binding of Ca^{2+}, the EF-hands 1 and 2 can partly move to open a hydrophobic groove to permit the cytosolic α-helix of the C-terminal to bind [94]. As a result of these movements glutamate and a proton can concomitantly enter the TM domain to induce the conformational changes (cytoplasmic to matrix state) leading to transport of the substrates (Figure 1-6, B) [94, 95].

As shown in Figure 1-6, C, the residues involved in the AGC1 binding site are E402 and K403, R490 and D491. Under physiological pH, E402 can repel IMS glutamate as a result of repulsion between the two sidechain negative ions [48]. However, co-transport of a proton with

glutamate might result in neutralization of E402, thereby facilitating binding of glutamate to K403 [48]. This is very similar to what happens in the co-transport of phosphate and proton through PICs [57]. The difference is that AGC is a proton-driven exchanger, whereas the PIC is a proton driven co-transporter/symporter. Translocation of aspartate from matrix to IMS is gradient driven, meaning that it is facilitated by the higher concentration of aspartate in the matrix, the weak cytoplasmic salt-bridge network (with a low energy barrier to overcome), and the membrane potential [57].

It has been shown that when the concentration of Ca^{2+} in the IMS increases the rate of electron transport also increases up to 5 times, as the proton gradient will constantly be dissipated by AGC activity [95]. The decrease in the membrane potential by AGC activity might also result in reducing ROS production because of the inverse relationship between the membrane potential and ROS production [97].

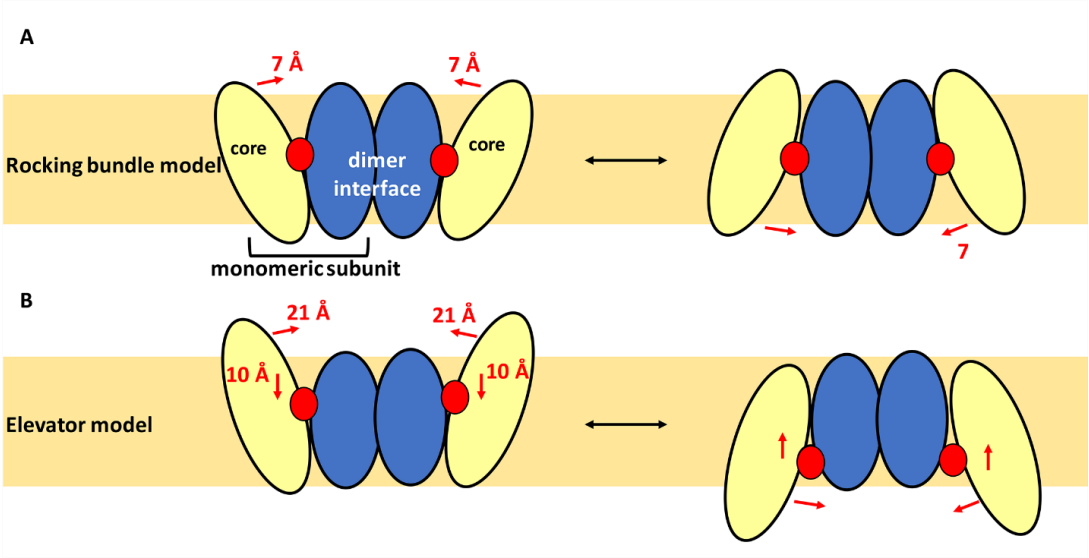

Figure 1-7 Rocking bundle model and elevator model are both sub-categories of the alternating access model for transport. These models are proposed for sodium and proton translocation by CPA1 and CPA2 families, respectively. In the rocking bundle model, the core domain has ~7 Å rocking motion and in the elevator model, the core domain rotates ~21° and shift ~10 Å. Both models lead the substrate SBS to become alternatively accessible to two different sides of the membrane. Figure generated by PowerPoint 365.

1.6.2.4 Non-proton driven antiporter: Ornithine/citrulline carrier

The mitochondrial ornithine/citrulline (ORC) exchanger is another proton translocator of the MCF [98]. However, in contrast to all other proton transporters in this family, proton translocation by ORC occurs against its concentration gradient and therefore requires energy [98]. The ORC carrier transports cytosolic ornithine across the IMM to the matrix in exchange for a citrulline molecule and a proton [98]. The energy required for this translocation could be provided by favorable gradients of the substrates across the IMM [98]. Since ornithine is positively charged in physiological pH, the net charge transfer resulting from the activity of this transporter is zero [98]. Ornithine and citrulline molecules are involved in urea synthesis. Citrulline is synthesized from ornithine in the matrix and transferred to the cytosol where it enters the urea cycle [99] via ORC [98]. In the urea cycle, urea is formed, citrulline is converted back to ornithine, and ornithine re-enters the matrix via ORC [100]. Two human isoforms of ORC have been discovered to date: ORC1 and ORC2 [101]. Even though ORC isoforms share 87% sequence identity, they have differences in substrate specificity; ORC2 is less specific compared to ORC1 [102].

A mutagenesis study of ORC1 and ORC2 shows that residue 179 is important in substrate specificity [102]. In the case of ORC1, ornithine binds to residues E180, R179 and E77 [102]. Close proximity of R179 to the matrix salt-bridge network might imply that R179 can also play a role in the ORC1 conformational change resulting in its transformation from cytoplasmic state to matrix state [102].

1.7 Proton leak in mitochondria by non-MCF members

In addition to the MCF members that are responsible for translocation of a wide range of substrates (such as, nucleotides, coenzymes and various ions) across the IMM, other carriers/channels are also present in the IMM which translocate cations [103]. Most studied of

these transporters are MCU (which is responsible for unidirectional import of Ca^{2+} into the matrix [104, 105]), Na^+/Ca^{2+} exchanger (NCLX) (which allows influx of Na^+ into the matrix and efflux of Ca^{2+} to the IMS [106]), as well as K^+/H^+ and Na^+/H^+ exchangers (KHE and NHE) (which translocate protons into the matrix in exchange for cytosolic K^+ and Na^+, respectively [107, 108]). Both NHE and KHE are able to translocate protons across the IMM; however, NHE is more active [109].

NHEs are members of the cation-proton antiporter (CPA) family [110]. Due to slow rate of electrochemical gradient-driven leakage of Na^+ (and K^+) cations across the IMM, mitochondria would never survive without transporters such as NHE (and KHE) to expel the cations out of the matrix [109]. NHEs are not exclusive to the mitochondria [111]. In fact, ten isoforms of NHEs (NHE1-NHE10) are differentially expressed in various tissues of the human body [111]. NHEs 1, 2 and 6 are reported to function in mitochondria. Among these, NHE6 is exclusively found in mitochondria [108, 111].

Members of the CPA family can be subdivided into CPA1 and CPA2 carrier subgroups. CPA1 carriers exchange one proton against one Na^+. Human NHEs are in the CPA1 branch [112]. CPA2 members exchange two protons against one Na^+ [112]. It has been proposed that the conformational changes leading to translocation of ions across the membrane is the same among CPA1 and CPA2 members [112].

Two models have been proposed for ion translocation by NHEs, which are both subclasses of the alternative access mechanism and both suggest a single site for ion-translocation: (i) the rocking bundle model, proposed based on structural analysis of a CPA1-type transporter, the *Methanocaldococcus jannaschii* NHE [112]; and (ii) the elevator model, proposed based on structural analysis of a member of the CPA2 sub-group, a NHE from *Thermus thermophilus* [113].

NHEs have been shown to be dimers, where the monomeric subunits are composed of 12 or 13 TM domains (CPA1: 13 [112], and CPA2: 12 [113]). The TM domains of each monomer are divided into a 6-helix bundle domain (core domain), which moves during the transport of ions, and a set of seven or six helices located at the dimer's interface (dimerization domain), which is stabilized in the membrane and does not move during transport [112, 113] (Figure 1-7).

In the rocking bundle model, the binding site becomes alternatively accessible to the two sides of the membrane upon a ~7 Å rocking motion of the core domain [112]. In the elevator model, a ~21° rotation of the core domain results in closure of the cavity on one side and opening of the cavity on the other side of the membrane. Parallel to this rotation, the core domain also shifts ~10 Å towards the side which will be exposed next [113].

Even though the details behind the conformational changes are not known, two aspartate residues (D156 and 157 on helix 5) are found in the binding site of the *T. thermophilus* NHE, which are highly conserved in all NHEs and have been shown to play a crucial role in the function of these proteins [113].

1.8 Disagreements about the functional forms of MCF members in lipidic environments

Formation of homo- and/or hetero-oligomers in the membrane to optimize/regulate protein functions is common among MPs [68, 114, 115]. Therefore, understanding oligomerization and interconversion between different oligomeric states can provide insights about a protein's mechanism of function [115]. An important example of oligomerization in the IMM is formation of the supercomplexes involved in the OXPHOS process [12], with different arrangements and stoichiometries. Lipids can influence and control protein oligomerization in the membrane [115]. The role of lipids in controlling oligomerization have been shown to be more important in MPs with weakly interacting subunits and small oligomerization interface(s) (small buried surface area

and no salt-bridge formation between the subunits) [114]. For example, NHEs of *E. coli* (no salt-bridges between the subunits, buried surface area: 684.4 $Å^2$) and *T. thermophilus* (two salt-bridges, buried surface area: 1800.9 $Å^2$) both form dimers in membranes. However, the former carrier protein can dimerize only in the presence of cardiolipin (CL) because of its small buried surface area and lack of inter-subunit salt-bridges [114] while the latter do not need lipids for dimerization [114]. It has also been suggested that cells can alter lipid composition of the membranes to regulate the presence and abundance of oligomeric species [114].

The quaternary structure and protein-lipid interactions of members of the MCF are not fully understood and in many cases researchers do not agree on the quaternary structures [66, 68, 116, 117]. Some reports suggest that all mitochondrial carriers function as monomers [67, 116], while others propose a dimeric structure for many of them [117]. Among proton transporters of the MCF, there has not been universal agreement on the functional molecular forms of AAC [67, 118, 119], UCP [65-68] and PIC [67, 117, 120]. It has been demonstrated that CL is tightly bound to AAC and PIC and is considered to be required for the transport function of these proteins [118]. UCP has no tightly bound CLs [118]; however, the presence of CL in UCPs 2,4 and 5 lipidic environment affects their proton and chloride transport function and enhances their helical conformation [80]. It has been suggested that AAC is either a monomer [67] or a dimer [118], or both [121] in the membrane. Out of six molecules of CL that are bound to subunits of dimeric AAC, two are thought to sit at the interface of the monomeric subunits and act as a "glue" [118]. Furthermore, it is suggested that CL might have a role in cross-talk between AAC subunits in the dimer [118]. Moiseeva et al. [121] showed that external factors (such as tonicity of the mitochondria or incubation at 4° C) can influence the oligomerization of AAC [121]. PICs are also proposed to function either as a monomer [67] or dimer [120].

The case of UCPs is more complicated, since monomeric [83], dimeric [65] and tetrameric [30, 68, 80] structures have been reported to be functional. A dimeric functional form was the first reported quaternary structure for UCP1 [65]. It has been shown that UCPs might be able to interact with other members of the MCF, such as AAC, to form hetero-dimers [122]. Also, different homologues of UCPs are proposed to be able to interact with one another and form hetero-dimers, such as UCP2+UCP3 [42]. It has been suggested that homo-tetrameric MPs are most probably formed by dimerization of dimers [30, 68, 123].

The presence of a GXXXG motif on TM helices has been shown to be involved in homo-oligomerization of MPs as a result of helix-helix interactions [124]. This motif was first shown to play an important role in dimerization of glycophorin A [125]. NMR structure of the glycophorin A showed that two glycine residues, that are apart from one another by three amino acid residues, form a groove that allows the helices to pack closely [126]. Furthermore, the GXXXG motif is known to be the most abundant sequence involved in helix-helix association of *E. coli* inner MPs (~80%) [124, 127]. In addition to GXXXG, πXXXπ (π = small residues such as G, A, S or T) and GXXXAXXG have also been shown to play an important role in oligomerization of proteins [124]. On the other hand, such oligomerization motifs are very abundant MPs and cannot be used as the only source for prediction of dimerization interface [124].

1.9 Research goal and objectives

The overall objective of this PhD dissertation is to provide novel insights into the structure and proton transport function of UCPs in lipid membranes. In order to accomplish this objective, two research goals are investigated:

1- The functional structure of UCPs in the membrane; and

2- The mechanism of proton transport by UCPs.

UCP2 was used as a model to answer these questions for several reasons: (i) its widespread expression in several mammalian tissues [19]; (ii) it has been shown to have multiple roles in mammals [41, 128, 129]; (iii) its high amino acid sequence identity with UCP1 (the prototypical UCP) [60]; and (iv) the availability of an atomic NMR structure [70].

1.9.1 Investigation of the functional structure of UCP2 in lipid environment

The hypothesis for the first goal was that *UCPs could exist and function as a tetramer (dimer of dimers), as well as monomers and dimers in the IMM*. The support for this hypothesis came from the previous observation that several UCP homologues reconstituted in lipid vesicles as functional tetramers [30, 68]. In order to evaluate this hypothesis, four specific aims were pursued to: (i) separately purify and characterize UCP2 as monomers as well as a mixture of monomers, dimers, and tetramers, and to reconstitute these two group of molecular forms (monomer and mixture) in liposomes; (ii) compare the structure and function of the reconstituted proteins that originated from these two groups of proteins (monomer and mixture); (iii) investigate the structural features (such as the overall shape and dimensions of the subunits), and the physicochemical characteristics of tetrameric UCP2 (such as dissociation energy of the tetramer and dynamics of the subunits) in lipidic environments; (iv) better understand the factors that stabilize the oligomeric structure of UCP2, such as inter-subunit salt-bridges or bound lipids.

To achieve these goals, UCP2 was expressed in the *E. coli* inner membrane and extracted first with lauryldimethylamine oxide (LDAO) detergent, which was switched at a later stage to a mild detergent (octyl glucopyranoside, OG) in its micellar form. Recombinant UCP2 was then purified in OG in two forms: as monomers and as a mixture of monomeric, dimeric, and tetrameric forms using immobilized metal affinity chromatography (IMAC). These two batches of proteins were then separately reconstituted in egg yolk PC vesicles using the detergent removal method to

study the structure and function of the protein in an environment that closely mimics the IMM [130, 131]. The structure and molecularity of UCP2 was then analyzed both in OG and large unilamellar vesicles (LUV) by far-UV CD spectroscopy [132] and semi-native sodium dodecyl sulfate–polyacrylamide gel electrophoresis (SDS-PAGE) techniques [68]. The function of UCP2 was studied using a fluorescence quenching assay [32, 68, 133]. The conformational features of the protein and the molecular interactions involved in oligomerization, were assessed by MD (Molecular Dynamics) simulations and related techniques [134]. Similar experimental and computational analyses were performed on AAC, (a structurally comparable MCF member for which the atomic x-ray structure is available) to validate our methods and compare the behavior of two proteins in lipid membranes.

Collectively, this part of the research provided in-depth information about the possible structures of UCP2 in the IMM, local conformational changes of the monomeric subunits upon tetramerization and the process of oligomerization. It is shown that UCP tetramerizes in the membrane as a dimer of dimers in which the monomers in one dimeric pair have comparable conformations that are different from the monomers in the other dimeric pair. The outcome of the experiments done to address the first specific objective imply that the subunits of the UCP2 interact and influence one another in the regulation of the proton transport function of the tetramer.

1.9.2 Evaluation of the mechanism of proton transport by UCP2

The second project focused on analysis of proton transport by UCP2 via the proposed "alternating access mechanism" [51]. The hypothesis was that *the matrix network in UCP2 plays a crucial role in regulation of proton transport*. UCP2 has an overall net charge of +15, and a cluster of positive charges are accumulated close to the matrix side of the protein. High charge density at the matrix interface could contribute to the formation of an electric field (potential-

sensitive area) that is capable of reacting to movement of charges/charged substrates and induction of conformational changes, which could contribute to substrate transport [32, 80]. Furthermore, the matrix network is in close proximity of three arginine residues (R88, R185 and R279) which have been suggested to be involved in inhibition and activation of UCPs in several studies [63].

The role of the matrix salt-bridge network in proton transport by UCP2 was studied through five specific aims: (i) Incorporate point mutations into UCP2 designed to partially or fully disrupt the matrix salt-bridge network; (ii) Test the integrity of the UCP2 matrix network by introducing three pairs of point mutations (6 mutations total) that maintain the integrity of the salt-bridges but switch the two ends of each bridge; (iii) compare the structures of UCP2 and its mutants in mild detergent (OG) and liposomes to ensure that the overall conformation of the native protein has been maintained in the mutants; (iv) compare the proton transport rate of UCP2 and its mutants in the presence and absence of purine nucleotide inhibitors; and finally (v) analyze and relate the proton transport function of UCP2 and its mutants to local conformational changes of the native protein.

To achieve these goals, UCP2 and its eleven mutants were expressed in *E. coli* membranes, purified, and reconstituted in vesicles using the same methods as in the first project. Conformations and conformational stabilities of the UCP2 and its mutants in OG detergent were evaluated by far- and near-UV CD and thermal denaturation techniques [132]. Proton transport rates were analyzed by a fluorescence quenching assay [80, 133], and molecular and atomic details of the structures were analyzed by MD simulation methods [134].

Overall, the second project provides detailed information about the proton transport mechanism of tetrameric UCP2 and its regulation. This part of the study led to the proposal of a biphasic model for proton transport by UCP2. Based on this model, protons can pass through the

central channels of monomeric subunits with the help of fatty acids via an alternating access mechanism. The two monomers within each dimeric unit are proposed to be in a similar stage/phase of transport (although not necessarily conformationally equivalent), but the dimeric units themselves are in opposite phases (when one is absorbing protons the other is releasing protons). Additionally, the monomeric subunits are not conformationally equivalent and their perpetual conformational changes could have a potential role in regulation of proton transport by influencing the neighboring subunits.

CHAPTER 2 - METHODOLOGIES

2.1 Experimental Methodologies

2.1.1 Recombinant overexpression and extraction of membrane proteins

The natural abundance/quantity of MPs is usually not sufficient for in vitro biochemical and biophysical analyses; therefore, researchers usually have to use overexpression techniques to produce enough material for their studies [135]. Obtaining properly folded pure proteins in high yields has always been a challenge in MP research [135]. Considering the crucial role of lipidic environments on the structure and function of MPs, it would be preferable to directly express these proteins in cell membranes, such as bacterial membranes [114, 115]. The most widely used host for overexpression of MPs is *E. coli*; however, the membrane expression yield of eukaryotic MPs, such as UCPs, in *E. coli* is not always satisfactory [136]. Approaches to address this issue can be classified into three categories [136]:

2.1.1.1 Engineering *E. coli* cells to make them more suitable for membrane protein expression

Alteration of *E. coli* cells to favor MP overexpression has been used in several studies. One strategy is to reduce the rate of protein production to better fit the capacity of the cell biogenesis machinery and to ensure that the produced proteins are folded and integrated properly in the membrane [136, 137]. There are several procedures for slowing the rate of protein expression, one of which is to reduce the production and/or activity of RNA polymerase [136]. Widely used MP expression strains C41(DE3) [138], C43(DE3) [138], and Lemo21(DE3) [135, 137] are examples of strains of *E. coli* that produce lower levels of RNA polymerase [137]. Reduction of protein

expression rate can also be achieved by lowering the incubation temperature, the concentration of inducer, or strength of the vector [136].

Overexpression yield of MPs can also be increased by improving the ability of *E. coli* cells to localize the protein in the membrane [136]. Co-expression of chaperones and/or other proteins that are involved in targeting MPs to the membrane [139] or increasing membrane fluidity for easier insertion [140] have proven to be successful methods for achieving higher MP expression yields.

2.1.1.2 Engineering the protein of interest to improve its yield of overexpression in the membrane

Another way to increase MP expression yield is to modify the N- or C-terminus of the protein [136]. Most MPs contain an N-terminal (or internal) sequence that directs the protein to the membrane [136]. Shortening the N-terminal [141] or changing its properties by incorporating point mutations can impact the expression yield of MPs [142]. Furthermore, fusion of leader sequences to N- or C-termini of proteins can result in membrane targeting [136]. Membrane targeting sequences from Mistic (a membrane-associated protein from *Bacillus subtilis*) [143], SUMO (a small ubiquitin-related modifier) [143, 144], and pectate lyase B (pelB) [145, 146] have all been shown to enhance yields of recombinant MPs in *E. coli* by directing proteins to the bacterial membrane. PelB is a 22-residue signal peptide first characterized in *Erwinia carotovora* [146]. This leader sequence has been shown to target soluble proteins to the *E. coli* cell membrane for export to the periplasm and to direct several MPs to the *E. coli* inner membrane [68, 145, 147, 148].

2.1.1.3 Using expression hosts other than *E. coli*

The reason behind the popularity of *E. coli* as a recombinant protein expression host is its ease of cultivation and availability of various genetic tools and biological methods for introduction of desirable changes [136]. Thus, other than convenience, there is no good reason for choosing *E. coli* as the only model organism for MP expression. Bacteria with more copies of MP chaperones (such as *Bacillus subtilis*) and/or slower growth rate (such as *Lactococcus lactis*) are promising alternatives to *E. coli* for overexpression of integral MPs, especially for those with multiple TM domains (more complicated folding) [136]. Furthermore, various eukaryotic hosts such as different yeast species, insect and mammalian cells can be used for expression of membrane proteins [60,72]. Throughout this thesis, *E. coli* has been used as the only host for expression of UCP2. Close homology relationship between gram negative bacteria and mitochondria makes *E. coli* a proper expression hosts for mitochondrial proteins. In fact, mitochondria are thought to have originated from gram negative bacteria about 1.6 million years ago [2].

Monitoring the cellular location of the overexpressed protein (either membrane or inclusion bodies or both), its quality and quantity are necessary steps in optimization of protein expression [136]. Fractionation of the host cells (to inclusion bodies, membrane fraction and soluble fraction) followed by determination of the protein abundance by SDS-PAGE and Western blot are common quality control steps of expression. Green fluorescent protein labeling could also be used for visualization of the protein in the whole cell [136].

2.1.1.4 Extraction and reconstitution of overexpressed membrane protein

Once overexpressed, MPs should be extracted from host cells using a system that mimics the membrane and stabilizes the protein in its native form [149]. MPs are usually extracted from the membrane using detergent micelles [149]. Once extracted and purified, the purity of the protein

should be evaluated. Denaturing, semi-native and native PAGE analyses are common methods to visualize and estimate the purity of proteins. The concentration of SDS in sample loading and running buffers are 2.5% (w/v) and 35 mM, respectively, in denaturing SDS-PAGE. These concentrations decrease to 1% (w/v) and 2 mM in semi-native conditions [68], while there is no SDS (neither in sample loading buffer nor in the gel and running buffer) in native PAGE analyses [150]. Semi-native and native conditions maintain inter-subunit interactions thus allowing visualization of oligomers [68]. After purification, detergents can be removed and replaced by more stabilizing molecules such as amphipols, or the MPs can be reconstituted into lipid bilayers that mimic membrane environments such as bicelles, liposomes and nanodiscs [149]. Figure 2-1 provides a summary of membrane mimetics that are frequently used in MP research.

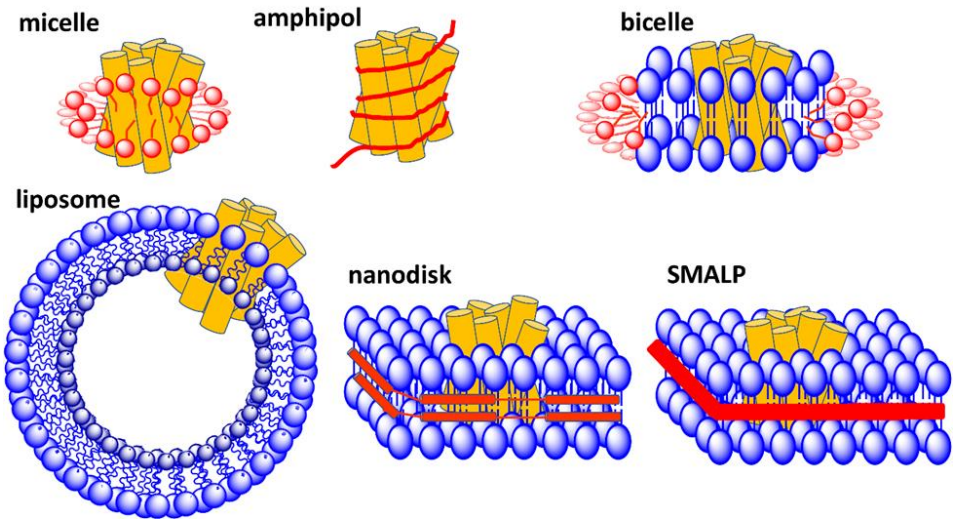

Figure 2-1 Schematic representation of various systems used for mimicking membrane environments. TM helices of MPs are shown in yellow. Lipids are shown in blue. Detergents in micelles and bicelles, amphiphilic polymers in amphipols, membrane scaffold proteins in nanodiscs and styrene maleic acid polymers in SMALP are all shown in red. Figure generated by ChemBioDraw Ultra 14.0.

Each membrane mimetic system has its own pros and cons. One important advantage of detergents is that their interference with spectroscopic analysis is minimal [132]. On the down

side, detergents cannot preserve all of the surrounding lipids around MPs and cannot fully mimic the MP lipidic environment in terms of packing constraint, charge, shape and size; consequently they can significantly impact/alter the structure and function of the native proteins [132].

Amphipols are amphipathic polymers composed of a polyacrylate backbone with hydrophobic and hydrophilic sidechains capable of solubilizing MPs by adsorbing onto their surface [151, 152]. Amphipols can better stabilize the structure of MPs compared to detergents, and modification of the sidechains provide the opportunity to optimize them for specific studies and introduce labels; yet lack of actual lipidic environment around the MPs is still an issue [149].

In liposomes and bicelles, the purified MP is reconstituted in a synthetic bilayer mimetic, which allows the protein to be studied in the presence of lipids and to analyze the effect of changes in the lipidic environment on a protein's structure and function [149, 153]. Large liposomes and bicelles usually interfere with spectroscopic analysis and special considerations should be taken into account [132, 149]. Furthermore, bicelles are usually unstable and can only be formed with limited types of lipids [149].

Nanodiscs are pieces of membrane bilayer that are surrounded by membrane scaffold proteins [149]. Small sizes of nanodiscs and the presence of lipids around the MP make them suitable environment systems for studying MPs; however, the proteins still need to be reconstituted in nanodiscs from detergent systems and if the detergents are not chosen carefully the structure of the proteins can be affected [149].

The most recently developed system for stabilization of MPs is the styrene maleic acid lipid particles (SMALP) [154]. Addition of styrene maleic acid polymers to the membrane (embedded with protein) results in spontaneous formation of disk-like particles (Figure 2-1). SMALP's environment is comparable to nanodiscs but the proteins are directly extracted from biological

membranes without the use of detergents [149, 154]. It has been suggested that the structure of an MP in a SMALP particle is very similar to their native structure and SMALP systems are considered promising tools for studying MPs.

2.1.2 Circular Dichroism spectroscopy for structural analysis of membrane proteins

CD spectroscopy is a robust technique for characterization of the secondary structures of proteins, protein folding, and protein interactions [132]. An important strength point of CD is its ability to provide information on dynamic structures of the proteins/molecules, which is more realistic compared to the data obtained from static molecular structures such as those obtained by x-ray crystallography [132]. Differences in the absorption of right- and left-handed circularly polarized light by chiral molecules or environments is the cause of production of a CD signal [132]. Information about the secondary, tertiary, and quaternary structures of proteins can be derived from near- (250-300 nm) and far-UV (190-240 nm) wavelength ranges [132]. The far-UV CD signal of a protein is mostly correlated with its backbone secondary structure and is the result of $\pi \rightarrow \pi^*$ (at ~190 and ~208 nm), and $n \rightarrow \pi^*$ (at ~222 nm) electronic transitions of the amide chromophores in the backbone sequence [132]. A protein's near-UV CD spectrum is usually derived from absorbance of aromatic and cystine residues and is sensitive to the microenvironment of these chromophores, and therefore provides qualitative information about the protein's tertiary structure [68].

The use of CD spectroscopy for structural analysis of MPs is limited compared to that for soluble proteins [132]. Peak shifts, absorption flattening, and light scattering are three common issues in CD spectroscopy of MPs, which result in uncorrectable and unpredictable distortions in the overall shape of CD spectra [132].

Red and blue shifts of the peaks are mostly because MPs are always shielded by stabilizing environments which are physicochemically different from aqueous solutions of which most of the reference databases of CD are generated from [132]. As a result, shifts in positive and negative minima of the spectra for MPs can result in large errors in data analysis [132]. In order to minimize these types of errors, CD data of MPs should be compared with libraries that include MPs in their datasets (such as SMP180 available DichroWeb Server) [132, 155].

Absorption flattening arises from nonuniform distribution of proteins in solution (since the solution is more concentrated inside a vesicle, a bicelle, or a nanodisc), and results in nonlinear reduction of the absorbance over the range of wavelengths, and thus could be minimized by increasing the homogeneity of the sample or decreasing the concentration of proteins per particle [132].

Light scattering by a particle is a consequence of comparable or larger size of the particles in a solution compared to the wavelength of the circularly polarized incident light, which results in the production of false signals. Thus, reducing the size of particles to less than the incident light wavelength can minimize the adverse effects of light scattering [132]. Since detergent micelles usually contain one protein complex per micelle and are smaller in size compared to vesicles, bicelles and nanodiscs, absorption flattening and light scattering issues are the lowest for detergents [132]; however, as mentioned earlier they cannot fully mimic a bilayer as there are no bilayer lipids surrounding the MP [149]. There is always a tradeoff between undesirable artifacts of lipidic environments on the CD spectrum and impact of detergent distortions on native conformations of MPs [132].

Some valuable information about the association state of proteins can be intuited by analyzing the relative intensity of the minima near 208 and 222 nm in a CD spectrum. It has been

experimentally shown that a higher ratio of 208/222 absorbance can indicate a higher probability of having a monomeric form and a lower ratio suggests the presence of more associated forms and higher density of helix packing [30].

2.1.3 Measurement of the rate of proton transport

In addition to ATP synthesis, translocation of many ions such as K^+, Na^+ and Ca^{2+} is regulated by the mitochondrial proton gradient across the IMM. [156]. Several techniques have been developed for measuring the rate of proton transport by mitochondrial transporters. Methods to evaluate the rate of ion transport across the IMM by transporters and channels can be classified as direct or indirect as described below.

One direct system for analyzing proton transport by UCPs involves the use of sensitive pH glass electrodes, which are able to detect decreases in pH on the external side of a membrane upon activation of reconstituted UCPs (in vesicles) [157]. The patch-clamp method also allows for the direct measurement of proton transport [158]. In addition to the ability to measure the number of transported ions across a transporter, patch-clamping can provide information about the biophysical properties of proteins, such as the number of active subunits within a complex [159]. In this method a pipette is pressed against a vesicle or a whole cell membrane in which the MP is embedded, to form a “seal”. The application of voltage can imitate the voltage difference across biological membranes and result in passage of ions through the channel, the resultant current is then amplified and detected [159]. Patch clamp can record currents as low as fractions of a picoampere [160]. Patch clamp studies on UCP1 have been used to detect currents of protons in mitoplasts and also suggested that UCPs might be oligomeric [161].

Indirect methods of measuring proton transport utilize an indicator to probe changes in the medium that occur as a result of proton transport. These changes include pH alteration of external

or internal media, changes in polarity of the liposome, or formation of anionic species inside the liposome upon efflux of protons. For example, pyranine (8-hydroxypyrene-1,3,6-trisulfonic acid, trisodium Salt) (HPTS) is a pH-sensitive fluorescent dye that has been used for detection of UCP-mediated proton transport [63]. The non-fluorescent dye Safranine O is another molecule that has been used to detect proton transport [64, 162]. Transport is detected by changes of Safranine O optical density (520 nm) upon polarization of liposomes as a result of proton transport by UCPs (negative inside, positive outside) [162]. An anion-sensitive fluorescent dye, 6-methoxy- N-(3-sulfopropyl) quinolinium (SPQ), has also been used for the detection of proton transport by UCPs in many studies [133]. Activated UCP is able to transport protons out of liposomes and increase the pH of the internal buffer. The anionic species formed due to the increase of pH inside the liposome can quench SPQ. Thus, the rate of proton transport can be indirectly measured by the rate of quenching of SPQ fluorescence (Figure A-2-1) [133]. To ensure that the calculated results are from the proton transport of UCP, and not the basal leakage from the liposomes, a batch of blank liposomes (with no protein) should be tested in all methods under the same experimental conditions (Figure A-2-1). Additional details about the application of the different methods that are available are covered in Chapters 3 and 4 of this thesis.

2.2 Computational methodologies

2.2.1 Molecular Dynamic simulations and related techniques

MD was first introduced as a computational approach to study molecules by Alder and Wainwright in the late 1950's [163, 164]. MD simulations allow particles to interact with one another and provide information about the dynamic evolution of the system under study with time [165]. This technique helps understand the physical basis of the structure and function of biological molecules [165]. The first protein simulations were conducted by McCammon and coworkers in

1977 [166]. The MD method has been widely used since then to study the motion of molecules and their constituent atoms in biological molecules such as proteins and DNA, and more complex systems such as biological membranes [134, 167, 168].

In MD, the motion of particles is determined by solving Newton's equations of motion. The particles' potential energies and the forces between the particles are calculated using molecular mechanics force fields [169]. A force field is defined by a series of physical equations and parameters designed to reproduce selected properties of a system such as geometry or potential energy [170]. Each force field includes a separate set of parameters such as bond lengths, angles, dihedrals, atomic masses, van der Waals radii, partial charges, and force constants for different atom types in different conditions [170]. These parameters are empirical, i.e. extracted from experiments or high-level calculations [170]. A force field is able to distinguish a carbon atom bound to a hydroxyl group from that in a carbonyl group and assign different values to their chemical bond, angle, dihedral, etc. [170].

Below is a list of popular force fields and the areas in which they are mostly utilized:

1. AMBER (Assisted Model Building and Energy Refinement): proteins and DNA [171]
2. CHARMM (Chemistry at HARvard Molecular Mechanics): macromolecules and small species such as organic ligands [172]
3. GROMOS (GROningen MOlecular Simulation): biomolecules, isolated molecules in gas phase [173]
4. OPLS (Optimized Potential for Liquid Simulations): macromolecules [174]

Regardless of the force field type, a typical MD simulation consists of several steps that are summarized below and presented in Figure 2-2 [165].

The first step is loading the particle coordinates (coordinates specify the relative position of particles with respect to one another; in protein systems, coordinates can be extracted from PDB files), force field, and velocities (randomly assigned based on the temperature) as an input of the MD simulation [165]. The potential energy of the system and forces imposed on each particle are calculated in the next step. The coordinates and velocities are then updated according to the equations of motion (Newton's laws, implemented in the force field) and the output is collected in a trajectory file [165]. A trajectory file includes all data related to particles' motions through space as a function of time. Trajectories are then subject to different types of analysis [165].

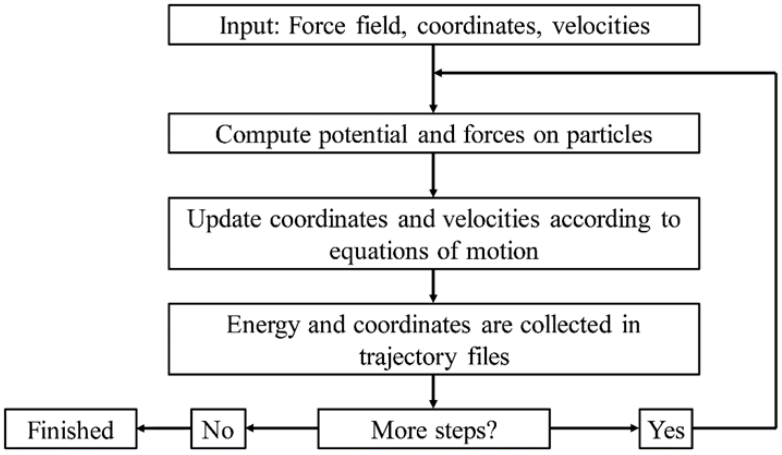

Figure 2-2 Flow chart representation of a typical MD simulation algorithm. Figure Generated by PowerPoint 365.

Ideally, the purpose of MD simulation is to explore all possible sets of coordinates (phase space) for all atoms of the system; however, in some cases some distinct regions are out of reach for a conventional MD simulation technique, e.g., when a potential energy barrier prevents the system from reaching particular coordinates [175]. The umbrella sampling technique has been developed to enhance sampling of the phase space for such systems, and to overcome and estimate the energy barrier (Figure 2-3) [175]. This technique uses a set of new coordinates with larger

energies (windows) in comparison to the system's initial energy. The system is moved from its initial coordinate (state) to the neighboring windows in a stepwise manner (Figure 2-3). This process continues until the barrier is surpassed [175]. The umbrella sampling method could be used to examine the dissociation of proteins, where tremendous interactions among the units separate the associated and dissociated forms by imposing a large barrier between the two.

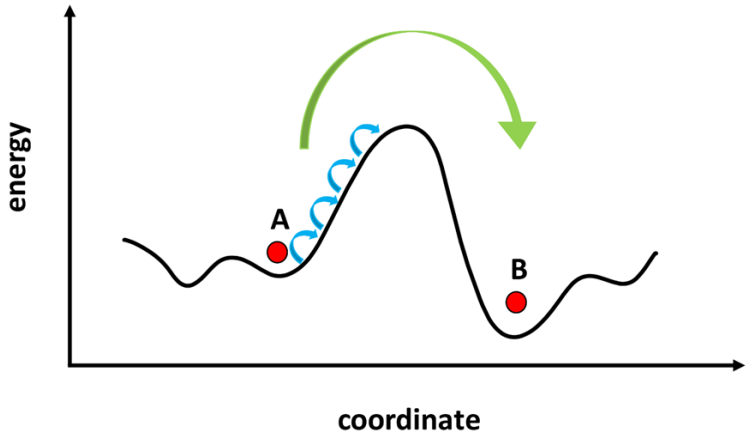

Figure 2-3 Schematic representation of a system for which umbrella sampling could be used. To change the state of the system (red circle) from A to B the energy barrier needs to be overcome (green arrow). To achieve this, the umbrella sampling technique increases the energy of the system in a stepwise manner until the barrier is passed. Each step (window, blue arrow) is a coordinate with a small increase in energy level in comparison to the previous one. Figure generated by PowerPoint 365.

Beside the various force fields, several simulation software programs are available to choose from based on the expertise of the researcher and the specifications of the system. Some of the most popular programs include AMBER [176] CHARMM [177] GROMACS [178], and NAMD [179]. Each program follows the steps outlined in Figure 2-2, using the chosen input data (force field, input coordinates, velocity/temperature) to run an MD simulation. More details about the application of computational methods for studying proteins are provided in Chapters 3 and 4 of this thesis.

CHAPTER 3 -FUNCTIONAL OLIGOMERIC FORMS OF UNCOUPLING PROTEIN 2: STRONG EVIDENCE FOR ASYMMETRY IN PROTEIN AND LIPID BILAYER SYSTEMS

3.1 Introduction

UCPs form a subfamily within the MCF superfamily, located in the IMM [60]. UCPs attenuate proton motive force by providing a back-flux route for protons to move from the IMS to the matrix, resulting in a decrease in the rate of ATP synthesis [180]. Five human UCPs have been identified. These proteins transport protons and anions across the IMM and possess comparable, dominantly helical, conformations [68].

UCP2 is unique among the UCPs in its ubiquitous expression in animal tissues [181]. The wide distribution of UCP2 in various tissues suggests that it may play different roles under different physiological/pathological conditions [182]. For example, UCP2's role in decreasing mitochondrial ROS concentration has been shown in several studies [183-185]. Moreover, UCP2 appears to be capable of transporting C_4 metabolites [34] and chloride ions [80]. Upregulation and anti-apoptotic properties of UCP2 in different cancerous cells have also been proposed [129, 186-190].

Comparable to other members of the MCF superfamily, UCPs contain a tripartite structure composed of three tandem repeats. Each repeat comprises about 100 amino acids folded into two TM α-helices that are connected by a hydrophilic loop positioned toward the matrix side of the mitochondrion [70, 180]. Monomeric [83], dimeric [66, 191] and tetrameric [30, 68] structures

have been reported as functional forms of UCPs. The monomeric structure of UCP1 has been supported by electrophoretic and size exclusion assays and isothermal titration calorimetry experiments in decyl maltose neopentyl glycol detergent, which was used (in combination with *n*-decyl-β-D-maltopyranoside) for the purification of the protein [83]. Lee *et al.* also reported that monomeric UCP1 was the only functional form of the protein; however, they were not able to convincingly justify the appearance of higher molecular masses in their assays [83]. Dimeric UCP1 structure has been a more traditional view based on cross linking [66], ultracentrifuge [65], and nucleotide binding studies [192]. Tetrameric form of UCP1 has been reported for recombinantly expressed proteins in bacterial membranes (not as inclusion bodies); and the possibility of co-existence of monomeric, dimeric and tetrameric UCPs as functional forms of the protein(s) was suggested [68]. Based on the analysis of mitochondrial Ca^{2+} uptake, Trenker *et al.* suggested that UCPs co-assemble to form homo- (UCP2+UCP2) or hetero-multimers (UCP2+UCP3) [42]. Moreover, assembly of UCPs with other MCFs, such as AAC proteins, has been reported [122]. Overall, the absence of a widely accepted high resolution structure for UCPs [64], variations in recombinant expression methodologies, and limitations accompanied by the choice and optimization of detergents for protein reconstitution in membranes are among the common shortcomings of all *in vitro* studies [59, 68].

Permanent and transient homo-oligomerization has been observed in many MPs [193]; among all enzymes listed in the Brenda enzyme database (https://www.brenda-enzymes.org), only 31.2% function as monomers and the rest (68.8%) are known to be oligomers [194]. Self-assembly of proteins is not limited to soluble proteins. In fact, co-assembly of integral MPs to functional oligomers has been reported for several systems [195-199]; proteins such as aquaporins and aquaglyceroporins (six membrane-spanning α-helices per subunit similar to UCPs) [195, 196], as

well as several potassium channels from bacterial, archaeal or eukaryotic sources [197, 198], can all form homo-tetrameric structures within the bilayer. Many homo- and hetero-tetrameric proteins are, in fact, functional in the form of dimer of dimers (containing two different molecular interfaces; one between the monomers within the dimeric unit and another between the dimers). Examples include streptavidin, transthyretin, hemoglobin [200] and GlpF [199].

Association of MPs is sometimes mediated and/or regulated by lipids, and delipidation by detergents can dissociate the multimeric proteins to monomers [114, 193]. It has been shown that lipids, such as CL, can also act as specific ligands to assist multimerization by bridging between monomers [36]. The lipid membrane therefore not only acts as a solvent medium for MPs, but also plays a crucial role in MPs' function, organization and assembly [201]. Reconstitution of proteins into lipid membrane models (*e.g.* liposomes) is an essential tool in MP research [202-204]. Lipid constituents of liposomes can assist the self-association of subunits of oligomeric proteins within the bilayer (also addressed as the chaperoning effect) [197, 204]. For reviews of lipid-protein interactions, see refs. [205] and [206].

In order to address the first goal of the thesis (analyse the functional structure of UCP2 in the membrane) , recombinantly produced UCP2 was reconstituted into vesicles composed of egg yolk lipid extract, which mainly contains PC and PE, the most abundant lipids in mitochondrial membranes [130]. Self-association of UCP2 was also investigated in the absence and presence of cardiolipin to evaluate the impact of lipid composition and specific lipid interactions on oligomerization of UCP2. UCP2 conformation, self-association and proton transport were investigated by CD spectroscopy, gel electrophoresis, western blotting and fluorescence ion transport assays. Moreover, conformation and self-association behavior of UCP2 in lipid membranes was compared to those of the structurally analogous bovine mitochondrial AAC1,

(PDB ID: 1OKC), under similar experimental conditions [60, 70, 207]. To further investigate the self-association of UCP2 in lipid membranes, atomistic MD simulations were performed.

3.2 Material and methods

3.2.1 Chemicals

L-α-Phosphatidylcholine type X-E (L-α-PC) was from Sigma-Aldrich (St. Louis, Missouri). This mixed lipid system was extracted from dry egg yolk and contained more than 60% (by weight) PC; the remaining lipids were mostly phosphatidylethanolamine and other phospholipids. C_8E_4 was from Bachem (Bubendorf, Switzerland). OG was obtained from BioVision (San Francisco, California). SPQ was from Biotium (Fremont, California). Other chemicals were from Sigma-Aldrich.

3.2.2 Overexpression and membrane extraction of proteins

The cDNAs encoding UCP2 and AAC were cloned into the pET26b(+) expression vector [68], and recombinant versions of UCP2 and AAC1 (UniProt Accession Codes UCP2 – P55851 and AAC1 – P02722, with poly-histidine affinity tags at their N-terminal) were expressed in *E. coli* BL21 (DE3)-RIL (codon plus) and BL21 (DE3) cells using the auto-induction method as previously described [68, 208]. Briefly, the bacterial cells were incubated for 22 hours in the auto-induction media [0.5% yeast extract, 0.5% glycerol, 1% tryptone, 0.2% lactose, 0.05% glucose, 50 mM KH_2PO_4, 50mM Na_2HPO_4, 1mM $MgSO_4$, 25 mM $(NH_4)_2SO_4$] at 22 °C. After 22 hours, the culture was centrifuged at 8000 g for 15 minutes and the bacterial cells were collected in the pellet. The pellets were resuspended in lysis buffer [500 mM NaCl, 20 mM Tris-HCl pH 8.0, one EDTA-free complete protease inhibitor tablet (Roche, Basel, Switzerland), 0.5 mg/ml DNase and 0.2 mg/ml lysozyme]. A high-pressure cell disruptor (Constant Systems Limited, Daventry, UK) was used to lyse the cells (at 20 kPsi). The lysate was centrifuged for 20 minutes at 20000 g to remove

intact cells or aggregated proteins. The supernatant was collected and ultracentrifuged at 50000 g (MLA 80 rotor, Beckman Coulter) for 1 hour to obtain the bacterial membranes in the pellet. NADH oxidase activity assay was used to confirm that the fraction was enriched in bacterial membranes [68]. In this assay the membrane-embedded enzyme NADH catalytic activity is assessed based on its ability to convert NADH from its reduced to oxidized forms, as explained previously [68].

3.2.3 Purification of proteins using immobilized metal affinity chromatography

Binding buffer containing 20 mM Tris-HCl, 1 mM THP [Tris (hydroxypropyl) phosphine], 500 mM NaCl, 1% LDAO detergent and 10 mM imidazole was used to solubilize the bacterial membrane. The solution was then incubated with nickel-nitrilotriacetic acid (Ni-NTA, Thermo Scientific Waltham, Massachusetts) resin for 2 hours and subsequently transferred to a column. Detergent exchange (from 1% LDAO to 1% OG) was performed on the column at the washing step. In the case of UCP2 the resin in the column was washed with buffer containing 12 mM imidazole and successively eluted with buffers containing 25, 40 and 400 mM of imidazole in 1% OG detergent. The mixture of monomers and associated molecular forms of proteins were eluted at 40 mM imidazole and the pure monomer was eluted at 25 mM of imidazole. For AAC1, the column was washed with 30 mM imidazole and eluted with 400 mM imidazole in 1% OG detergent. Econo-Pac 10DG Columns (Bio-Rad, Hercules, California) were used to desalt the fractions in desalting buffer (20 mM Tris-HCl, 1% OG, 1% glycerol, pH 8.0). Purity and concentration of proteins were analyzed with semi-native PAGE (polyacrylamide gel electrophoresis) and modified Lowry assay [209], respectively. The desalted proteins were stored in desalting buffer at –80 °C.

3.2.4 Semi-native PAGE analysis

To analyze proteins using semi-native PAGE [68], SDS was excluded from the sample buffer, and its concentration was considerably reduced in the gel and running buffer as compared to SDS-PAGE conditions ([SDS] in the running buffer = 2 mM in semi-native *vs.* 35 mM in denaturing conditions). Moreover, samples were not heated before loading on the gel. The gels were run at 120 volts, stained with 0.2% w/v solution of Coomassie Brilliant Blue R-250 in acetic acid, methanol and water (10:45:45 by volume) for 2 hours and destained overnight.

3.2.5 Western blot analysis

The identity of overexpressed recombinant wild-type UCP2 and AAC1 were confirmed by immunoblotting. Proteins (5-10 μg) were loaded on semi-native PAGE gels, and using the semi-dry technique, the proteins were transferred (75 minutes -110 volts) to nitrocellulose. The filters were stained with Amido Black to confirm transfer efficiency [210]. The nitrocellulose filters were blocked for at least 60 minutes in Tris buffered saline containing 0.1% tween-20 and 5% dry skim milk. The primary antibody used to detect UCP2 was 1:2000 dilution of anti-UCP1/2/3 raised in rabbit (Santa Cruz Biotechnology Inc. Dallas, Texas), and for AAC1 the primary antibody was 1:5000 dilution of rabbit IgG anti-AAC1 (Bio-Rad). The secondary antibody was 1:5000 dilution of horseradish peroxidase (HRP) conjugated antibody raised in a goat against rabbit IgG (Rockland, Limerick, Pennsylvania). Luminata Crescendo Western HRP substrate (Millipore Sigma) was used as a chemiluminescent reagent to achieve immunodetection. A Bio-Rad VersaDoc imaging system was employed to capture the images.

3.2.6 Reconstitution in lipid vesicles

Reconstitution of UCP2 and AAC1 into lipid vesicles followed a previously described procedure [30, 80], with minor modifications. Briefly, solutions of egg yolk PC in MeOH:

chloroform (1:3) were dried for 8–12 hours under vacuum. The dried lipids were solubilized in an appropriate reconstitution buffer (supplemented with 3 mM SPQ fluorescent probe in proton transport assays) to generate multilamellar vesicles which were consequently solubilized in C_8E_4 detergent to form lipid-detergent mixed micelles [at a lipid/detergent ratio of 1/2.5 (w/w)]. Pure proteins were added to the mixed micelles to reach the final 3 μM concentration. Protein/lipid ratio was ~1/6000 (mol/mol) for proton transport assays and ~1/600 (mol/mol) for CD experiments. Unilamellar proteoliposomes were spontaneously generated by removing the detergent using SM-2 Biobeads (Bio-Rad). The average radii of the prepared proteoliposomes for the proton transport assays and CD measurements were 76.87±2.29 nm and 31.46±1.68 nm, respectively, as determined by dynamic light scattering. On average, the radii of the blank liposomes were ~13% larger than the proteoliposomes in both cases. In proton transport assays, part of the added SPQ was entrapped inside the liposomes and the external SPQ was removed by size-exclusion chromatography, using a Sephadex G25-300 (GE-Healthcare, Chicago, Illinois) spin column. Blank (protein-free) liposomes were prepared simultaneously in parallel with proteoliposomes.

3.2.7 CD spectroscopy and fluorescence measurements

Far-UV CD measurements were performed at 25 °C, at 1 nm resolution, on an AVIV 215 spectropolarimeter (Aviv Biomedical, Lakewood, New Jersey). Quartz cells with 0.1 cm path length were used for measuring the CD spectra in OG detergent and in liposomes. Ellipticities were converted to mean residue ellipticity, [θ]. Each spectrum was an average of 6–12 measurements.

Steady-state fluorescence measurements of the liposomes were performed using a Cary Eclipse spectrophotometer (Varian, Palo Alto, California) with a band width slit of 5 nm and a scan speed of 600 nm/min. Excitation and emission of the SPQ fluorescence signal were at 347

and 442 nm, respectively. The fluorescence scans were performed at 25 °C. Each proton transport analysis was an average of 10 independent measurements.

3.2.8 Proton transport measurements

Proton transport rates were measured following reconstitution in lipid vesicles, as described previously [80]. Anions quench SPQ by a dynamic collision mechanism. In proton transport assays, 40 μL of liposomes were mixed with 1.96 mL of external buffer. The internal buffer was composed of TEA_2SO_4 (TEA: tetraethylammonium, 54 mM), TES buffer (20 mM) and EDTA (0.7 mM). The external buffer had a similar composition to the internal buffer, with TEA_2SO_4 replaced by K_2SO_4 (54 mM). The pH of both buffers was kept constant at 7.2. Palmitic acid (as palmitate) [PA, [PA]=100 μM] was used to activate the UCP2-mediated proton flux. The addition of valinomycin mediated the influx of K^+ which triggered fatty acid dependent proton efflux of UCP2. Proton efflux by UCP2 resulted in deprotonation of the TES buffer. TES^- anions quenched the SPQ emission. The rate of decrease in the SPQ fluorescence signal was correlated to the rate of fatty acid activated proton transport of UCP2. The latter was measured by monitoring the decrease in SPQ's fluorescence signal intensity within the first 30 seconds after addition of valinomycin [68]. All proton transport data in liposomes were corrected for the basal non-specific leakage by subtraction of blank liposomes proton efflux. Furthermore, the proton transport data were calibrated for internal volume, SPQ's fluorescence response and protein concentration. The concentration of protein in proteoliposomes was calculated using a modified Lowry assay [80, 209], No significant proton transport/leakage has been observed for the proteoliposomes in the absence of valinomycin. The inhibitory role of ATP on proton transport rates of reconstituted UCP2 was assessed by incubating the proteoliposomes with 500 μM ATP for 2 minutes prior for measurements.

3.2.9 MD simulations

The NMR structure of UCP2 (PDB ID: 2LCK) [70] was used as the starting structure for the monomeric UCP2. The same structure was used to build the dimeric and tetrameric forms. To form multimeric UCP2, the monomer units were aligned in such a way that the *GXXXG* [127], *GXXXAXXG* [211], and *SmXXXSm* (*Sm* = Gly, Ala, Ser, Thr) [124, 212] motifs were involved in the interactions with the neighboring unit(s) (Figure A-3-1); these motifs have been proposed to promote helix-helix interaction.[48] Moreover, in the case of dimer, several relative orientations for the monomers were examined. From these, the parallel orientation with maximal (distance-based) favorable interactions (electrostatic and hydrophobic) was chosen for the simulations. The tetramer was then built analogously from two dimers. The X-ray structure (PDB ID: 1OKC) was adopted as the initial AAC1 structure.

The protein-membrane systems were built using CHARMM-GUI [213] Membranes were built with 300, 316, and 498 1-palmitoyl-2-oleoylphosphatidylcholine (POPC) lipids for the monomeric, dimeric, and tetrameric UCP2, respectively. In the case of AAC1, 160 and 200 POPC lipids were used for monomeric and dimeric forms, respectively. POPC was chosen to model the membranes, since PC is the main constituent of IMM [131, 214].

Each system was solvated in an explicit TIP3P water [215] box (total of 24195, 28463, and 47881 water molecules for monomer, dimer, and tetramer, respectively. For AAC1 systems the numbers are 9806 and 13555) and 0.15 M KCl (65, 78, and 134 K^+, and 80, 108, and 194 Cl^- for the monomer, dimer, and tetramer, respectively. For AAC1, 25 and 36 K^+, and 42 and 70 Cl^- for the monomer and dimer, respectively). Overall charge neutrality was always maintained. CHARMM36m/CHARMM36 protein/lipid force fields were used [216, 217]. All systems were first energy minimized using the steepest descents algorithm followed by 500 ps of pre-

equilibration under constant volume and temperature (NVT), and constant pressure and temperature (NPT) conditions. MD simulations were conducted for 350 ns with 2 ps time steps using GROMACS/2018 [218]. Chemical bonds were constrained using the linear constraint solver (P-LINCS) algorithm [219]. The Nosé-Hoover thermostat [220, 221] was employed to maintain the temperature at 300 K with a 1.0 ps coupling constant and the Parrinello–Rahman barostat [222] with a compressibility of 4.5×10^{-5} bar^{-1} and a 5 ps coupling constant was used. The particle mesh Ewald method [223, 224] was used for the long-range interactions. The above protocol and methods have been shown to be reliable in a number of previous studies (e.g., Refs. [225-227] and references therein).

We tested the force field dependence by studying the protein structure in POPC bilayers employing CHARMM36m, CHARMM36 and CHARMM27 force fields neutralized by either Cl^- ions or KCl salt in the absence and presence of GDP^{3-}. MD simulations were carried out for 100 ns for a total of 12 additional individual systems. The robustness of the results was further examined by additional simulations using different initial conditions.

To study the dissociation process of the multimers, umbrella sampling [228] was conducted on the final structures obtained from the 150 ns MD simulations. Selected windows of 0.1 nm along the pulling trajectories were first equilibrated for 100 ps and production runs were carried out for 5 ns. Theses trajectories are short since the aim was not to determine the absolute free energy curve, but rather to have an estimate for the binding energies. Protein subunits were pulled from their centers of masses until the subunits were separated by at least one layer of POPC. The weighted histogram analysis method (WHAM) was used for the analysis [229]. Potential of mean force was monitored to confirm the end of the process. The bootstrap technique was used to estimate the statistical errors [230].

3.3 Results

3.3.1 Expression and purification of UCP2 and AAC1

Cloning the cDNAs of UCP2 and AAC1 into pET26b(+) resulted in the pelB signal peptide being added to the N-termini of the proteins, which targets the proteins to the *E. coli* inner membrane [68], followed by His-tag. The pelB signal peptide normally directs secreted proteins to the periplasmic space. The TM segments of UCP2 and AAC1, however, prevent full translocation and lead to insertion into the membrane due to hydrophobic interactions with the bacterial membrane [30, 68]. Expression of proteins in bacterial membranes allows the protein and its surrounding tightly attached membrane lipids to be extracted with mild detergents and co-purified with protein. These co-purified membrane lipids can shield the protein from potential denaturing interactions with the solubilizing detergent, and thus help UCP2 to remain relatively intact/folded. The His-tagged proteins were purified on nickel-containing columns. Purity was confirmed by semi-native PAGE (Figure 3-1). Bands of approximately 33, 66 and 132 kDa were observed for UCP2 on polyacrylamide semi-native gels. Furthermore, Western blot analysis using an α-UCP1,2,3 antibody reacted with all three bands (Figure 3-1), suggesting that they correlate as monomeric, dimeric and tetrameric forms of UCP2, respectively - as has been observed previously [30, 68]. Under similar conditions, only monomeric and dimeric forms were detected for AAC1 (Figures 3-1 and A-3-2).

3.3.2 Semi-native PAGE analysis of UCP2 and AAC1 before and after reconstitution

As shown in Figure 3-1, UCP2 existed as a mix of monomeric, dimeric and tetrameric forms when purified in the presence of OG detergent. OG was chosen on the basis of conformational and thermal stability analysis of UCP1 in different detergents [such as OG, DDM (*n*-dodecyl-β-D-maltopyranoside) and LDAO] [68]. Overall structural integrity of the protein was most stable when

purified and stored in OG micelles [68]. Once reconstituted in lipid vesicles from detergents, the electrophoretic analysis showed that only tetrameric forms of UCP2 are present in liposomes (lanes 3 and 5 in Figure 3-1). Interestingly, the electrophoretic analysis showed that regardless of the lipid composition and presence/absence of cardiolipin, only tetrameric forms of the reconstituted UCP2 are present in liposomes.

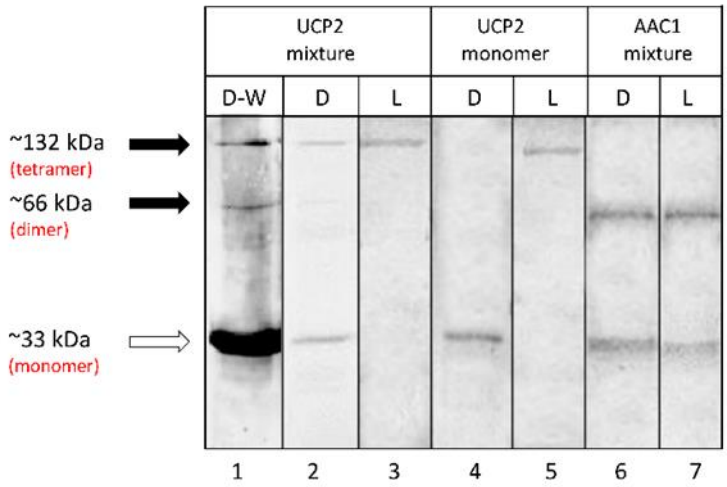

Figure 3-1 Semi-native PAGE analysis of purified UCP2 and AAC1 in OG detergent (D) and in liposome (L) detected by Coomassie blue staining (lanes 2-7) and Western blot (W) (lane 1) methods. Mixture and monomer terms displayed at the top refer to the protein sample that was used for reconstitution. The solid arrows show the locations of oligomers and the open arrow shows the monomers. Western blot detection of UCP2 in OG detergent was probed with an α-UCP 1, 2, 3 antibody. Collectively, the data confirm the presence of tetrameric UCP2 and the absence of tetrameric AAC1 in lipid vesicles. The protein/lipid molar ratio in lanes 3 and 5 was 1/6000.

To further investigate the spontaneous oligomerization of UCP2 in lipid membranes, the protein was isolated from *E. coli* membranes in its monomeric form in the OG detergent and reconstituted in liposomes. The electrophoretic analysis results show that reconstituted UCP2 monomers also spontaneously self-associate into tetramers (lanes 4 and 5 in Figure 3-1). To test the reliability of the reconstitution process and the possibility of tetramerization of other MCF proteins, a purified mix of AAC1 monomers and dimers were reconstituted into liposomes under comparable experimental conditions. The carrier protein AAC1, with structural similarities to

UCP2, did not form tetrameric complexes in lipids; instead, it maintained its original mix of monomeric and dimeric forms (lanes 6 and 7 in Figure 3-1).

Other evidence for spontaneous self-association of UCP2 into homo-tetramers in liposomes comes from its proton transport function (Figure 3-2). Both reconstituted forms of UCP2 resulted in similar ion transport profiles (Figure 3-2, right). This observation confirms the functional equivalence of reconstituted proteins from different preparations (monomeric *vs.* mixed monomeric/multimeric). The proton transport rates of tetrameric UCP2 from reconstituted monomeric and mixed species in liposomes were comparable: 5.16±0.03 and 5.24±0.09 μmol/min/mg of protein, respectively.

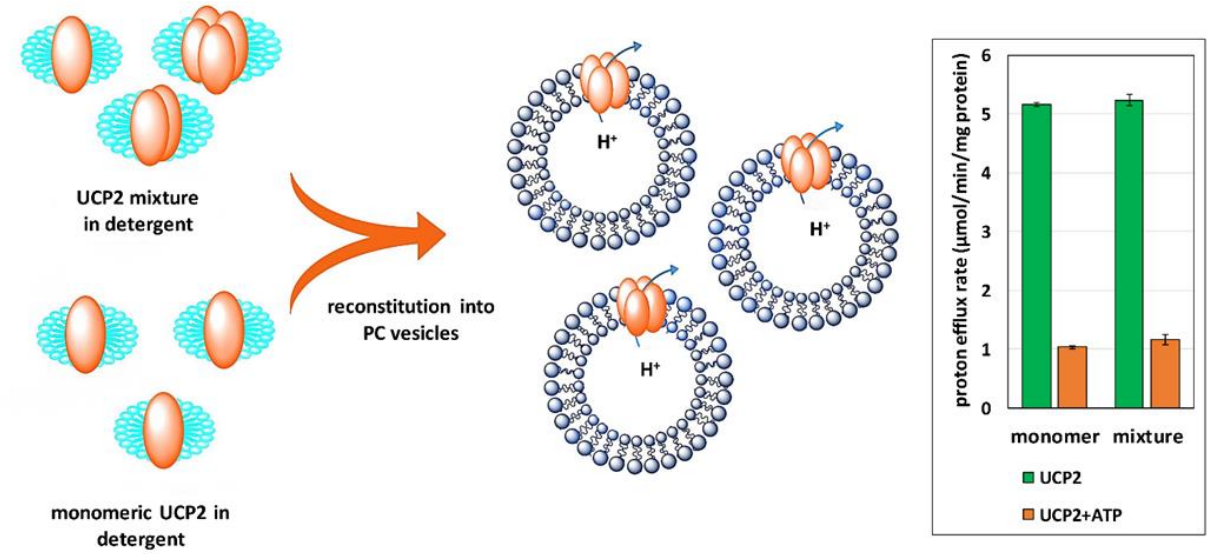

Figure 3-2 Formation of functional UCP2 tetramer after reconstitution in vesicles. Regardless of its molecular composition in detergent (monomeric or mixed monomeric/multimeric, before reconstitution), UCP2 adopts a tetrameric form in lipid vesicles. The bar graph on the right, shows the comparable rate of proton efflux for UCP2 in proteoliposomes generated either from monomeric or mixed molecular species. Each bar represents the average transport rate of 10 repeats and the error bars show the standard deviations. Figure generated by ChemBioDraw Ultra 14.0

The proton transport function of the tetrameric proteins was further examined in the presence of a common inhibitor (ATP, 500 μM). Results showed that, in both cases, the rate of proton

transport was ~80% less compared to that of uninhibited proteins (1.03±0.02 and 1.17±0.09 for UCP2 tetramers from reconstituted monomeric and mixed proteins, respectively). These results also exclude the possibility of non-specific proteoliposome leakage. The observed proton transport and inhibition rates are comparable with previous independent studies [30, 71, 231].

3.3.3 CD spectroscopic conformational analyses of UCP2 and AAC1

Conformations of UCP2 and AAC1 in OG and liposomes were characterized and compared by CD spectroscopy (Figure 3-3). The CD spectra of both proteins exhibited helical backbone structures with a characteristic double negative maxima at 208 nm and 222 nm, as well as a positive maximum around 193 nm (not shown), corresponding to $\pi \rightarrow \pi^*$ (193 and 208 nm) and $n \rightarrow \pi^*$ (222 nm) transitions of the peptide bond [232].

In UCP2, the far-UV CD signal was notably enhanced after reconstitution in liposomes, indicating a higher helicity compared to that of protein in OG detergent (Figure 3-3, A). This marked conformational change, reflected as enhancement of negative ellipticity and reversal of the relative intensity of minima ($\theta_{208}/\theta_{222}$), reveals the essential role of the lipid environment in folding and structural stabilization of UCP2. In addition to their difference in signal intensity, the shape of the CD spectrum of UCP2 in proteoliposomes differed from that of the monomer (and the mixed monomer/multimer) in OG. Particularly, in lipid vesicles, a shoulder-like $\pi \rightarrow \pi^*$ parallel transition band around 208 nm replaced the minimum band in OG, and also a considerably more intense $n \rightarrow \pi^*$ transition band appeared at 222 nm. The $\theta_{208}/\theta_{222}$ ellipticity ratio of UCP2 monomer spectrum changed from 1.07 to 0.68 after reconstitution in liposomes (Figure 3-3, A). The $\theta_{208}/\theta_{222}$ ellipticity ratios lower than one has been previously reported for human UCPs' helical bundle motifs and their self-associated oligomers [30]. Relative decrease in molar ellipticity at 208 nm (in comparison to ellipticity at 222 nm) and its red shift, due to intramolecular interactions between

TM helical motifs and intermolecular protein association, have also been reported for UCP1 and other MPs [68, 233-235]. The CD spectra (Figure 3-3, A) related to the tetrameric form of UCP2 is in good agreement with our previously reported studies [30, 68]. CD spectra of the mixed molecular forms of UCP2 (monomer, dimer and tetramer) and AAC1 (monomer and dimer) in OG detergent exhibited comparable helical conformations (Figure 3-3, B), as expected based on the known structural similarities and co-presence of different monomeric and associated molecular forms in these proteins.

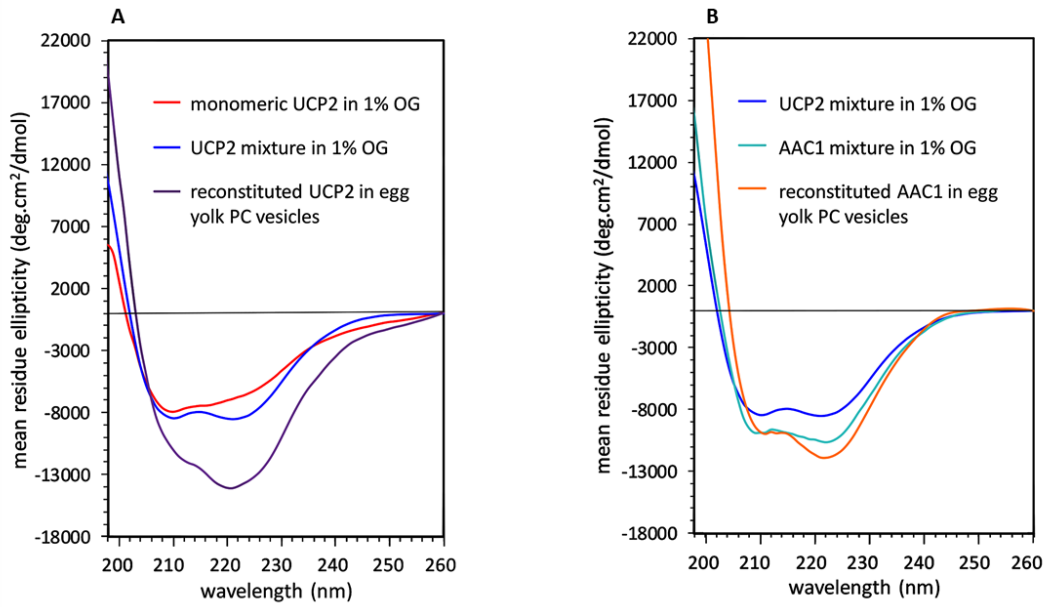

Figure 3-3 CD spectra of purified UCP2 and AAC1 before (in OG detergent) and after reconstitution in liposomes at 25 °C. A) Tetramer formation of UCP2 in liposomes, regardless of its original molecular composition in detergent, resulted in a drastic change in CD spectrum. B) Comparable CD spectra of AAC1 before and after reconstitution implies a comparable molecular composition of the protein in liposome vs. detergent. Concentrations of proteins were 5 – 8 μM in OG and ~ 1 μM in lipid vesicles. Each spectrum is an average of 6-12 measurements.

Compared with UCP2, the negative ellipticity for AAC1 in liposomes was less enhanced (Figure 3-3, B). The $\theta_{208}/\theta_{222}$ ellipticity ratio of AAC1 changed from 0.89 in OG detergent to 0.84 after reconstitution in liposomes, which is consistent with the protein maintaining similar

conformations in these environments (mix of monomeric and dimeric forms) (Figure 3-3, B). The differences between the CD spectra of reconstituted UCP2 and AAC1 show that the two proteins acquire different molecular forms after reconstitution in vesicles. In liposomes, both the lower negative ellipticity and higher $\theta_{208}/\theta_{222}$ ellipticity ratio of AAC1 compared to UCP2 (0.84 *vs.* 0.68) are consistent with a lower degree of association in AAC1. In summary, our experimental results show that UCP2 and AAC1 behaved differently in liposomes. UCP2 associated into a functional tetramer, while AAC1 did not form tetramers in liposomes.

3.3.4 MD simulations

3.3.4.1 Protein Properties

It is well established that interactions of TM helices within lipid bilayers have crucial roles in folding [236], stability [237-239], and function [240] of MPs. All-atom MD simulations were conducted on monomeric, dimeric and tetrameric UCP2 in POPC model bilayers, and monomeric and dimeric AAC1. PC is one of the main constituents of the mammalian IMM (~40%) [130, 214]. CL is another important component of IMM (~18%); however, our experimental results indicated that the presence or absence of cardiolipin in the membrane did not affect the oligomerization of UCP2, Accordingly, and in order to keep the systems simple and comparable to other studies [241], we did not include this lipid in our model bilayers. Average root-mean-square-deviations (RMSDs), radius of gyration (R_g), principal component analysis (PCA), solvent accessible surface area per chain (SASA), and pore radius and free radius were determined. Moreover, umbrella sampling simulations were carried out to examine the stability of the multimeric forms of UCP2 and to provide further insights into the protein's subunit interactions and oligomerization process.

The general structural features of the protein were always preserved in all three UCP2 systems through intensive interactions with the phospholipid bilayer. This was the case

independent of the force field and reproducible in repeated simulations with different initial conditions. Figure 3-4 compares the initial and final (350 ns) structures of monomeric UCP2 and shows the final arrangement of the dimeric and tetrameric forms. RMSD is a measure of flexibility of the structure and indicates the deviation of atomic positions from the initial structure. RMSD of the protein backbone over the course of simulations (Figure A-3-3) indicates that in POPC bilayers, all three forms had reached a steady-state or equilibrium and were stable. The tetrameric UCP2 showed the smallest fluctuations in RMSD, suggesting it to be more stable than the other two forms. AAC1 structures are provided in Figure A-3-4 and as suggested by the backbone RMSD, both monomeric and dimeric forms remained stable in the phospholipid bilayer (Figure A-3-3).

Figure 3-4 shows that over the simulation time, both dimeric and tetrameric UCP2 adopted asymmetric conformations, that is, the deviations from the initial structure were not similar among their constituting subunits. The differences between the monomeric and oligomeric forms of the protein arise from the changes in the local environment of the monomeric UCP2 upon association, altering the modes of protein-environment interactions and protein motions in the lipid bilayer. The effect of environment on protein motion was further explored with PCA of the proteins (Figure A-3-5 and A-3-6). PCA analyses indicated greater motions in the TM helices for the multimeric UCP2 in comparison to the monomeric protein during the simulation. As seen in Figure A-3-6, certain parts of the subunits of dimer and tetramer moved in different manners resulting in an overall contraction of the protein. This contraction was especially observable in the tetramer. It is likely to arise from its structure as a dimer of dimers as will be discussed below in connection with salt-bridges. R_g is a measure of compactness of the structure and SASA is the surface area of the protein that is exposed to the solvent. While R_g remains relatively similar for the two AAC1 forms, SASA for the dimeric form decreases compared to that of the monomeric AAC1.

In agreement with a previous MD study of monomeric UCP2 [64], the SASA of all three molecular forms of UCP2 (Figure A-3-3) were reduced in the lipid bilayer compared to the initial structure (monomeric) in detergent micelles. Variation of protein SASA in different environments is common and has been reported for a number of proteins [242-244]. As seen in Figure A-3-3, the SASA of UCP2 monomer and dimer are very similar and the changes are only considerable upon dimerization of UCP2 dimers (tetramerization of subunits). SASA of the tetramer was not only the smallest among the considered UCP2 forms, but also closely resembles that of AAC1 with widely accepted structure and transport features (discussed later).

The loops on both matrix and cytoplasmic sides of the protein were able to move more freely throughout the simulation and might form transient hydrogen bonds with one another and solvent, keeping the multimeric structures intact and protecting the transport controller gates on matrix or intermembrane side of the protein. These gates are salt-bridge networks that are proposed to regulate the transport in MCF carriers with consecutive opening and closures [51].

Dimeric and tetrameric UCP2 were subjected to umbrella sampling simulations to evaluate the energy of dissociation of the dimer to monomers, and the tetramer to dimers (Table A-3-1 and Figure A-3-7). Smaller dissociation energy of the tetramer into two dimers (60.2 kcal/mol) compared to the dissociation energy of the dimer (78.7 kcal/mol) is consistent with our previous experimental reports on UCP [30, 68], which suggests that the tetrameric complex of UCPs is in fact a dimer of dimers (see Discussion section).

In the UCP2 dimer, stabilizing salt-bridges between the monomeric subunits (chains 1 and 2) of the dimer (K109···D202, E112···K206 and K164···E46) were observed. Interestingly, in the tetramer contacts between chains 1 and 2 (K109···D202 and K164···E264) and chains 3 and 4 (K104···D202 and K164···E264) within the tetramer were present (Table A-3-1 and Figure A-3-8).

Importantly, no salt-bridges were formed between the two dimers. This is also consistent with UCP2 tetramer being a dimer of dimers.

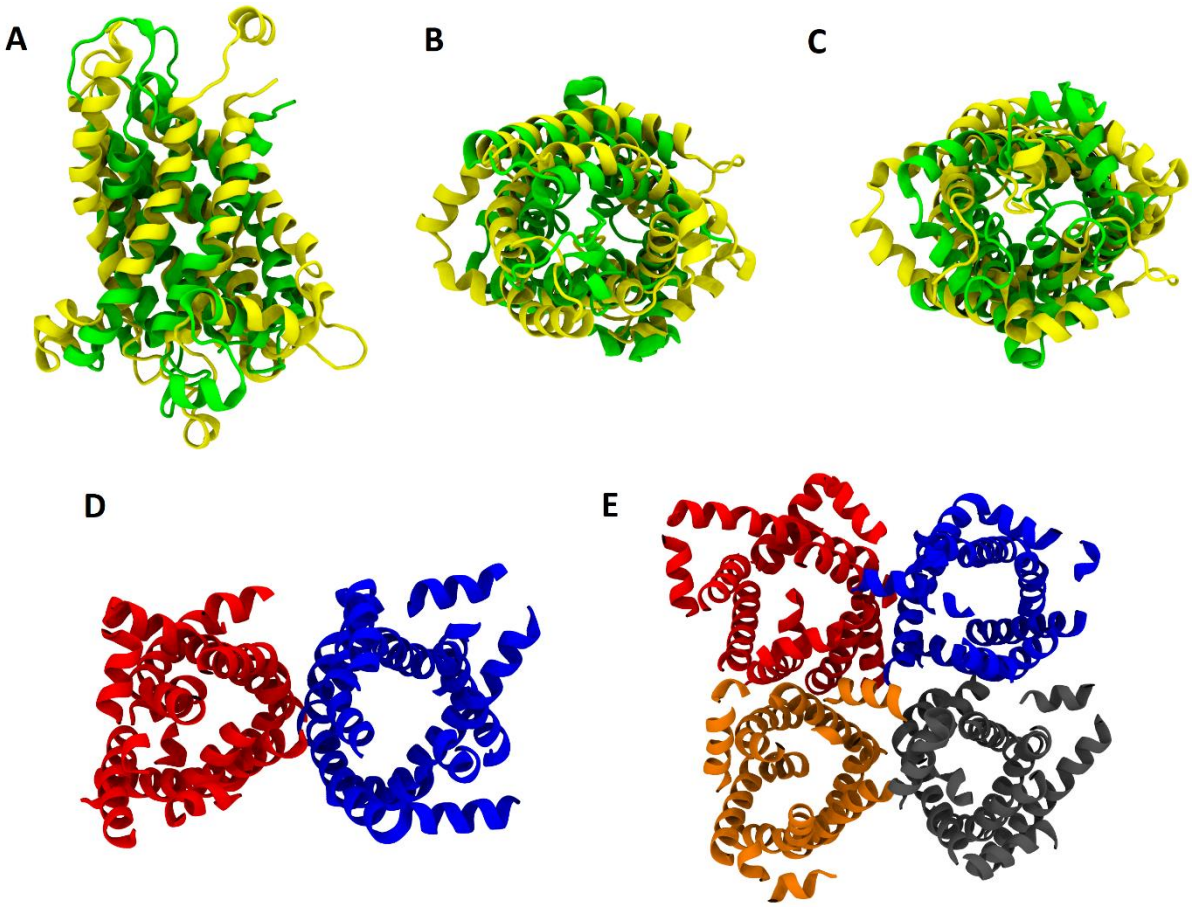

Figure 3-4 Overlay of the UCP2 monomer (A-C) initial (PDB ID: 2LCK, yellow) and final (350 ns, green) structures. (D) final dimer and (E) tetramer structures. An overall shrinkage is observed upon insertion of the protein into the POPC bilayer. The monomeric subunits within the dimeric and tetrameric structures are not identical, leading to asymmetric protein oligomers. Figure generated by VMD 1.9.3.

UCPs are transporters and the existence of pores across the individual monomers were determined using MoleOnline software [245]. The results were also compared to those calculated with CAVER [246] and found to be consistent. Two different pore radii were determined, 1) the free radius that uses the closest three protein backbone atoms and 2) simple radius which uses all the atoms of an instantaneous configuration. The free radius is a more realistic measure and was

used in data analysis. Comparison between the initial and final free radii of UCP2 structures in Figure 3-5, A shows that in the monomeric form it shrinks on the matrix side. The free radii of the dimer's subunits do not change significantly and are comparable to that of the initial monomer. In the tetramer, free radii of two of the subunits markedly reduce on the matrix side, while the other two have smaller free radii on the cytoplasmic side. Free radius analysis of AAC1 indicates a large change on the matrix side for both monomeric and dimeric forms compared to the initial structure, Figure 3-5, B.

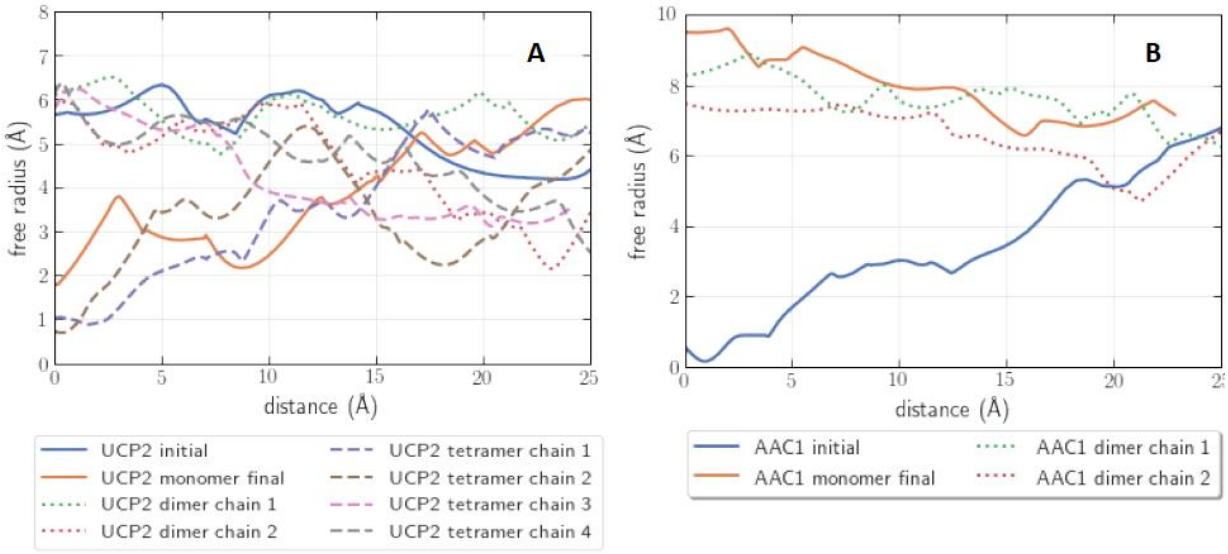

Figure 3-5 Protein pore free radius for initial and final structures of UCP2 (A) and AAC1 (B). For all UCP2 and AAC1 forms the free radius changes quite drastically from its initial structure. Distance of zero is on the matrix side. Free radius is measured by fitting spheres within the channel limited by the three closest main chain atoms.

We compared our free radii of the monomeric forms to the effective radii reported by Zoonens *et al*. [64] While they only report UCP2-GDP^{3-} system shrinking on the cytoplasmic side in a POPC bilayer, our simulation shows a contraction on the matrix side (distance = 0 nm in Figure 3-5) for UCP2 in absence of the inhibitor (Figure 3-5). Moreover, in the case of AAC1, the pore radius opens up on the matrix side over the simulation and becomes slightly larger than the radius on the cytoplasmic side (Figure 3-5).

3.3.4.2 Membrane Properties

To evaluate the effects of the protein oligomerization on the membrane, several bilayer properties such as area per lipid (APL), APL distributions and lipid distribution s were examined. APL is a measure of membrane compactness. Higher density leads to a lower APL and thicker membranes. Figure 3-6, A shows the APL distribution and the average APL for the monomeric UCP2 system. As the figure shows, APL is smaller for the upper leaflet. The situation, however, reverses for both oligomeric forms (Figures 3-6, B-C). This data shows how multimerization of UCP2 has marked impacts on bilayer properties.

Figure 3-7 represents 2D averaged (over the last 50 ns) APL distribution in the two leaflets. The contours can be considered as the protein's lipid "fingerprint" [247], i.e., how the protein affects the packing of its neighboring lipids. While originally the fingerprint idea was used to determine what kind of a local lipid environment (in terms of lipid species) a protein recruits, here we have a single lipid species and use the fingerprint to characterize the local modulations the protein causes. The area with the deep blue color in the middle is where the protein(s) is (are) located. The plots show a strong asymmetry between the leaflets in all cases. Close to the protein, the deep red color and larger APL appears to indicate that lipids at the interface are very fluidic (since volume of a bilayer is usually considered to be roughly a constant). That, however, is not the case here. Instead, the interfacial lipids have very low mobility due to the strong interactions with the protein and their tails become distorted. This is what leads to the observed higher APL.

This is also reflected in local membrane height distribution along the z-axis, Figure 3-8. The areas of lower thickness correspond to larger APL close to the protein. As Figure 3-8 shows, the distribution is different for the two leaflets and the different protein oligomeric states. The distribution for the lower leaflet (matrix side) obtains a fat tail toward the membrane interior

(smaller thickness) and the average lipid z-position (shown with dashed lines) changes upon oligomerization. In the case of the tetramer, there is also a small but clear contribution from the membrane interior (i.e., few phospholipids that penetrated deeper, indicated by the arrow in Figure 3-8A). It was also observed that a few lipids insert their headgroup partially in one of the cavities on the tetramers' side. Upper leaflet (cytoplasmic side) lipid distributions of the monomeric and dimeric UCP2 systems are practically indistinguishable and have overlapping averages (the blue dashed line is behind the orange one). For the tetramer, the distribution curve becomes significantly broader and the average lipid position changes. The two leaflets show opposite behaviors: On the matrix side the z-positions move toward smaller values (center) and on the cytosol side toward larger (away from the center). Thus, tetramerization causes a relatively large impact on both leaflets with skewed distributions.

In the case of AAC1, there is only a negligible change in the lipid distribution on the matrix side upon dimerization (Figure A-3-9), while on the cytoplasmic side (upper leaflet) the average lipid position has moved toward the bilayer center. Overall, dimerization of AAC1 has only a small impact on the average lipid position on both leaflets.

3.4 Discussion

Several functions, including proton motive force attenuation and ROS regulation, have been proposed for UCP2 [183-185]. On the other hand, the only published atomic structure of any UCP is that of UCP2, using a semi-empirical fragment searching NMR analysis [70]. The functional molecular form of UCPs (in particular UCP1) in mitochondria has been a subject of debate, with some researchers proposing monomers [67] and others proposing oligomers as possible functional

forms [30, 66, 68], Molecular characterization of the functional structure(s) of UCPs is essential for understanding their mechanisms of physiological action.

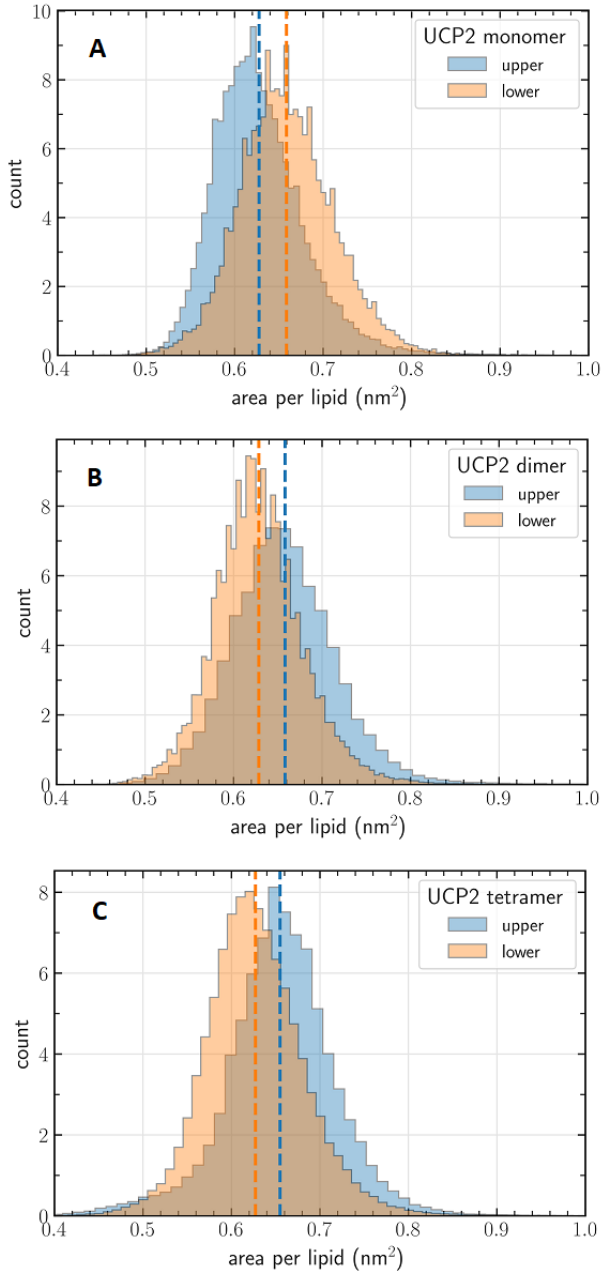

Figure 3-6 The APL distribution in upper and lower leaflets in the cases of (A) monomeric, (B) dimeric, and (C) tetrameric UCP2. Average values are shown with dashed lines. As is seen, there is clear change in the distribution in both leaflets upon oligomerization of UCP2.

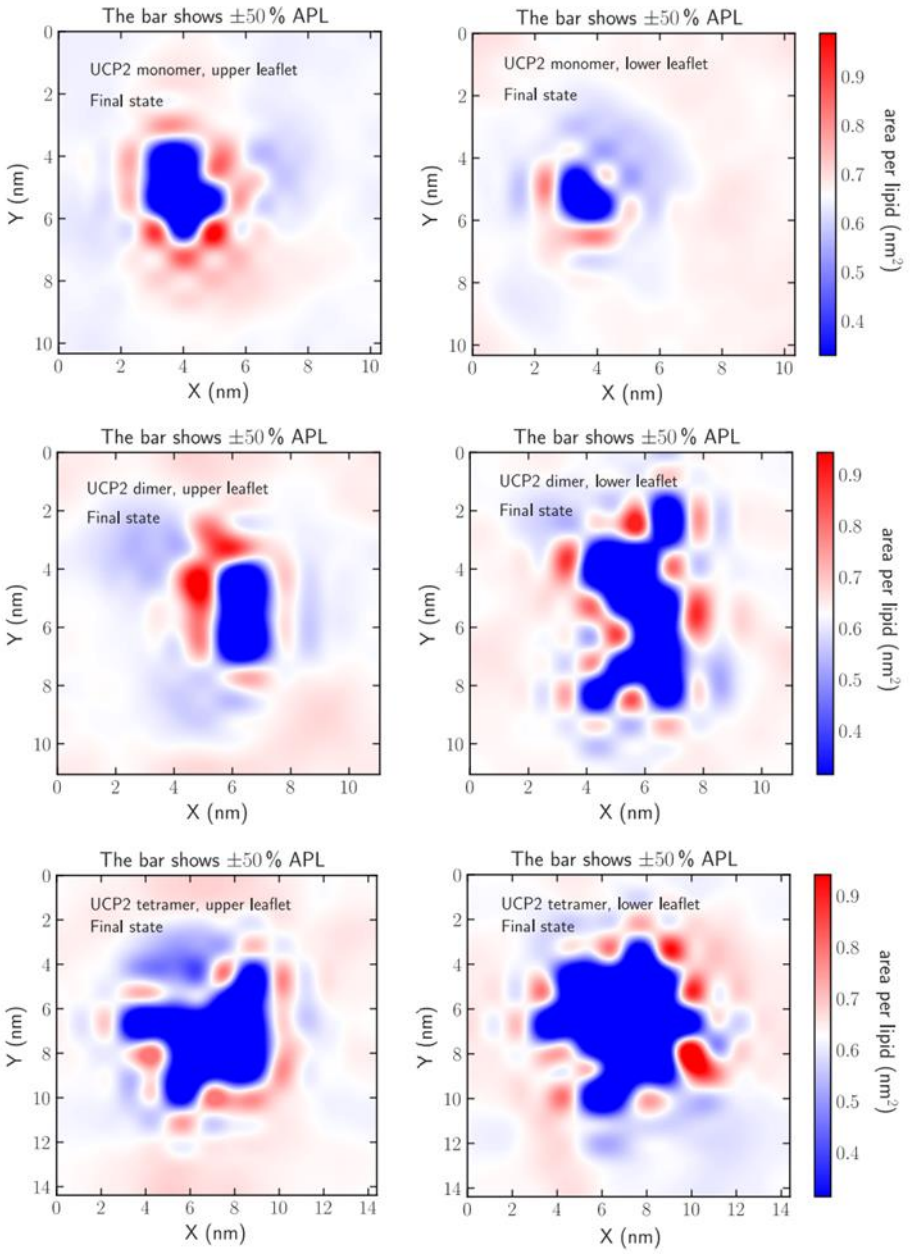

Figure 3-7 APL averaged over the last 50 ns of the simulations for the upper (left panel) and lower (right panel) leaflets for the monomeric, dimeric, and tetrameric UCP2. The color is adjusted such that the range gives 50% variation over the average (white color ~ 0.6 - 0.7 nm^2). Deep blue color represents the protein(s) location. Such contours can be considered as UCP2-lipid interaction "fingerprints"

In the current study, we have experimentally shown that UCP2 spontaneously self-associates to form tetramers (M_w ~132 kDa) in lipid membranes (Figure 3-1). This tetrameric UCP2 was shown to be capable of transporting protons (Figure 3-2), a general characteristic of all UCPs [30,

66, 68]. On the other hand, AAC1, a mitochondrial carrier protein with comparable three-dimensional structure to UCP2, does not form tetramers in lipid membranes. These observations indicate the specific tendency of UCP2 to form tetramers in phospholipid bilayers, which cannot be generalized to all MCF members. Association and stability of the tetrameric state are consistent with our previous studies of other UCPs [30, 68] using analytical ultracentrifugation and mass spectrometric methods. Importantly, the analysis of salt-bridges from our MD simulations also confirms the experimental results [30, 68] that the tetrameric UCP2 complex is in fact a dimer of dimers, in which the interactions between the monomers forming the dimer are stronger than the interactions between the dimers within the tetramer.

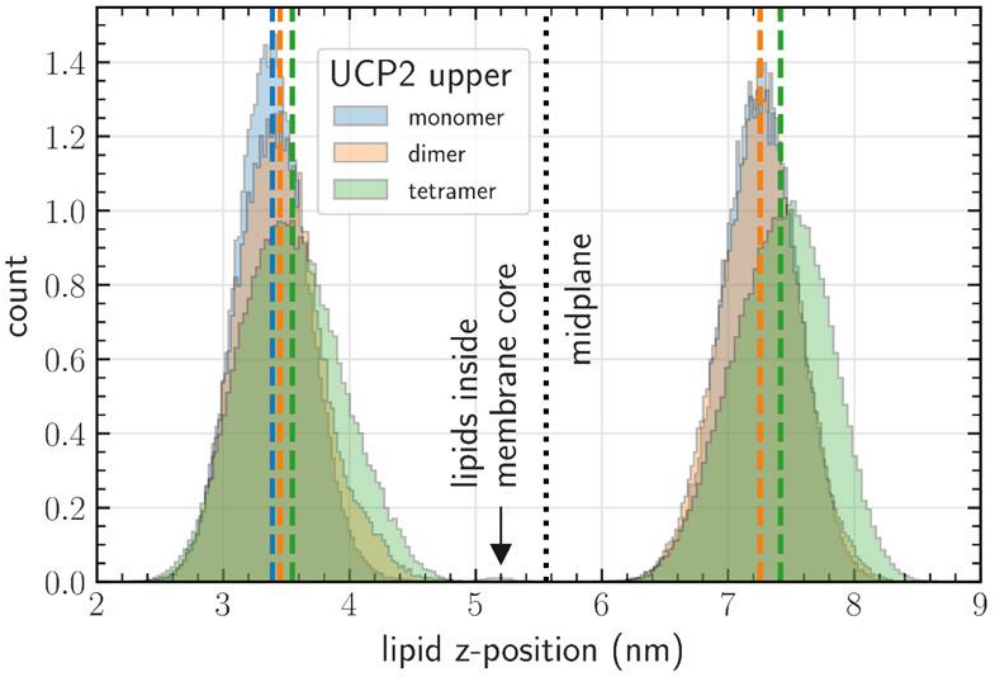

Figure 3-8 Distribution of the lipid head groups (phosphate was used as the marker) in lower (left; matrix side) and upper (right; cytoplasmic side) leaflets for all three UCP2 forms. The vertical dashed lines show the corresponding averages. The arrow shows a small but persistent contribution of lipid head groups located deep inside the membrane; some of the lipids in this band were found to be oriented perpendicular to the membrane surface. On the cytoplasmic side, the average values for the monomers and dimers overlap (the blue dashed line is behind the orange one). The distribution is different depending on the leaflet and oligomerization state of the protein.

In addition to the formation and stability of the tetrameric protein, the reversal of the ellipticity ratio ($\theta_{208}/\theta_{222}$) after reconstitution of the monomeric proteins (from OG detergent) into liposomes (Figure 3-3, A) implies both a more compact interhelical packing of monomers and a stronger intermolecular interactions between these monomers [30, 68]. The low rate of proton transport and its inhibition by common UCP inhibitors such as ATP also confirms that the tetrameric UCP2 is functional in lipid membranes and is more likely to be a transporter than a channel. This is also supported by the measurements of the free UCP2 monomer radius from the MD simulations.

The MD simulations of the tetramer in the lipid bilayer shows that despite the compaction of all constituting monomers over the course of simulation - comparable to changes in the ellipticity ratio mentioned in the previous paragraph - these subunits do not adopt similar structures and lateral orientations (Figure 3-4). Moreover, asymmetric conformations of monomeric units in the tetramer were also observed along the z-axis. Previous computational analyses of the members of MCF have proposed two structural states leading to transport of the substrates: 1) the matrix state with the protein cavity open to the matrix side and 2) cytoplasmic state with the cavity open to the IMS side [46]. It might be concluded from Figure 3-5, A (dashed lines) that every two monomers within the dimer are in the same state of transport and there is a phase difference between the two sets of dimers in a tetramer (two members of one dimer are in the matrix state while the two members of the other dimer are in the cytoplasmic state). The phase difference between the dimers within the tetramer and the asymmetric nature of the tetramer could provide a scaffold for regulating the activity of individual units, and also facilitate cooperative intercommunication between the subunits. Concomitantly, all individual monomeric subunits might not be active at the same time. Asymmetric oligomerization has also been reported for other

proteins such as tetrameric D-glyceraldehyde-3-phosphate dehydrogenase [248] and dimeric tryptophanyl-tRNA synthetase [249].

Detailed analysis of the MD data of the interactions stabilizing the dimeric and tetrameric UCP2 indicates that comparable salt-bridges are formed between the monomers within the dimer and between the monomers within the dimeric units constituting the tetramer (Table A-3-1). No salt-bridges were found between the two dimeric units of the tetramer. This finding renders direct support to our notion that tetrameric UCP2 is indeed a dimer of dimers (Figure A-3-8). This conclusion is further supported by the pulling simulations that showed higher dissociation energy of monomeric subunits of a dimer compared to dimeric subunits of a tetramer by 18.5 kcal/mol.

Further experiments are required to establish the roles of lipid species in the stability and ion transport function of UCPs; the role of lipids cannot be easily generalized as has been shown in the case ATP binding cassette proteins where results have shown both dependence and independence of lipid specificity depending on the systems and properties of interest [250-252]. The importance of non-specific protein-lipid interaction is also exhibited in the increased helicity of the protein in lipid bilayers (Figure 3-3, A). The role of bridging lipids in stabilizing the multimeric complexes of MPs has been shown for several proteins such as dimeric *Aquifex aeolicus* leucine transporter, dimeric *E. coli* NHE and tetrameric aquaporin (aqpZ) [114]. Finally, the scope of *in vitro* studies is always limited by the use of detergents in MPs purification and reconstitution steps, and by not being able to mimic the exact dynamics of the IMM lipid/protein membranes. These limitations can lead to deviations from the structure and function of proteins in living cells, and the real-time *in vivo* analysis of IMM, considering the complexities involved, is still to be anticipated.

3.5 Conclusions

Detailed structural and ion transport studies and atomistic MD simulations have been utilized to investigate UCP2 oligomerization in lipid membranes. The findings suggest a simultaneous co-existence of functional monomeric, dimeric and tetrameric forms of the protein, under various conditions and different membrane lipid compositions. Our experimental data and salt-bridge analysis from MD data shows that UCP2 tetramers are dimers of dimers. In addition, MD simulations suggest that UCP2 tetramers are asymmetrical, and that there is a phase difference between the two sets of dimers in a tetramer. The full implications to proton (or other substrate) transport are currently not known, but it can be hypothesized that this asymmetry, which also influences the membrane structure, may help to regulate the protein's activity and communication between the individual monomers.

CHAPTER 4 - ON THE MECHANISM OF PROTON TRANSPORT IN UNCOUPLING PROTEIN 2

4.1 Introduction

Inducible proton leak across the IMM is accomplished by UCPs [22]. UCPs belong to the largest family of solute carriers in humans known as the MCF [46, 60]. UCPs translocate protons from the IMS to the matrix, thus dissipating the electrochemical gradient [253] and uncoupling the electron transport process from ATP synthesis [253].

Among the five human UCPs (UCPs 1-5), UCP2 is unique due to its more widespread expression in various tissues compared to other members of the family [19, 60, 180]. UCP2 also has an important role in regulation of mitochondrial ROS concentration [183-185]. Several studies show that the expression of UCP2 is remarkably up-regulated in different types of cancer, including cancers of the, skin, prostate, colon, and breast [186-188, 190]. It has recently been reported that expression of UCP2 in melanoma is positively related to diffusion of T cells in the tumor microenvironment, thus increasing the sensitivity of cancerous cells to therapeutics [189]. It has also been suggested that changes in expression levels of UCP2 in various tissues could be among the causes of diabetes, obesity and heart failure [254].

A NMR structure of UCP2 was reported in 2011 [70]. Although not universally agreed upon [59, 64], it is still the only available structure of UCPs in the PDB. Based on sequence similarities, UCPs and other members of the MCF are thought to have comparable secondary and tertiary structures [46, 60, 70, 207]. These proteins typically contain three domains each comprised of about 100 amino acids and folded into two TM α-helices (Figure 4-1, A). Hydrophilic helical motifs have been identified in loops that connect the TM helices and that extend into the matrix

and IMS [49, 70, 253]. It has been suggested that UCPs function as monomers [83], dimers [66, 191], and a dimer of dimers (tetramers) [30, 68, and this thesis]; however, these functional forms are somewhat controversial, and none have been universally accepted. Controversies are not limited to the quaternary structure of UCPs; there is also no consensus on the general or specific mechanism of function of these proteins [255].

Although proton transport activity is considered to be a common function of all UCPs, its detailed mechanism is not yet fully understood. Different studies have shed light on several aspects of the proton transport mechanism in UCPs, with a focus on UCP1 [61, 62, 72, 73]. Despite some inconsistencies, all agree that proton flux through UCPs is activated by fatty acids and inhibited by purine nucleotides [30]. To date, proposed mechanisms of UCP activation by fatty acids can be summarized into four models: the fatty acid cycling model [61], the buffering/cofactor model [62], the long-chain fatty acid shuttling model [73], and the ITF model [72]. In the fatty acid cycling model, protonated fatty acids that reside in the IMS "flip-flop" across the IMM and release their proton into the matrix. The fatty acid anion is then transported back from the matrix to IMS by UCP [61]. In the buffering model, fatty acid anions bind to the UCP, accept and transport protons via their carboxylate group to the buffering amino acids of the protein, one by one, all the way to the matrix side through this translocon channel [60, 62]. The shuttling model proposes that carboxylate head of a long chain fatty acid moves alongside the protein's cavity, back and forth toward the IMS and the matrix. It gets protonated in the IMS and deprotonated in the matrix, while the fatty acid remains bound to the protein [72, 73]. The ITF model could be considered as a modified version of the shuttling model, where in parallel with/as a result of the movement of the polar head group of the fatty acid across the IMM, UCPs can alternate between two conformational states in which the protein's cavity is either open to the IMS side (cytoplasmic state) or the matrix

side (matrix state) of the membrane [72]. It has been suggested that alternating between the cytoplasmic and matrix state in response to substrate binding (alternating access mechanism) is a common mechanism of transport in all MCF members [46, 51, 53] (Figure 1-3).

Based on homology modeling and amino acid alignment of MCF members, two types of conserved motifs at the water-accessible interfaces are anticipated to form salt-bridge networks; these networks can assist the conversion of cytoplasmic and matrix states through successive disruption and reformation of the salt-bridges [51]. The Px[D/E]xx[R/K] motif, located on the odd-numbered helices (1, 3 and 5), forms the matrix network; and the [F/Y][D/E]xx[R/K] motif, located on the even-numbered helices (2, 4 and 6), forms the cytoplasmic network [46, 51]. The structure of UCP2 in the cytoplasmic state is depicted in Figure 4-1, A-C; a cone shaped structure in which the formation of the matrix network salt-bridges (D35-K141, D138-K239, and D236-K38) results in narrowing of the matrix side of the protein, and a simultaneous disruption of the cytoplasmic network (D101-K295, D198-K10, and E292-K20) leads to the opening of the cavity on the IMS side of the protein [51]. Several studies also highlighted the involvement of three arginine residues (R88, R185, and R279), located in the vicinity of the matrix network of UCPs, in proton transport [52, 63, 72] and transport inhibition mechanisms [52, 63, 74]. A high-resolution X-ray structures of AAC1 locked in either cytoplasmic [49] or matrix states [50] provided evidence in support of the alternating access model mechanism [50, 56, 76].

In order to analyze the mechanism of proton transport by UCPs (the second goal of the thesis), the role of the matrix network and its electrostatic features in the proton transport mechanism of oligomeric UCP2 was investigated. Eleven UCP2 mutants were prepared, of which ten had partially or fully disrupted matrix networks (single, double and triple mutants) and one had an altered, yet intact, matrix network (Hexamutant, HM) (Figure 4-2). UCP2 and its mutants were

expressed in *E. coli* membranes and reconstituted in lipid vesicles for proton transport and transport inhibition analyses. Spectroscopic conformational analyses and thermal stability experiments were performed to investigate the structural similarity/stability of UCP2 and its mutants in membrane-mimicking environments. MD simulations [134] were also employed to provide insights into the local structural changes in tetrameric UCP2 and its mutants and the interaction between UCP2 and its inhibitor (ATP in this case). Our results suggest that the matrix network plays key roles in both the proton transport regulation of tetrameric UCP2 and the interaction of the protein subunits with ATP.

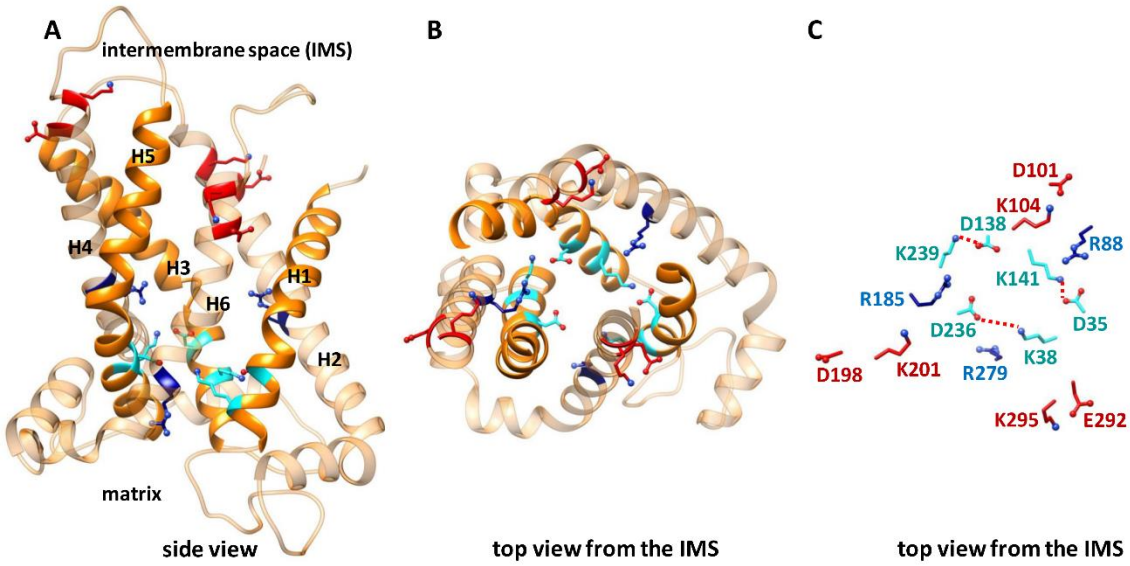

Figure 4-1 Sideview (A), and IMS/cytoplasmic (top) view (B and C) of simulated (300ns) structure of UCP2 in the cytoplasmic state. An intact matrix network between the residues (cyan) present on odd numbered helices (dark orange), and a disrupted cytoplasmic network between the residues (red) present on even numbered helices (light orange) is represented. The conserved arginine residues R88, R185, and R279 (blue) can be seen in the vicinity of the matrix network. In C, the helices are hidden for clarity and the suggested salt-bridges of the matrix network are shown with dashed red lines. The oxygen and nitrogen molecules are shown in red and blue respectively. Figure generated by USCF Chimera 1.13rc.

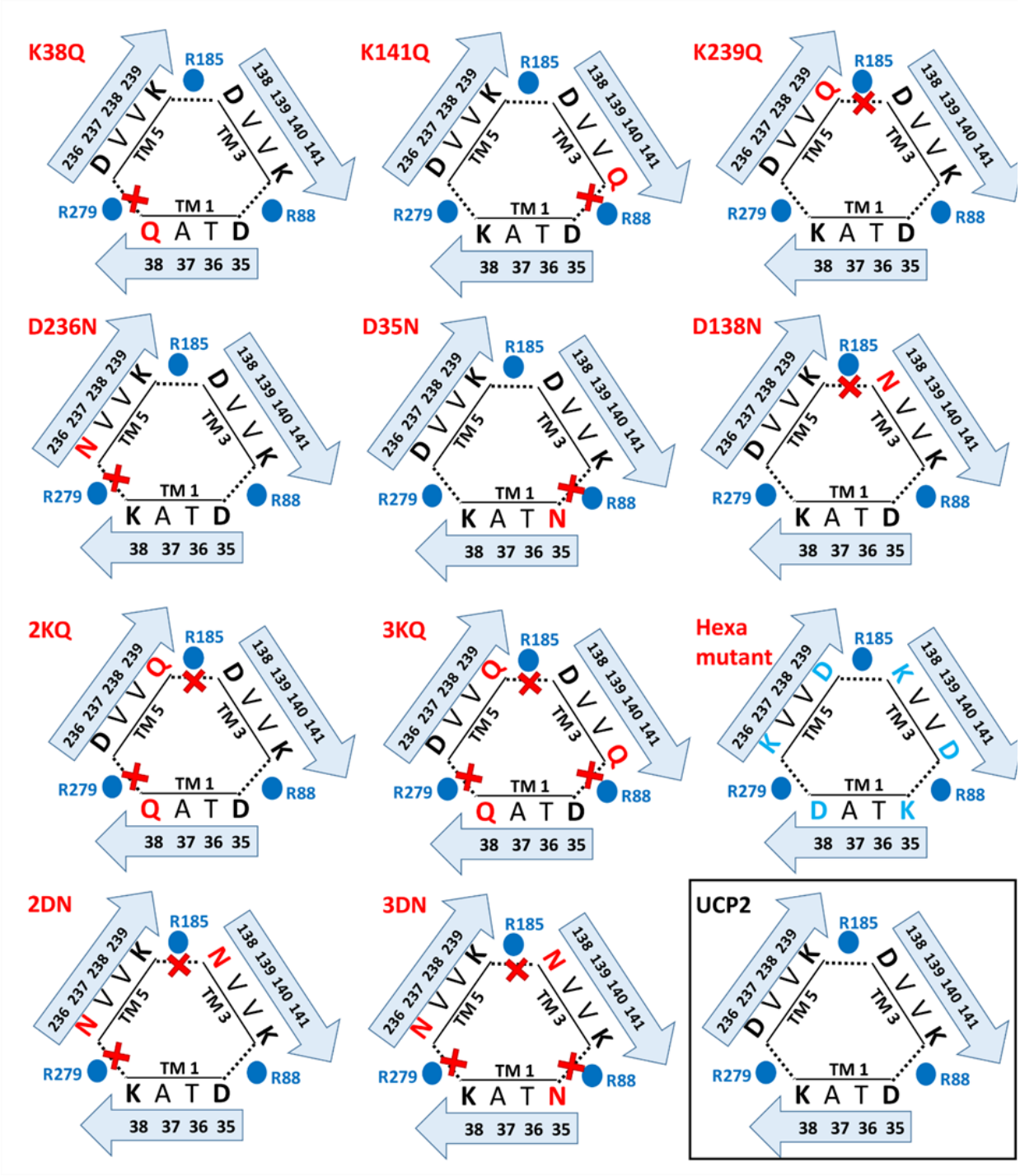

Figure 4-2 Schematic representation of the suggested matrix network in UCP2 and its mutants. disrupted salt-bridges are shown with red crosses. Figure generated by PowerPoint 365.

4.2 Materials and methods

4.2.1 Chemicals

Egg yolk extract with more than 60% (by weight) PC (egg yolk PC or L-α-PC) was obtained from Sigma (St. Louis, Missouri).; the remaining ~40% of the egg yolk extract were mostly phosphatidylethanolamine and other phospholipids. OG was from BioVision (San Francisco, California) and C_8E_4 was obtained from Bachem (Bubendorf, Switzerland). The fluorescent dye SPQ was from Biotium (Fremont, California). The rest of the chemicals were from Sigma-Aldrich.

4.2.2 Construct design and site-directed mutagenesis

Four cDNAs, encoding three single mutants (K38Q, K141Q and K239Q) and one double mutant (K38Q/K239Q, 2KQ) of UCP2 were generated by site-directed mutagenesis of the wild-type human UCP2 [30]. Overlap extension PCR was used to incorporate the mutations [256]. The recombinant proteins that were produced contained an N-terminal pelB, followed by a His-tag, followed by the protein [68]. Codon-optimized cDNAs of the remaining mutants were synthesized and cloned into pET26b(+) (Millipore Sigma, Gene synthesis and cloning services provided by Biobasic, Markham, ON). The pET26b(+) vector was used for cloning in all cases. The fusion proteins produced with a pelB leader sequence on the N-terminus are directed to the cell membrane and the pelB leader is cleaved [30, 68]. The recombinant vectors encoding UCP2 and mutants were transformed into BL21-Codon Plus- RIPL *E. coli* (BL21 CD+), or BL21(DE3) cells in the case of codon-optimized constructs, by heat shock.

4.2.3 Overexpression and extraction from membranes

Recombinant UCP2 and its mutants were expressed in *E. coli* using the auto-induction method as previously described for UCP1 and other UCPs [30, 68, 208]. In brief, *E. coli* cells were grown with vigorous shaking (250rpm) in the auto-induction medium [0.05% glucose, 0.2%

lactose, 0.5% glycerol, 0.5% yeast extract, 1% tryptone, 25 mM $(NH_4)_2SO_4$, 1 mM $MgSO_4$, 50 mM KH_2PO_4, 50 mM Na_2HPO_4,] for 22 hours at 22 °C. After incubation, the cells were spun for 15 min at 8000 g to collect the bacterial cells (pellets). *E. coli* cells were resuspended in extraction buffer [20 mM Tris-HCl pH 8.0, 500 mM NaCl, 0.2 mg/ml lysozyme, 0.5 mg/ml DNase and one ethylenediaminetetraacetic acid (EDTA)-free protease inhibitor cocktail (Roche, Basel, Switzerland)]. The cells were lysed by passing three times through a high-pressure cell disruptor at 20 kPSi (Constant Systems Limited, Daventry, UK). The cell lysate was spun at 20000 g for 20 min to remove unwanted cell debris, aggregated proteins, and intact cells. The supernatant was removed to a clean screwcap centrifuge tube and centrifuged at 50000 g (MLA 80 rotor, Beckman Coulter) for 1 h to pellet the bacterial membranes.

4.2.4 Purification of UCP2 and its mutants

Pellets containing bacterial membranes were solubilized and incubated for 15-16 h in binding buffer [15 mM imidazole, 1% (w/v) LDAO detergent, 500 mM NaCl, 20 mM Tris- HCl, 1 mM Tris (hydroxypropyl) phosphine (THP)]. The solution was then rotated with 1 mL of Ni-NTA resin (Thermo Scientific, Waltham, Massachusetts) for 1 h and transferred to a 0.7 cm diameter glass column. The same protocol was used for purification UCP2 and all of its mutants. The resin in the column was washed with 15 mM imidazole in 1% OG detergent and eluted with 40 mM imidazole in 1% OG detergent. The concentration of NaCl, Tris-HCl and THP in wash and elution steps were the same as binding buffer. Imidazole was removed from the purified proteins (collected upon elution with 40 mM imidazole in 1% OG) by Econo-Pac 10DG Columns (Bio-Rad, Hercules, California). Semi-native SDS-PAGE [68] and modified Lowry assay [209] were used to assess the purity and concentration of the proteins, respectively [68].

4.2.5 Western blot characterization

The identity of recombinant UCP2 was confirmed by immunoblotting. 5-10 μg of purified recombinant UCP2 was separated using SDS-PAGE and transferred to nitrocellulose using the semi-dry method (110 v for 75 minutes). Transfer efficiency was confirmed by Amido-Black staining [257]. The filter was blocked for a minimum of 60 min in Tris-buffered saline (TBS) containing 5% (w/v) dry skim milk and 0.1% (v/v) tween-20. A 1:2000 dilution of rabbit IgG anti-UCP1/2/3 (Santa Cruz Biotechnology Inc. Dallas, Texas) was used as the primary antibody for detection of UCP2 and HRP conjugated antibody (1:5000 dilution), raised in goat against rabbit IgG (Rockland, Limerick, Pennsylvania), was utilized as the secondary antibody. Detection of the secondary antibody was achieved using chemiluminescent reagent Luminata Crescendo western HRP substrate (Millipore Sigma). The image was captured using a Bio-Rad VersaDoc imaging system.

4.2.6 Reconstitution in lipid bilayers

UCP2 and its mutants were reconstituted into lipid vesicles by following the procedure described in references [30, 80] with minor modifications. Briefly, a thin layer of lipids was formed in round bottom flasks by drying solutions of egg yolk PC in MeOH: Chloroform (1:3) for about 10 hours under vacuum. The thin layer of dried lipids was solubilized in proper reconstitution buffer (3mM SPQ fluorescent dye was added for proton transport assays) in order to form multilamellar vesicles (MLV). C_8E_4 [at detergent/lipid ratio of 2.5/1 (w/w)] was added to solubilize the MLVs to form mixed micelles. The mixed micelles were supplemented with pure and desalted proteins to a final concentration of 3 μM. The molar ratio of lipid to protein was ~6000 and ~600 for proton transport and CD experiments, respectively. SM-2 Biobeads (Bio-Rad) were finally used to remove extra C_8E_4 and OG in solution resulting in formation of unilamellar

proteoliposomes. For proton transport analysis experiments, size-exclusion chromatography [Sephadex G25-300 spin column (GE-Healthcare, Chicago, Illinois)] was used for removal of external SPQ (SPQ should be encaged inside the vesicles). In parallel to every step of formation of proteoliposomes protein-free liposomes were prepared to be analyzed as negative controls.

4.2.7 CD and fluorescence spectroscopic measurements

Far- and near-UV CD measurements were performed at 1 nm resolution and at 25 °C, using AVIV 215 spectropolarimeter (Aviv Biomedical, Lakewood, New Jersey). For measurements of far-UV CD spectra (in OG detergent and in liposomes) quartz cells with 0.1 cm path length were used and for measurements of near-UV CD spectra (only in OG detergent) quartz cells with 0.5 cm was used. Ellipticities were converted to mean residue ellipticity, [θ]. All Individual CD spectra were an average of 6-12 measurements. Thermal denaturation curves of UCP2, triple mutants and HM in detergents were obtained by monitoring the proteins ellipticity at 222 nm in the range of 25-90°C [68].

Steady-state fluorescence of proteoliposomes and blank liposomes was performed at 25°C, at a scan rate of 600 nm/min and a band width slit of 5 nm using a Cary Eclipse spectrophotometer (Varian, Palo Alto, California). SPQ was excited at 347 and emission signal was collected at 442 nm. The fluorescence scans were performed at 25°C. Each reported proton transport rate was obtained by averaging of at least 10 different scans.

4.2.8 Proton transport assay

Following reconstitution of UCP2 and its mutants in egg yolk PC vesicles the rate of proton transport was measured as described previously [80]. In brief, 0.040 mL of vesicles were mixed with 1.96 mL of external buffer. The internal buffer of liposomes prepared for proton transport measurements was composed of 0.7 mM EDTA, 54 mM tetraethylammonium sulfate (TEA_2SO_4),

and 20mM TES buffer. The composition of the external buffer was similar to that of internal buffer, with 54 mM TEA_2SO_4 replaced by 54 mM potassium sulfate K_2SO_4. The pH of internal and external buffers was 7.2. Proton transport of UCP2 and its mutants was activated by palmitic acid at a final concentration of 100 μM. Valinomycin was used to influx K^+ and form an electrochemical gradient between inside and outside of the liposome which initiates the proton flux of UCP2 and its mutants. Efflux of protons by UCP2 and mutants led to deprotonation of TES buffer and formation of anionic TES (TES^-). TES^- is able to quench SPQ fluorescence emission by collision. The rate of proton transport by UCP2 and its mutants was thereby correlated to the reduction of SPQ signal intensity. The rate of palmitic acid activated proton efflux was evaluated by monitoring the reduction of SPQ's fluorescence signal intensity during the first 0.5 minutes after injection of valinomycin [68]. Non-specific proton leakage of blank liposomes was deducted from the proton transport rate of the proteoliposome for all cases. Moreover, the proton transport data were corrected for internal volume of the liposomes, fluorescence response of SPQ and protein concentration [80, 209].

4.2.9 MD simulations

The only available NMR structure of UCP2 (PDB ID: 2LCK) [70] was used as the starting structure for the monomeric UCP2.

CHARMM-GUI online server [213] was used to prepare the protein-membrane systems. Membranes consist of POPC lipids, since PC is the main constituent of IMM [130, 214].

In order to build the tetrameric form, a monomeric system was first prepared and was subjected to MD simulation. The final simulated structure was then used to build the UCP2 tetrameric form. Details of building the tetrameric form is discussed in Chapter 3.

The monomeric system was built using 239 POPCs, 11965 water molecules, and 46 and 31 chloride and potassium ions, respectively. Initial minimization was followed by 1 ns of equilibration under NVT and NPT conditions. The production phase included 250 ns.

For the tetrameric systems, the membranes included (400) POPC lipids. Amino acid mutations were made using Pymol [258]. Each system was solvated in an explicit TIP3P [215] water box (total of 47881 water molecules) and CHARMM36m/CHARMM36 protein/lipid force field were used [216, 217].

All tetrameric systems were first energy minimized using the steepest descents algorithm followed by 2 ns of pre-equilibration under NVT and NPT conditions. MD simulations were conducted for 250 ns with 2 ps time steps using GROMACS/2018 [218]. The constraints on the chemical bonds were maintained using the linear constraint solver (P-LINCS) algorithm [219]. The Nosé-Hoover thermostat [220, 221] with a 1.0 ps coupling constant was employed to maintain the temperature at 300 K. To preserve the systems' pressure, the Parrinello–Rahman barostat [222] with a compressibility of 4.5×10^{-5} bar^{-1} and a 5 ps coupling constant was used. For the long-range interactions the particle mesh Ewald method [223, 224] was used. The mentioned procedure and methods have been employed in a number of previous studies (e.g., Refs. [225, 226, 251]) and shown to provide reliable results. Root-mean-square deviations were monitored to ensure the systems were well equilibrated.

4.2.10 Statistical analysis and graphical representations

The statistical method that was used for data analysis was the One-way analysis of variance (ANOVA), in which $P<0.05$ was considered as statistically significant. Graphical representations of the proteins were made by USCF Chimera [259] version 1.13rc and Visual Molecular Dynamics version 1.9.3 [260].

4.3 Results

4.3.1 Expression, purification, and reconstitution of UCP2 and its mutants

In order to evaluate the role of the matrix network in the proton transport mechanism of human UCP2, eleven mutants were prepared (Figure 4-2), of which ten were generated by single or multiple point mutations of K→Q or D→N resulting in partial or full disruption of the matrix salt-bridge network. These mutants included six single mutants: K38Q, K141Q, K239Q, D35N, D138N, and D236N, two double mutants: K38Q/K239Q (abbreviated as 2KQ) and D138N/D236N (2DN) and two triple mutants: K38Q/K141Q/K239Q (3KQ) and D35N/D138N/D236N (3DN). Finally, one mutant was prepared by swapping the positions of the lysines and aspartates that participate in salt-bridge formation, by simultaneously mutating K→D and D→K, resulting in a Hexamutant (D35K/K141D/D138K/K239D/D236K/K38D, abbreviated as HM) with an intact, but inversed matrix salt-bridge network.

All proteins were expressed in the membrane of *E. coli* and purified as a mixture of monomers, dimers, and tetramers in OG detergent. Purity and identity of all three oligomeric forms of UCP2 and its mutants were confirmed by semi-native SDS-PAGE and Western blot analysis (using anti-UCP1/2/3 antibody), respectively (Figure A-4-1). Once purified in OG, UCP2 and its mutants were reconstituted in egg yolk PC (~60% PC) vesicles for proton transport functional analysis. As shown in Figure 4-3, UCP2 and its mutants associated to form a single multimeric (tetrameric) complex when reconstituted into liposomes regardless of the number and type of mutations. Homo-oligomerization of UCP2 and other UCPs to dimer of dimers in lipid vesicles have been demonstrated in our previous reports [30, 68]. The oligomeric structure of UCP2 and the interactions involved in the formation of a dimer of dimers in lipidic environments have been discussed in detail in Chapter 3 [30, 68].

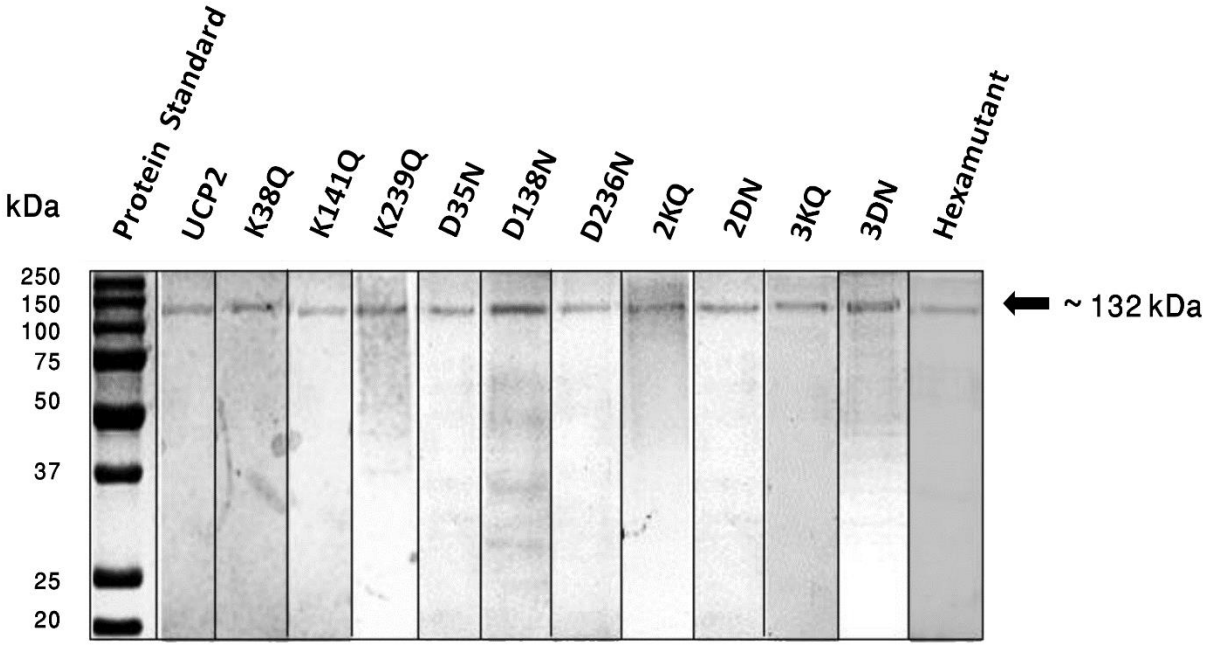

Figure 4-3 Semi native SDS-PAGE analysis of proteoliposomes stained with Coomassie Blue, showing the presence of the tetrameric form of UCP2 and its mutants in lipid vesicles. Vertical black lines separate individual gels.

4.3.2 CD spectroscopic analysis of UCP2 and its mutants

Conformations of UCP2 and its mutants in OG detergent were characterized using CD spectroscopy. Distinctive spectral features of α-helical backbone secondary structures (two negative maxima at 208 nm and 222 nm, and a positive maximum around 193 nm [232]) were observed for all proteins (Figure 4-4, A). Also, the ellipticity ratio ($\theta_{208}/\theta_{222}$) in all spectra was in the range of 0.9-1.0, which is typical of α-helical protein structures [261]. This suggests that purified UCP2 and its mutants are dominantly α-helical in OG. Moreover, all twelve proteins exhibited conformational similarities, indicating that the mutations did not alter the overall conformation of the protein. However, minor local structural differences between UCP2 and its mutants were revealed by near-UV CD analysis. Such minor changes in local structures were

revealed by up to a ~5 nm red shift of the peak at ~280 nm and/or alteration of the overall shape of the near-UV CD spectrum in some cases (Figure 4-4, A, inset). These changes could be due to differences in the microenvironment of aromatic residues, especially those close to the site of mutations such as W283.

To ensure that introducing multiple mutations (i.e. in triple mutants and HM) did not affect the overall structure of proteins in lipid environments, UCP2 and these mutants were reconstituted in lipid vesicles and examined using far-UV CD spectroscopy (Figure 4-4, B). Comparison of the far-UV CD spectra before and after reconstitution reveals that CD signals of the reconstituted proteins were considerably enhanced compared to those in detergent, indicating that all four proteins had higher helical contents in liposomes. This emphasizes the important role of lipids in enhancing secondary structures in MPs [201]. Furthermore, spectra of reconstituted proteins showed a red shift of the negative maximum at 208 nm (towards 210 nm), which has been attributed to enhanced helix-helix interactions and protein association [30, 68, 233-235].

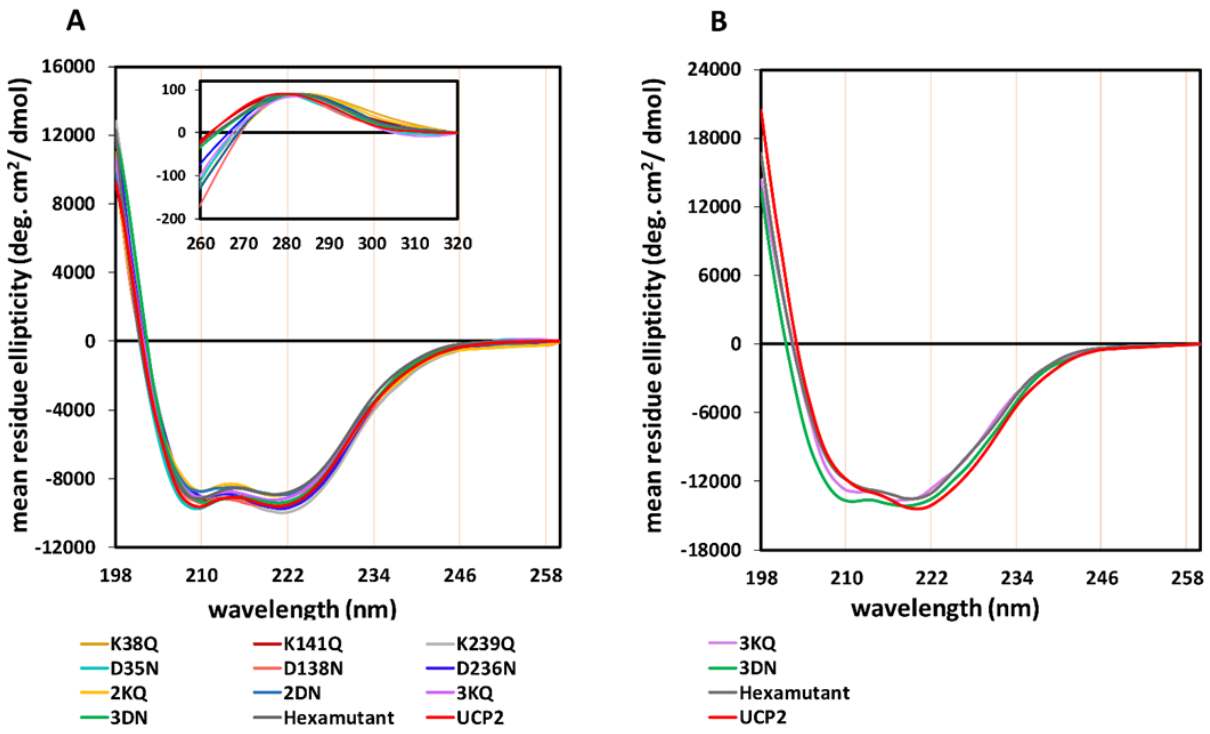

Figure 4-4 Far-UV CD spectra of UCP2 and its mutants in A) OG detergent and B) in lipid vesicles show an overall α-helical structure for all proteins in both environments. **Near UV-CD spectra of the proteins in detergent (A-inset)** indicate that local structure of the mutants at the microenvironment of aromatic residues are comparable as well. This suggest that mutations did not impact the overall structure of the proteins. Each reported CD spectrum is an average of minimum 6 scans. The concentrations of proteins were 5 – 8 μM in OG and ~1μM in vesicles.

The shape of far-UV CD signals of reconstituted proteins were comparable and deconvolution using DichroWeb [155] showed similar helical contents for UCP2 and mutants (~50-60%). Despite the similarity of the CD signal of reconstituted proteins in liposomes, slight differences were observed in the ellipticity ratio $\theta_{208}/\theta_{222}$ (UCP2: 0.74, HM: 0.82, 3KQ: 0.92, 3DN: 0.95). Differences in the ellipticity ratios between the mutants and UCP2 could be indicative of changes in the degree of protein association and/or alteration of interhelical interactions [68, 233, 235]. Higher ellipticity ratios of 3DN and 3KQ compared to those of UCP2 and the HM protein imply that more relaxed (less compact) conformations could be found in the mutants with disrupted matrix network. Collectively, the data indicate that the overall structures of UCP2 and its mutants were comparable both in OG detergent and in liposomes.

4.3.3 Thermal denaturation experiments

To further evaluate the proper folding and structural similarity of UCP2 and its mutants with multiple mutations (3DN, 3KQ and HM) in OG, the ellipticity at 222 nm was monitored over the temperature range of 25-90 ºC. As shown in Figure 4-5, A, UCP2 and all three mutants showed comparable cooperative denaturation curves and with no significant difference (P>0.05) between the melting points (T_m). The T_m of UCP2 in these experiments was 59.8 ± 0.7 ºC, which is very close to the reported T_m of the prototypical UCP1 in OG (T_m= 59.2 ºC) [68], and relatively close to that of AAC in dodecyl-maltoside detergent plus CL (T_m=50.0 ºC) [262].

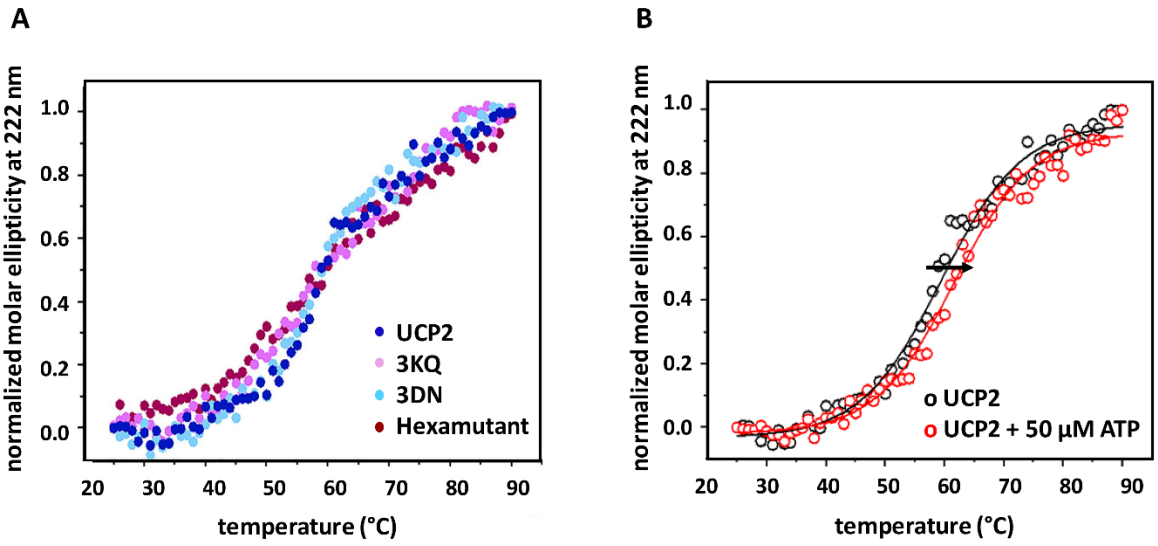

Figure 4-5 A) Comparative thermal denaturation curves of UCP2 and its mutants in OG reveal that multiple mutations of UCP2 did not impact the thermal stability of the protein. **B) Thermal denaturation curve of UCP2 in the absence and presence of ATP** shows an increase in Tm upon addition of ATP (indicated by the arrow) as a result of formation of new salt-bridges between ATP and UCP2**.** Tm was calculated by Boltzmann equation for fitting the data**.**

Appropriate folding of extracted proteins from bacterial membranes was further supported by the elevated T_m of the proteins after addition of their inhibitor ATP (Figure 4-5, B). Elevation of UCP2 T_m to 61.8 ± 0.4 ºC in the presence of ATP suggests that UCP2 interacts with ATP and

is folded in its native-like functional form, which provides an appropriate binding site for the inhibitor. Addition of ATP to 3DN and 3KQ also increased the T_m in both cases, albeit less compared to that for UCP2 (the increase of T_m was 2.0 ºC, 1.2 ºC, and 1.4 ºC for UCP2, 3DN and 3KQ, respectively). This could be a consequence of direct or indirect impact of the mutations in the interaction with ATP (discussed later).

Overall, denaturation experiments specified that UCP2 and its mutants were relatively stable in OG detergent, and neither extraction and purification steps, nor multiple point mutations resulted in loss of structural stability.

4.3.4 The role of the matrix salt-bridge network on proton transport function of UCP2

Proton transport rates were studied using a fluorescence quenching assay, as described previously (Figure A-2-1) [80]. All proteins were only able to transport protons after addition of palmitic acid (PA). This is consistent with previously reported data on the inability of UCP1 (in proteoliposome systems and mitoplasts) to transport protons in the absence of free fatty acids [72, 263]. Table A-4-1 and Figure 4-6 represent proton transport rates of UCP2 and its eleven mutants. The rate at which UCP2 transported protons was 5.24 ± 0.09 μmol/min/mg protein, which is within the range of previously reported proton transport rates for UCP2 (1.2-30 μg/min/mg protein) [for a full list see Ref. [80]]. Our results showed that disruption of the matrix network by elimination of the charged residues (K→Q and D→N mutations) significantly ($P<0.05$, P less than 0.05 means a significant difference between the results was obtained in our SPSS, One-Way ANOVA test) increased the rate of proton flux. In contrast, mutations that maintained the integrity of the matrix network did not affect the proton transport rate as no significant difference was observed in the proton transport rate of UCP2 and the HM version ($P>0.05$).

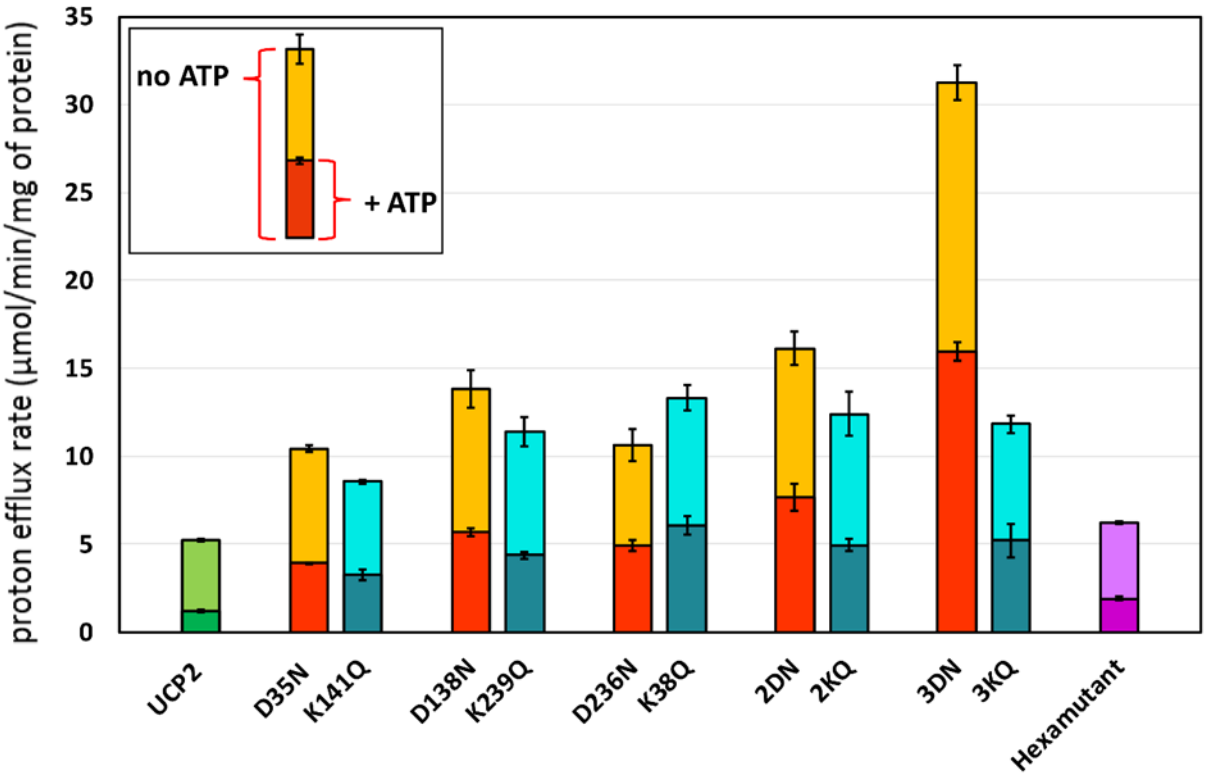

Figure 4-6 Proton transport rate of UCP2 and its mutants. Mutations of K → Q are shown in orange shades and mutations of D→N are shown in blue shades. For the numerical values see Table A-4-1. Every two bars close to one another were predicted to disrupt the same salt-bridge(s). The full length of each bar represents the rate of proton transport in the absence of ATP and the darker shade on the bars shows the rate of proton transport in the presence of ATP. Each bar represents the average transport rate of 10 repeats and the error bars show the standard deviations.

To compare the structural features of the proteins at the site of the matrix network, atomistic MD simulations were carried out on tetrameric UCP2 (Figure A-4-2) and selected mutants (D138N, 2DN, 3DN, 3KQ, and HM) in a POPC bilayer. Interestingly, MD simulation analyses showed that the matrix network is composed of more salt-bridges than what has been previously suggested [51]. In fact, instead of the three suggested salt-bridges between aspartate and lysine pairs of the signature motifs on odd numbered helices (D35-K141, D138-K239 and D236-K38), the MD simulations indicate that the matrix network is composed of five salt-bridges (D35-K141, D138-K239, D138-R88, D236-R185, and D236-R279) of which two are amongst the previously

suggested matrix network and three are formed upon interaction of aspartate residues of the signature motifs with R88, R185 and R279. Consequently, in order to properly investigate the role of the matrix network in proton transport by UCP2 all potential salt-bridges should be considered.

Figure A-4-3 represents a single snapshot (at 250 ns) of the matrix network in the four monomeric subunits of tetrameric UCP2 (labelled as chains A-D). The average length of the matrix network salt-bridges over the last 100 ns of simulation are listed in Table 4-1. A 0.4 nm cut off was used to determine salt-bridge formation [264]. Even though the distances between the residues of the three originally suggested salt-bridges are reported in this table, K38 and D236 did not form a salt-bridge in any of the subunits (average distance > 0.4 nm) during the simulations. RMSD analysis (Figure A-4-4) showed that all the systems have reached equilibrium and the proteins did not completely or partially change their conformational state (from matrix state to cytoplasmic state and vice versa) over the last 100 ns. Table 4-1 reveals that the matrix network did not have similar conformations in the four subunits of UCP2; e.g., the salt-bridges that were formed within chain A of the wild-type UCP2 (D138-R88, D236-R185 and D236-R279) were different from those in chains B, C, and D. This is consistent with our recent work showing that individual subunits do not obtain 100% identical conformations (Chapter 3) and the tetrameric UCP2 is in fact a pseudosymmetrical dimeric complex of dimers. The dissimilarity between the matrix network salt-bridges of UCP2 subunits (also seen in mutants) implies that not all subunits are in the same phase of transport, which means protons do not enter and exit all four subunits concurrently.

Comparison of UCP2 and D138N tetramers indicated that upon single mutation of D→N more than half of the salt-bridges of the matrix network were lost (changed from a total of 12 per

Table 4-1 Average distance (nm) for salt-bridges in different system over the last 100 ns of simulation.

	UCP2				Hexamutant (HM)			
	Chain A	Chain B	Chain C	Chain D	Chain A	Chain B	Chain C	Chain D
D35-K141	1.06	0.42	**0.20**	**0.31**	**0.18**	0.55	**0.18**	**0.17**
D138-K239	0.69	**0.20**	**0.34**	**0.35**	**0.21**	**0.25**	**0.18**	**0.17**
D236-K38*	0.90	0.70	0.64	0.92	0.97	0.75	0.96	0.84
D35-R279*	0.77	0.73	0.92	0.62	**0.18**	**0.25**	0.64	**0.22**
D138-R88	**0.29**	0.78	0.66	0.49	1.43	0.58	**0.31**	**0.21**
D236-R185	**0.40**	0.67	**0.39**	0.42	0.60	0.53	0.61	0.59
D236-R279	**0.19**	**0.36**	**0.27**	**0.24**	0.80	0.82	0.75	0.96
number of SB	3	2	4	3	3	2	3	4
	D138N				**D138N/D236N (2DN)**			
	Chain A	Chain B	Chain C	Chain D	Chain A	Chain B	Chain C	Chain D
D35-K141	0.89	0.57	**0.17**	**0.40**	0.74	**0.36**	**0.38**	**0.40**
D138-K239	-	-	-	-	-	-	-	-
D236-K38	0.84	1.68	0.96	0.66	-	-	-	-
D35-R279	0.64	1.46	0.80	0.69	**0.39**	0.55	0.85	0.70
D138-R88	-	-	-	-	-	-	-	-
D236-R185	0.42	0.48	0.58	0.48	-	-	-	-
D236-R279	**0.27**	**0.19**	**0.29**	0.46	-	-	-	-
number of SB	1	1	2	1	1	1	1	1
	D35N/D138N/D236N (3DN)				**K38Q/K141Q/K239Q (3KQ)**			
	Chain A	Chain B	Chain C	Chain D	Chain A	Chain B	Chain C	Chain D
D35-K141	-	-	-	-	0.90	0.84	0.87	0.58
D138-K239	-	-	-	-	1.09	0.80	0.55	0.60
D236-K38	-	-	-	-	0.96	1.33	1.95	0.87
D35-R279	-	-	-	-	**0.19**	**0.39**	**0.20**	0.58
D138-R88	-	-	-	-	0.58	**0.23**	**0.26**	0.41
D236-R185	-	-	-	-	0.42	0.50	0.45	0.50
D236-R279	-	-	-	-	0.49	0.43	1.43	**0.19**
number of SB	0	0	0	0	1	2	2	1
	UCP2-ATP							
	Chain A		Chain B		Chain C		Chain D	
D35-K141	1.07		0.73		**0.25**		0.41	
D138-K239	**0.40**		**0.18**		0.56		0.55	
D236-K38	1.13		1.19		0.77		0.70	
D35-R279	0.96		0.70		**0.37**		**0.18**	
D141-R88	0.47		**0.31**		**0.26**		**0.18**	
number of SB	1		2		3		2	
K38-ATP	0.83		**0.19**		0.66		0.66	
K141-ATP	**0.17**		**0.17**		0.43		**0.38**	
K239-ATP	0.91		0.64		**0.35**		**0.21**	
R88-ATP	**0.19**		**0.19**		**0.17**		**0.20**	
R185-ATP	0.42		0.50		**0.18**		**0.19**	
R279-ATP	**0.23**		**0.41**		0.45		**0.18**	

-The salt-bridges shown with * sign did not form in the UCP2.

-The originally proposed salt-bridges are shown in black, the interactions involving arginine residues are shown in blue, and the numbers ≤ 0.40 nm (the salt-bridge cut off) are shown in bold.

tetramer to a total of 5). This decrease in the number of salt-bridges together with ~2 times increase in the rate of proton transport (Figure 4-6) suggest an important "filtering" role for the matrix network in limiting the proton leakage across the protein. The total number of salt-bridges in tetrameric 2DN and 3KQ was found to be 4 and 6, respectively (comparable to that of D138N). This agrees with the similar rates of proton transport observed in D138N, 2DN and 3KQ ($P>0.05$). The data suggest that the matrix network of UCP2 is interconnected, and disruption of one component could impact other components; thus one single mutation can reduce the filtering effect of the network as much as three mutations (3KQ) (in the network) can do. As shown in Table 4-1, our MD simulations showed no salt-bridge formation in the matrix network for 3DN, the mutant with the highest rate of proton transport (31.26 ± 0.09 μmol/min/mg protein). Such uncontrolled proton leakage could be a result of total loss of the filtering effect of the matrix network. Moreover, the significant contribution of newly identified salt-bridges (D138-R88, D236-R185, and D236-R279) in controlling proton leak across UCP2 could be distinguished upon comparison of the rate of proton transport by 3DN and 3KQ. In both mutants all original K-D salt-bridges of the matrix network were disrupted, thus the difference in the rate of proton transport (11.82 ± 0.48 for 3KQ *vs.* 31.26 ± 0.95 for 3DN) could be related to the difference in the number of the newly identified salt-bridges (6 in 3KQ *vs.* 0 in 3DN). Finally, the only mutant with similar number of salt-bridges to UCP2 was HM (12 salt-bridges per tetramer), which also showed a comparable rate of proton transport with UCP2 ($P>0.05$). Overall, the proton transport results suggested that the rate of proton transport is inversely related to the number of salt-bridges per tetramer: UCP2 and HM > 3KQ > D138N > 2DN > 3DN, (Table A-4-1).

Importantly, MD simulation analyses together with our experimental approach strongly supported a cooperative tetrameric function for UCP2 (and its mutants). In all cases, the four

subunits were analyzed as one interconnected tetrameric unit and the total number of salt-bridges per tetramer were considered. Our results also showed a correlation between the proton transport rate and structural compactness of UCP2; mutants with a more relaxed conformation (less compact monomeric units) compared to UCP2 showed increased proton transport rates, while the HM protein, with similar interhelical packing to that of UCP2, had a comparable proton transport rate. Such correlations were previously reported by Hoang *et al.* [32].

4.3.5 Inhibition of proton transport by ATP

In order to investigate the mechanism of inhibition of proton transport by purine nucleotides, the proton flux rate of UCP2 and its mutants was analyzed in the presence of ATP (Figure 4-6 and Table A-4-1). Molecular features of the interaction of UCP2 with ATP were also analyzed using MD simulations. The highest rate of inhibition (~78%) was observed for UCP2, decreasing the rate of proton transport to 1.17 ± 0.09 μmol/min/mg protein. Partial inhibition of UCPs by purine nucleotides has been reported previously in several studies [71, 80]. Figure 4-7 shows a snapshot of UCP2 and ATP contacts at 250 ns. Arginine (R88, R185 and R279) and lysine residues (K38, K141 and K239) of the matrix network could interact electrostatically with the phosphate groups of the ATP molecule (Figure 4-7 and Table 4-1) in all four subunits of the tetrameric UCP2 leading to tight binding of protein to its inhibitor (one ATP molecule/every subunit). Binding to ATP was not identical among the subunits of UCP2 neither in terms of the number of interactions nor in the interacting protein residues involved (for example in subunit A, ATP was interacting with K141, R88 and R279 while in subunit B it was interacting with K38, R88 and R279 but not K141) (Figure 4-7 and Table 4-1). Therefore, the experimental inhibition rate (~78% inhibition) could be an average outcome of four different types of UCP2-ATP contacts. A basal proton leak might take place in subunits which are less tightly bound to ATP, which explains the reason behind not

reaching a 100% inhibition by purine nucleotides [71, 80]. Residues R88, R185, R279 and K141 were previously proposed as potential binding sites of purine nucleotides in the structure of UCP2 [30, 63, 74]. To the authors' knowledge, residues K38 and K239 are reported for the first time in this study as potential binding sites of ATP.

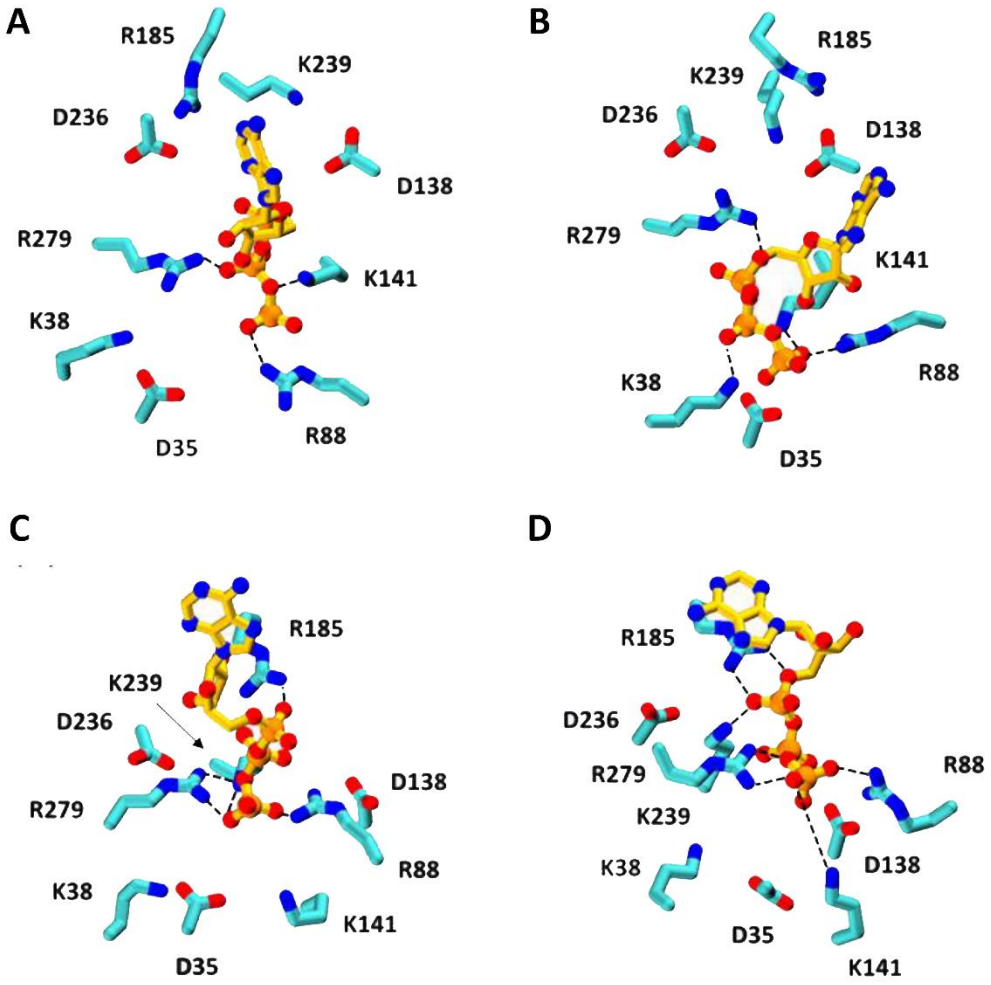

Figure 4-7 The interactions between ATP and subunits A-D of the tetrameric UCP2 (top view from the IMS side). Protein helices are omitted for clarity. Average length for the interactions is provided in Table 4-1. Carbon, nitrogen, and oxygen are shown in cyan, blue, and red, respectively. Carbon and phosphorous of the ATP molecule are shown in yellow and orange, respectively. Figure generated by VMD 1.9.3.

Since a total of six residues were able to interact with ATP, mutations of K→Q and D→N could only lower (but not fully interrupt) the inhibition mechanism, thus the rate of inhibition was

in the range of ~ 50-60% (Table A-4-1) for such mutants. Even though aspartate residues did not directly bind to ATP, the inhibition rates of K→Q and D→N mutants were comparable. This observation implies that D→N mutations indirectly influenced the inhibition process by conformational distortions that could result in loosening the packing of helices near the binding site of ATP and/or lowering the availability of ATP-interacting residues. The similarity ($P>0.05$) of inhibition rate between the HM and UCP2 supports the importance of tight helix-helix interactions in binding of UCP2 to ATP. The data suggest that ATP can bind to the center of monomeric subunits of the UCP2 tetramer upon interaction with basic residues of the matrix network and the integrity of the network impacts this binding.

Binding of ATP to UCP2 resulted in increased thermal stability (higher T_m) of the protein (Figure 4-5, B). Addition of ATP to 3DN and 3KQ also increased the T_m; however, to a lesser extent. This is consistent with the lower inhibitory effect of ATP on triple mutants compared to that for UCP2 (Table A-4-1 and Figure 4-6), and the importance of local structure in UCP2-ATP interactions.

4.4 Discussion

Signature motifs present on helices 1, 3, and 5 of MCF members have been suggested to form matrix salt-bridge networks in multiple studies [46, 51, 56]; however, it seems that this suggestion was extrapolated from structural analysis of AAC1 in the presence of CATR inhibitor [49, 265]. Here we demonstrated the engagement of arginine residues 88, 185 and 279 in the matrix network of human UCP2 and provide evidence of a more complex network compared to what was originally proposed [51]. Similarly, a more complex and broader matrix network has recently been offered for AAC1 (without inhibitor) based on MD simulation analyses in POPC [265]. Under our experimental conditions, low proton transport rates of UCP2 and its mutants were in better

agreement with the behavior of a transporter/carrier as compared to an ion channel [72]. However, the possibility of increased transport rates under different physiological conditions [such as larger electrochemical potential across the mitochondrial membrane and interactions of other proteins and specific lipids (such as CL) in the IMM)] cannot be excluded.

A combination of the electrophoresis (Figure 4-3), CD (Figure 4-4), thermal denaturation (Figure 4-5) and proton transport (Figure 4-6 and Table 4-1) analyses of UCP2 and its mutants revealed that the mutations did not have a substantial impact on the overall conformation and the molecularity of the proteins in lipid-like environments. The differences in proton transport rates can thus be attributed to the disruption of the salt-bridge network and its relative impact on local conformation rather than perturbing the overall tertiary structure of the proteins.

By comparing the proton transport rates and structures of UCP2 and its mutants, we can conclude that the matrix network plays a dual role in regulating the proton transport function of UCP2. First, by formation of a cumulative electric field as a result of electrostatic interactions between lysine and arginine residues with aspartates, which can have a filtering effect on proton transport. Secondly, by holding the TM helices in the monomeric subunits close to one another, enhancing their non-covalent interactions, and maintaining the dense packing of the funnel-like structure of the protein. The regulatory role of the matrix network is consistent with the reported gating role of cytoplasmic and matrix networks of MCF members to prevent undesirable proton leak across the IMM [46].

Structural differences in the local interior conformations and the matrix network states (Figure A-4-3 and Table 4-1) of the monomeric subunits of tetrameric UCP2, indicate that the subunits do not undergo identical changes concurrently and there might be a phase difference in the transport cycle of the neighboring subunits. In Chapter 3 we analyzed the internal cavities of

all four subunits of UCP2 along the central z axis normal to the membrane aided by MD simulations and found that in UCP tetramers the orientation of cavities of monomers in each dimeric subunit was similar but opposite to the monomers of the other dimeric unit (Figure 4-8). In other words, in tetrameric UCP2, monomers in one of the dimers were open towards the IMS and the monomeric subunits of the other dimeric pair were open towards the matrix side of the membrane. This two-state or biphasic conformation of UCP tetramers could be the functional mode of the protein in ion/proton transport. For example, for the proton transport function of the tetrameric UCP2, on the basis of this two-state model, it can be suggested that one of the two dimeric units that is open to the IMS side (cytoplasmic state; closed to the matrix side) allows the protons to enter the open cavities of its monomeric subunits (open mode); while, simultaneously, the other dimeric unit that is closed to the IMS side (matrix state; open to the matrix side) does not allow protons to enter from the IMS side of the membrane (closed mode) (Figure 4-8). These open and closed functional modes of the protein are interconvertible but always oppose each other. To better understand the synchronicity in the biphasic behavior of UCP2, one can visualize the dimeric unit in the cytoplasmic state (or open mode) is about to absorb protons from the IMS side, and at the same time the dimeric unit in the matrix state (or closed mode) is about to release protons to the matrix side (matrix state). At a certain stage of proton absorption on the IMS side and proton release on the matrix side the dimeric units in the protein inverse their conformations and in the next stage their roles switch. This general **biphasic two-state molecular model** (Figure 4-8) primarily aims to explain the proton transport in tetrameric UCP2 (and other UCPs). In addition, this general biphasic model could also help explain the co-transport (antiport) of protons and certain anions (such as chloride) in tetrameric UCPs [30]. The matrix state of the dimeric units with low affinity for positively-charged protons could have a high affinity for anions such as

chloride; therefore, after being attracted to the open cavity of the matrix state (with a positive electric field), chloride ions will have an opportunity to be transported to the IMS side of the membrane after conversion of the matrix state to cytoplasmic state.

To summarize, all subunits are functional in a tetrameric UCP2 complex, monomers of each dimer are in similar transport states (cytoplasmic or matrix states), and the function of one dimeric unit could be regulated by the other dimeric unit.

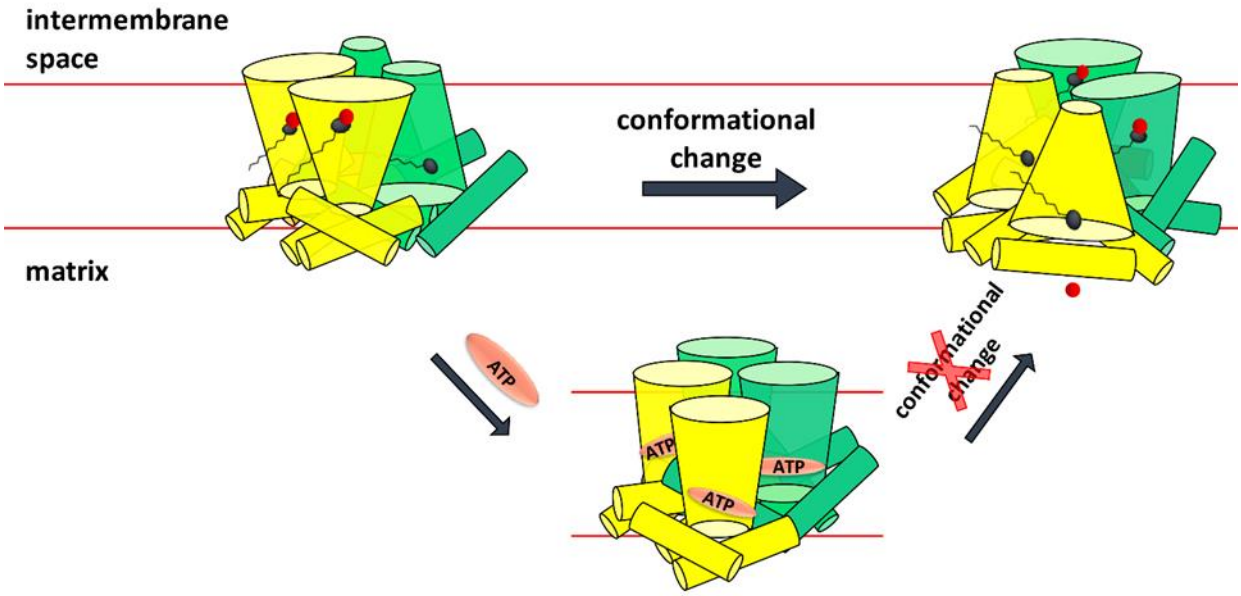

Figure 4-8 The biphasic two-state model for proton transport and inhibition of tetrameric UCP2. The monomeric subunits within a dimeric unit are functional and conformationally correlated. Dimeric unit 1 (yellow) is in cytoplasmic state first and changes to matrix state as the protonated head group of fatty acid moves form the IMS towards the matrix. Dimeric unit 2 (green) is in matrix state first, and changes to cytoplasmic state upon the movement of fatty acid's head group towards the IMS. None of the four monomeric subunits of the tetramer have identical conformations; however, the monomers within one dimeric unit are at the similar conformational state or phase (compare the subunits with the same color) which is opposite to the second dimeric unit (compare yellow and green subunits). Fatty acids are shown in deprotonated (black) and protonated (red sphere attached) forms. Fatty acids are protonated in the cytoplasmic state and deprotonated in the matrix state. Conformational changes in one dimeric unit can simultaneously induce change of conformation in the other dimeric unit. Binding of ATP (orange) locks the conformational changes of the proteins and blocks the path of fatty acid. Figure generated by PowerPoint 365.

4.4.1 Mechanism of proton transport by the subunits of a tetrameric UCP2 complex

The mechanism of proton transport by monomeric subunits of the tetramer in the proposed two-state model could be explained by the ITF model, describe above [72]; however, in a tetrameric complex the transport mechanism becomes more complicated as the subunits mutually impact one another (Figure 4-8). Based on the ITF model, when a UCP2 monomer is in the cytoplasmic state (intact matrix network) a long chain fatty acid and a proton can interact with three arginine residues (R88, R185, R279) present at the center of the protein and induce a set of conformational changes which eventually transforms the protein to the matrix state [72]. When UCP2 is in the matrix state (disrupted matrix network), the arginine residues and the protonated fatty acids are exposed to the matrix side where the proton is released [72]. Another set of conformational changes is required to return the fatty acid back to the IMS side in order to start another transport cycle [72]. The fatty acid's hydrocarbon chain remains anchored to its binding site (hydrophobic pocket) on the protein by hydrophobic interactions throughout the transport cycle [72]. The fatty acid's head can move back and forth across the protein upon changes from cytoplasmic to matrix state and vice versa. Very similar mechanisms have been proposed for the symport of protons and anionic species across the IMM by other members of the MCF, such as PICs and glutamate carriers [57]. The ITF model can be expanded to the dimeric units of the tetrameric UCP2, assuming that each unit binds to two fatty acids (one for each monomer) and is either protonated (cytoplasmic state) or deprotonated (matrix state). However, based on the inherent asymmetry of monomeric subunits in UCP2 (Chapter 3), it is feasible that dissimilar asymmetric conformations of monomeric subunits offer different binding affinities for fatty acids and one or more of these subunits may not even properly bind to fatty acids (therefore not active).

Stoichiometry of fatty acid to protein subunit in tetramer may therefore be different from the 1:1 stoichiometry in the monomer.

This possibility brings us back to the potential regulatory role of the matrix network in proton transport, which could be assisted by cooperative interaction of UCP2 non-equivalent subunits. The inverse relationship between the packing density of the TM helices and the rate of proton transport (comparison between the native protein and single, double and triple mutants) could be related to easier movement of fatty acid across the protein in mutants with disrupted matrix network. The ITF mechanism supports the observed elevation of UCP2 proton transport function by increasing the fatty acid chain length [32]. In this case, stronger hydrophobic interactions in longer hydrocarbon chains enable the fatty acid to remain bound and participate in more transport cycles. The ITF hypothetical model may also explain the inhibitory role of fatty acids on the chloride transport function of UCP2 reported previously [30]. Since the fatty acid and chloride might share the same path, the anionic form of the fatty acid (present in the matrix state of the transporter) could interrupt chloride transport from matrix to IMS.

4.4.2 Cycling and buffering models

We have reported that the chloride transport rate of UCP2 was much less than its proton transport rate [30, 32]. This conflicts with the fatty acid cycling model in which the anion transport activity of UCPs is a prerequisite of their proton transport function [61, 76]. Moreover, the passage of a fatty acid hydrocarbon tail from the relatively hydrophilic core of UCP2 seems to be energetically unfavorable and should be lowered (should not be enhanced) as the hydrophobicity and bulkiness of the hydrocarbon chain increases, yet we saw a direct relationship between the length of the fatty acid and the proton transport activity of UCP2 [30, 32]. Also, bulky and long-chain fatty acids such as arachidonic acid have been shown to activate UCP2 at a higher rate than

shorter and less bulky fatty acids [30, 32]. The fatty acid cycling model was proposed based on the ability of the AAC to transport anionic fatty acids [19, 61], however, a recent patch clamp analysis clearly showed the inability of AAC to transport such species [90].

Our results do not support the buffering model either [62]. First, because neutralization of titratable residues of the matrix network resulted in a higher rate of proton transport compared to UCP2, which is in contrast with the stepwise passage of protons to titratable amino acids. Secondly, partial or full disruption of the matrix network considerably increased the transport rate of protons, and in the buffering model no role was identified for any of the two networks. Furthermore, the observed inhibitory role of fatty acids on chloride transport of UCP2 (and other UCPs) [30] could not be explained by the buffering model.

4.4.3 Inhibition of proton transport with ATP

Upon disruption of the matrix network and formation of new salt-bridges with basic residues (K38, K141, K239, R88, R185, and R279), MD simulations revealed that ATP could bind to UCP2 in its cytoplasmic state at a position near the center of the cavity (Figure 4-7). ATP binding might block the movement of fatty acid, preventing it from moving between the IMS and the matrix, thereby stopping the protein from changing conformation or locking it in an intermediate state (neither cytoplasmic nor matrix state). ATP inhibition might also be attributed to neutralizing the positive charges of the arginine residues through interaction with the phosphate groups. These arginine residues (R88, R185 and R279) have been proposed to attract fatty acids towards the protein cavity to initiate proton transport [72]. Our hypothesis on the presence of ATP in the translocon channel of UCPs and its interaction with matrix network residues is consistent with a previous report on the ability of ATP to induce a local conformational change in UCP1 with minor alteration of the overall protein structure [68].

In our mechanistic model supported by MD simulations, similar to the case of fatty acid binding in proton transport, each of the four ATP molecules can have different binding affinities for non-equivalent monomeric subunits of UCP2. Considering the influence of local conformation of the protein cavity in the cytoplasmic state on ATP interaction with UCP2 and the mutual interaction of subunits within the tetrameric functional unit (discussed above), we conclude that intercommunication between subunits could dictate the rate of inhibition.

4.5 Conclusions

In the current study we suggest a model for proton transport in tetrameric UCP2 that we term the biphasic two-state proton transport model. We also introduced the possibility of a larger matrix salt-bridge network (composed of five salt-bridges D35-K141, D138-K239, D138-R88, D236-R185, D236-R279 of which the last three have never been reported previously) for UCP2 and demonstrated that the matrix network plays an important filtering role in controlling proton transport. Based on this biphasic two-state proton transport model for tetrameric UCP2 (Figure 4-8), the conformation of each functional dimeric unit is either in one or the other mode of transport, acting as an on /off switch. The presence of ATP can occlude the translocon channel via interaction with specific basic residues (K38, K141, K239, R88, R185, R279), and also inhibit proton transport by preventing switching between the cytoplasmic and matrix state conformational changes as well as movement of fatty acids.

CHAPTER 5 - CONCLUSIONS AND FUTURE DIRECTIONS

UCPs have attracted a great deal of attention since their discovery in 1978. A total of ~17000 studies have been published on UCPs to date, of which about half have been in the last decade (Figure 5-1) [266]. This is because UCPs not only mediate non-shivering thermogenesis in mammals, but they have also been linked to several metabolic diseases (such as obesity, diabetes, hypertension and cancer), making them intriguing drug targets [19].

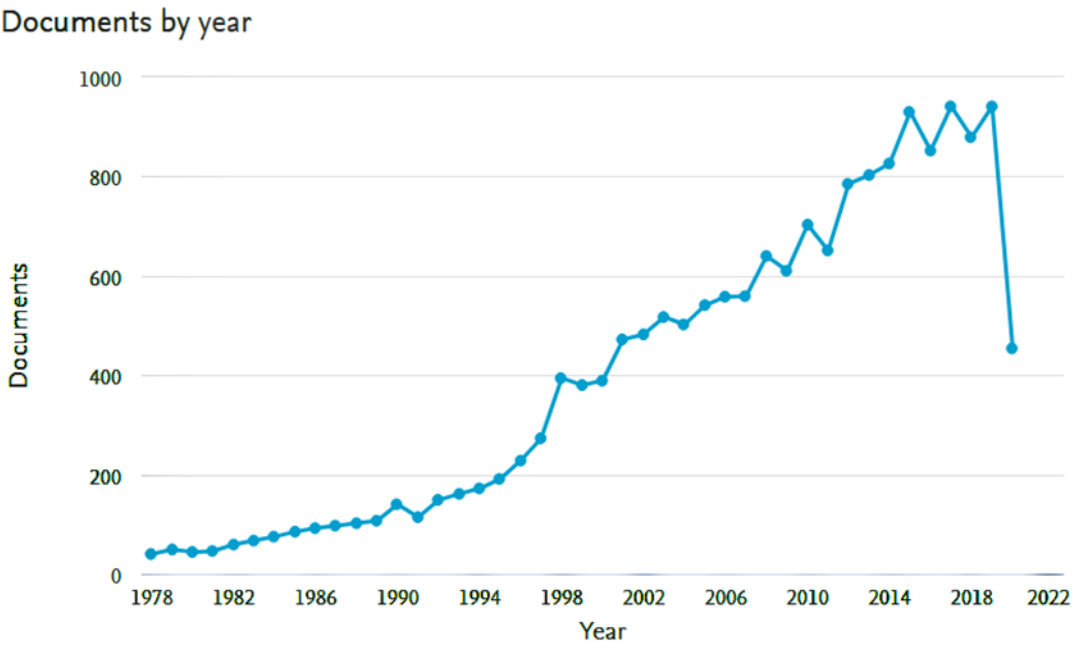

Figure 5-1 Number of published documents per year, with the phrase 'uncoupling proteins' in the abstract, title and keywords. The graph is obtained from Scopus analysis website Ref. 266

To treat obesity, energy intake should be less than expenditure and increasing uncoupling activity causes the cell to consume more energy in order to generate the same/required amount of ATP. Several chemical agents induce mitochondrial uncoupling; however, these agents have

serious side effects on human health [45]. Activation of UCP1 has shown promising effects in the regulation of body weight in mice and human studies and, contrary to chemical anti-obesity drugs, might have additional metabolic benefits [45]. The physiological functions of UCPs 2-5 are less well defined than that of UCP1. But several studies show that UCP2 can regulate/balance ROS formation [45, 183, 267, 268]. Furthermore, expression of UCP2 in tumor cells makes them more resistant to anti-tumor agents [254]. It has been reported in different studies that inhibition, down regulation and decreased expression levels of UCP2 in cancer cells result in increased sensitivity of tumors to various chemotherapeutic agents [254].

Despite their important potential as therapeutic targets, UCPs' structure and mechanism of activation are not clear. Even though the NMR structures of UCP1 [69] and UCP2 [70] have been reported, but there is not overall agreement on the functional structures of UCPs and their state of oligomerization [59, 255]. Inconsistencies about UCPs' mechanism of function, structure and primary substrates mostly originate from differences in protein preparation and functionalization methods [59, 255].

With the goal of making a contribution to the current knowledge on UCPs, the current study reports new findings on the structural features and mechanistic aspects of UCP2 proton transport at the molecular and atomic levels.

Experimental and computational results from this thesis support self-association of UCPs into tetramers, as dimers of dimeric units, in lipidic environments. The study highlights the residues that play key roles in maintaining UCP2 structure and function, such as those involved in subunit association or essential residues in proton transport activation and inhibition. The research also demonstrates the structural changes that the protein and its surrounding bilayer undergo upon oligomerization and reveals the importance of the subunit's internal cavity conformation and inter-

and intra-subunit helix-helix interactions/associations during proton/anion transport activity of UCP2. Finally, by focusing on one of the main constituents of the alternating access mechanism (the matrix network, explained in the Introduction section), the main outcome of this thesis is summed up in a molecular model describing proton transport by tetrameric UCPs. This model can provide insights into the regulation of uncoupling activity in biological environments.

5.1 UCP2 self-associates as a pseudosymmetric dimer of dimers in model lipid membranes

Oligomerization of MCF members in the IMM has long been a subject of controversy [66, 68, 116]. As mentioned in the Introduction section, the molecular states of proton transporters of the MCF has been debated among researchers in the field and UCPs are not an exception in this regard. In the case of UCPs, the existence of monomeric [83] and dimeric [65] functional states have been suggested previously by some researchers and the tetrameric functional state has been suggested by our group [30, 68]. This thesis, using both experimental and computational methodologies and approaches, provides additional support and evidence for the tendency of UCP2 to form tetramers (dimer of dimers) in model lipid membranes. We observed that regardless of the starting molecular state of UCP2 used for reconstitution, the protein spontaneously assembles into tetrameric complexes when reconstituted in lipid membranes (Figures 3-1 and 3-2).

The structure of the UCP2 tetramer in a PC bilayer was also characterized using computational methods, which revealed that this functional tetramer is likely a pseudosymmetric/asymmetric dimer of dimers capable of inducing asymmetry in the bilayer leaflets (Figures 3-7 and 3-8). Each dimeric unit (in a UCP2 tetramer) was stabilized via formation of salt-bridges and hydrogen bonds between the two monomers; however, no salt-bridges were formed between the two dimeric units within the tetramer. Furthermore, the energy needed to

dissociate the dimers to monomers was higher than that needed to dissociate the tetramers to dimers. Our data suggest that UCP2 is a dimer of dimers with two different interfaces, one loose interface between the two dimers and one tight interface between the two monomers within the dimeric unit, the findings of the current thesis are consistent with our original reports about the possibility of UCPs to exist as dimer of dimers [68]. Formation of salt-bridges between monomeric subunits of MPs is a critical factor in stabilizing oligomers and their ability to self-oligomerize without the need for lipids [114]. In other words, the presence of two salt-bridges stabilize the dimeric units, independent of lipids. Conversely, lack of salt-bridges between the dimeric units result in a loose association that may require lipids at the interface to stabilize. This might suggest that UCPs could exist as dimeric units in the membrane with capability to further oligomerize to form a functional tetramer. Equilibrium between two oligomeric states in response to factors such as alteration of membrane lipidic composition have been reported previously for other proteins such as bacterial sugar transporter SemiSWEET [114]. Furthermore, it has been reported that the presence of lipids such as CL in the model membranes could promote the ion transport ability of UCP2 (and other UCPs) [80]. Thus, changing the membrane lipid composition is a possible signal that could regulate the abundance of the functional tetrameric UCP2.

Computational conformational analysis of the asymmetric UCP2 tetramer showed a biphasic molecular structure (Figure 3-5), meaning that the monomers within the dimeric units have comparable (but not necessarily equivalent) conformations with their cavities exposed to one side of the membrane, and the dimeric units have opposite orientations. For example, the two monomers within one dimeric unit had cavities open to the matrix (matrix state), while the two monomers in the other dimeric unit had cavities open to the IMS (cytoplasmic state). This

tetrameric structure implies a cooperative interconnection between the two dimeric units where the conformational of one unit could impact the conformational changes of other units.

To validate our experimental methods, and to evaluate the oligomeric state of other MCF members we purified AAC as a mixture of monomers and dimers using the same methods as were used for UCP2, and observed that reconstitution did not induce oligomerization as was the case with UCPs (Figure 3-1). We also applied similar computational analyses to both proteins to compare the structural features of UCP2 and AAC; these proteins behaved differently, supporting the experimental results.

To observe the structure of UCPs in lipid membranes by experimental methods in the future, these proteins can be analyzed by mass spectroscopy techniques [115]. Recent advances in this technique allow for the study of specific and nonspecific lipid interactions with proteins in order to determine the role of lipids in inducing oligomerization in cell membrane mimics [115]. Furthermore to evaluate the role of specific lipid species on oligomerization (such as CL, which is proposed to play a significant role in oligomerization of MCF members), UCPs could be expressed in bacteria with specific lipid deficiencies such as CL deficient *E. coli* [114]. Such strains provide the opportunity to better control the lipid environment and compare the impact of presence and absence of these molecules on oligomerization.

UCP proteoliposomes could also be studied by atomic force microscopy (AFM) in imaging mode [269] in the future. AFM is able to scan surfaces with sub-nanometer resolution, thus can visualize protein folding, oligomeric states, and height [269]. Human aquaporin 1 (six TM helices) is an example of a MP for which the tetrameric structure has been visualized using AFM [270].

5.2 UCP2 transports protons as a biphasic dimer of dimers

Fatty acid-activated proton transport is a well-defined function of all UCPs [80]. But the exact mechanism of UCP activation by fatty acids and inhibition by purine nucleotides is not universally agreed upon. Various research groups have proposed different models of proton transport by UCPs (see section 1.6.1) [61, 62, 72, 73]. The existence of multiple models may have arisen because of dissimilar experimental approaches and sometimes incomplete interpretation of the data [255]. The alternating access mechanism model (Figure 1-3) was proposed as a common mechanism of non-regulated proton transport by all MCF members [51]. A recent whole cell patch clamp study on mitoplasts from various mouse tissues demonstrated that UCP1 and AAC are both fatty acid-activated proton transporters of the IMM and unequally responsible for regulated proton transport in mitochondria, with UCP1 as the main transporter [90]. Patch clamp analyses also supported the alternating access mechanism in both proteins and suggested that alternation between cytoplasmic and matrix states occurs in parallel to shuttling of fatty acids across the protein's interior [90].

In the current study, we examined the importance of one of the main functional elements of the alternating access model - the matrix network - by investigating the structure and proton transport activity of UCP2 and eleven mutant versions. Extensive structural evaluation of UCP2 and the mutants revealed a more comprehensive matrix network than had been previously proposed, consisting of five (instead of three) salt-bridges (D35-K141, D138-K239, D138-R88, D236-R185, D236-R279), which was not only able to act as an electric filter to prevent basal proton leak across UCP2, but also could hold the helices close to one another on the matrix side giving rise to the V shape (conical) structure of the cytoplasmic state. Both of these roles agree with the proposed role of the matrix network in the alternating access mechanism [51].

Consistent with the apparent pseudosymmetrical structure of UCP2, we observed that monomeric subunits of the UCP2 tetramer do not undergo similar changes during the transport cycle (Figures 3-4, A-4-3, and Table 4-1); however, their change of conformation could impact one another. This observation together with the biphasic tetrameric conformation of the protein (Figure 3-5), led us to suggest a *biphasic molecular model* for the proton transport function of tetrameric UCPs (Figure 4-8). Based on this model, each monomer is able to separately transport protons via the alternating access mechanism, with each monomer within a dimeric unit in the similar stages of transport. At the same time, conformational changes of one dimeric pair can influence the active/inactive conformation of the other pair. Considering the loose interface between the two dimeric pairs, we suggest that dimerization of dimers might represent a higher level of regulation of proton transport by UCPs.

The study also provides more insight into the inhibition of UCPs by purine nucleotides (Figure 4-7 and Table 4-1), by characterizing the protein residues interacting with ATP and comparing it to previous studies by other researchers [63, 74, 271]. We showed that despite some suggestions by other researchers [63], ATP could block the internal cavity of the monomeric subunits (Figure 4-7), thereby not only preventing the movement of fatty acids across the protein but also neutralizing key arginine residues that might play critical roles in attracting fatty acids towards the protein.

One approach to test the proposed model and advance our knowledge about the structure and function of UCPs in continuation of this work is to neutralize the suggested key amino acids by point mutations and to re-evaluate the structure and function. Mutations could be targeted to neutralize the three arginine residues in the vicinity of the matrix network (R88, R185 and R279 for UCP2) or residues involved in the electrostatic interaction of the monomers within a dimeric

pair, such as K164 and E264 for UCP2. Design and synthesis of oligomerization interfering peptides [272] is another approach which could be used to prevent oligomerization of UCPs in liposomes. This method would provide the opportunity to analyze ion transport by the monomeric state and to study the impact of oligomerization on the proteins' function.

To support and complete the proposed model and to expand it to the anionic substrates of UCP2, chloride transport of UCP2 and the eleven mutants (Chapter 4) should be studied in future, and the observed trend should be compared with proton transport results. These types of analyses should reveal whether anions and protons are transported using the same path and provide a deeper understanding of the general mechanism of ion transport in UCPs.

Finally, to gain a better knowledge about the regulation of proton transport, UCPs could be reconstituted together with other proton transporters of the MCF such as AAC to investigate the mutual impact of the two proteins on proton transport function of one another. Mutual regulatory impact of AAC and UCP was suggested previously as a mechanism for controlling energy in the cells [90].

Despite several advancements in understanding the structure and function of UCPs in recent years, there is still a considerable lack of consensus among researchers in the field. To achieve a commonly accepted model for the molecular and physiological behavior of UCPs in mitochondria, a comprehensive study is required to correlate and rectify the various models and proposed structures. Historically, the source of UCPs used in biochemical and biophysical studies have been diverse, as UCPs were expressed and analyzed in different biological systems including bacteria, yeast, mammalian cell lines and animal tissues. Although time consuming, a multi-component research project will provide a better insight about the molecular state and function of UCPs in different systems and gives researchers an opportunity to compare results from previous reports.

APPENDICES

Appendix 1 (Chapter 1 appendix)

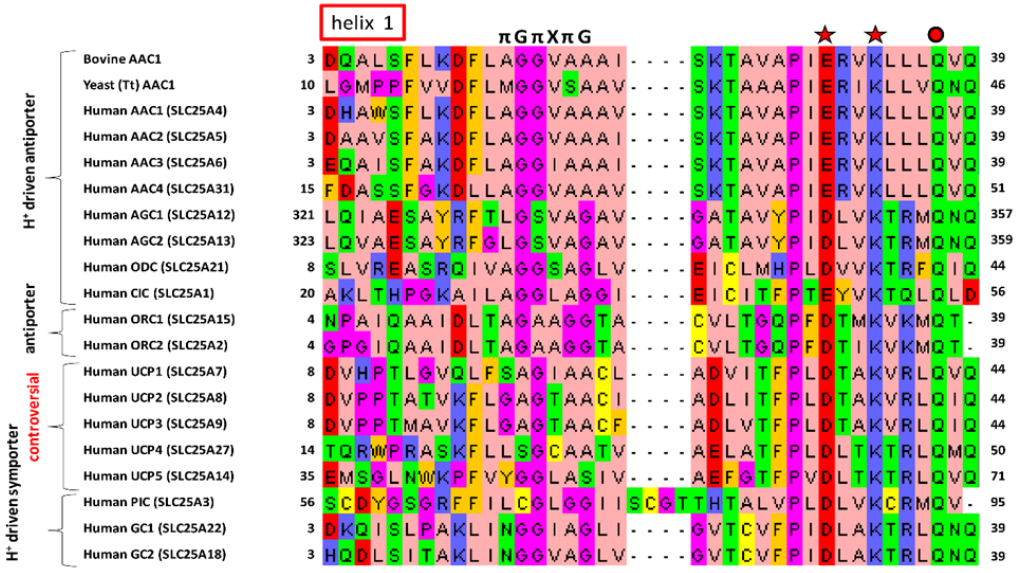

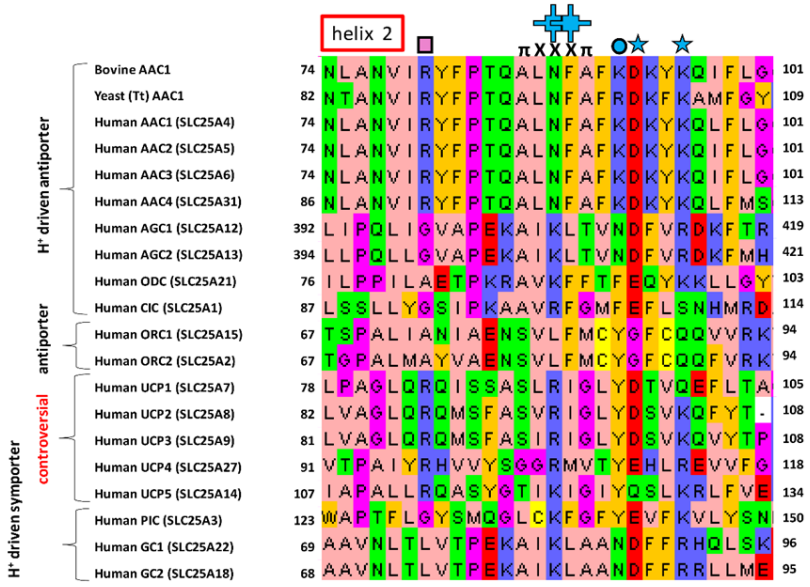

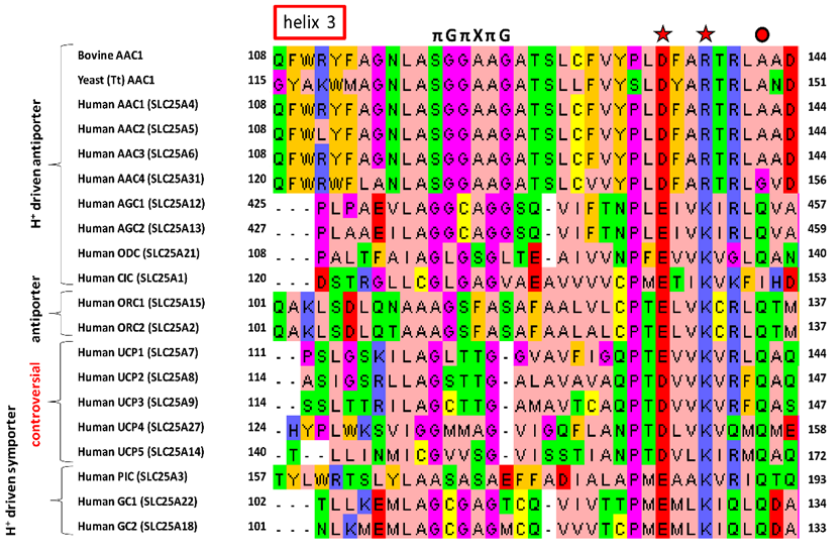
helix 3
πGπXπG
H+ driven antiporter
antiporter
controversial
H+ driven symporter
Bovine AAC1 108 QFWRYFAGNLASGGAAGATSLCFVYPLDFARTRLAAD 144
Yeast (Tt) AAC1 115 GYAKWMAGNLASGGAAGATSLLFVYSLDYARTRLAND 151
Human AAC1 (SLC25A4) 108 QFWRYFAGNLASGGAAGATSLCFVYPLDFARTRLAAD 144
Human AAC2 (SLC25A5) 108 QFWLYFAGNLASGGAAGATSLCFVYPLDFARTRLAAD 144
Human AAC3 (SLC25A6) 108 QFWRYFAGNLASGGAAGATSLCFVYPLDFARTRLAAD 144
Human AAC4 (SLC25A31) 120 QFWRWFLANLASGGAAGATSLCVVYPLDFARTRLGVD 156
Human AGC1 (SLC25A12) 425 ...PLPAEVLAGGCAGGSQ-VIFTNPLEIVKIRLQVA 457
Human AGC2 (SLC25A13) 427 ...PLAAEILAGGCAGGSQ-VIFTNPLEIVKIRLQVA 459
Human ODC (SLC25A21) 108 ...PALTFAIAGLGSGLTE-AIVVNPFEVVKVGLQAN 140
Human CIC (SLC25A1) 120 ...DSTRGLLCGLGAGVAEAVVVVCPMETIKVKFIHD 153
Human ORC1 (SLC25A15) 101 QAKLSDLQNAAAGSFASAFAALVLCPTELVKCRLQTM 137
Human ORC2 (SLC25A2) 101 QAKLSDLQTAAAGSFASAFAALALCPTELVKCRLQTM 137
Human UCP1 (SLC25A7) 111 ..PSLGSKILAGLTTG-GVAVFIGQPTEVVKVRLQAQ 144
Human UCP2 (SLC25A8) 114 ..ASIGSRLLAGSTTG-ALAVAVAQPTDVVKVRFQAQ 147
Human UCP3 (SLC25A9) 114 ..SSLTTRILAGCTTG-AMAVTCAQPTDVVKVRFQAS 147
Human UCP4 (SLC25A27) 124 .HYPLWKSVIGGMMAG-VIGQFLANPTDLVKVQMQME 158
Human UCP5 (SLC25A14) 140 .T..LLINMICGVVSG-VISSTIANPTDVLKIRMQAQ 172
Human PIC (SLC25A3) 157 TYLWRTSLYLAASASAEFFADIALAPMEAAKVRIQTQ 193
Human GC1 (SLC25A22) 102 ...TLLKEMLAGCGAGTCQ-VIVTTPMEMLKIQLQDA 134
Human GC2 (SLC25A18) 101 ...NLKMEMLAGCGAGMCQ-VVVTCPMEMLKIQLQDA 133

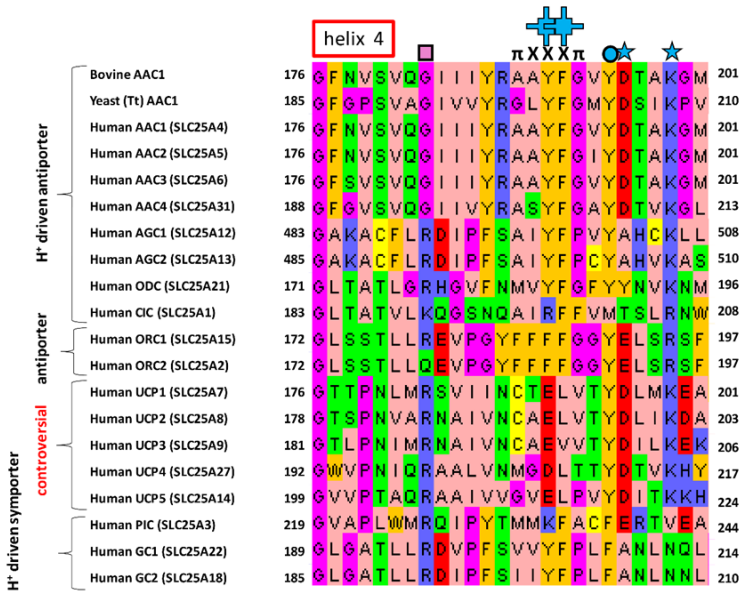
helix 4
πXXXπ
H+ driven antiporter
antiporter
controversial
H+ driven symporter
Bovine AAC1 176 GFNVSVQGIIIYRAAYFGVYDTAKGM 201
Yeast (Tt) AAC1 185 GFGPSVAGIVVYRGLYFGMYDSIKPV 210
Human AAC1 (SLC25A4) 176 GFNVSVQGIIIYRAAYFGVYDTAKGM 201
Human AAC2 (SLC25A5) 176 GFNVSVQGIIIYRAAYFGIYDTAKGM 201
Human AAC3 (SLC25A6) 176 GFSVSVQGIIIYRAAYFGVYDTAKGM 201
Human AAC4 (SLC25A31) 188 GFGVSVQGIIVYRASYFGAYDTVKGL 213
Human AGC1 (SLC25A12) 483 GAKACFLRDIPFSAIYFPVYAHCKLL 508
Human AGC2 (SLC25A13) 485 GAKACFLRDIPFSAIYFPCYAHVKAS 510
Human ODC (SLC25A21) 171 GLTATLGRHGVFNMVYFGFYYNVKNM 196
Human CIC (SLC25A1) 183 GLTATVLKQGSNQAIRFFVMTSLRNW 208
Human ORC1 (SLC25A15) 172 GLSSTLLREVPGYFFFFGGYELSRSF 197
Human ORC2 (SLC25A2) 172 GLSSTLLQEVPGYFFFFGGYELSRSF 197
Human UCP1 (SLC25A7) 176 GTTPNLMRSVIINCTELVTYDLMKEA 201
Human UCP2 (SLC25A8) 178 GTSPNVARNAIVNCAELVTYDLIKDA 203
Human UCP3 (SLC25A9) 181 GTLPNIMRNAIVNCAEVVTYDILKEK 206
Human UCP4 (SLC25A27) 192 GWVPNIQRAALVNMGDLTTYDTVKHY 217
Human UCP5 (SLC25A14) 199 GVVPTAQRAAIVVGVELPVYDITKKH 224
Human PIC (SLC25A3) 219 GVAPLWMRQIPYTMMKFACFERTVEA 244
Human GC1 (SLC25A22) 189 GLGATLLRDVPFSVVYFPLFANLNQL 214
Human GC2 (SLC25A18) 185 GLGATLLRDIPFSIIYFPLFANLNNL 210

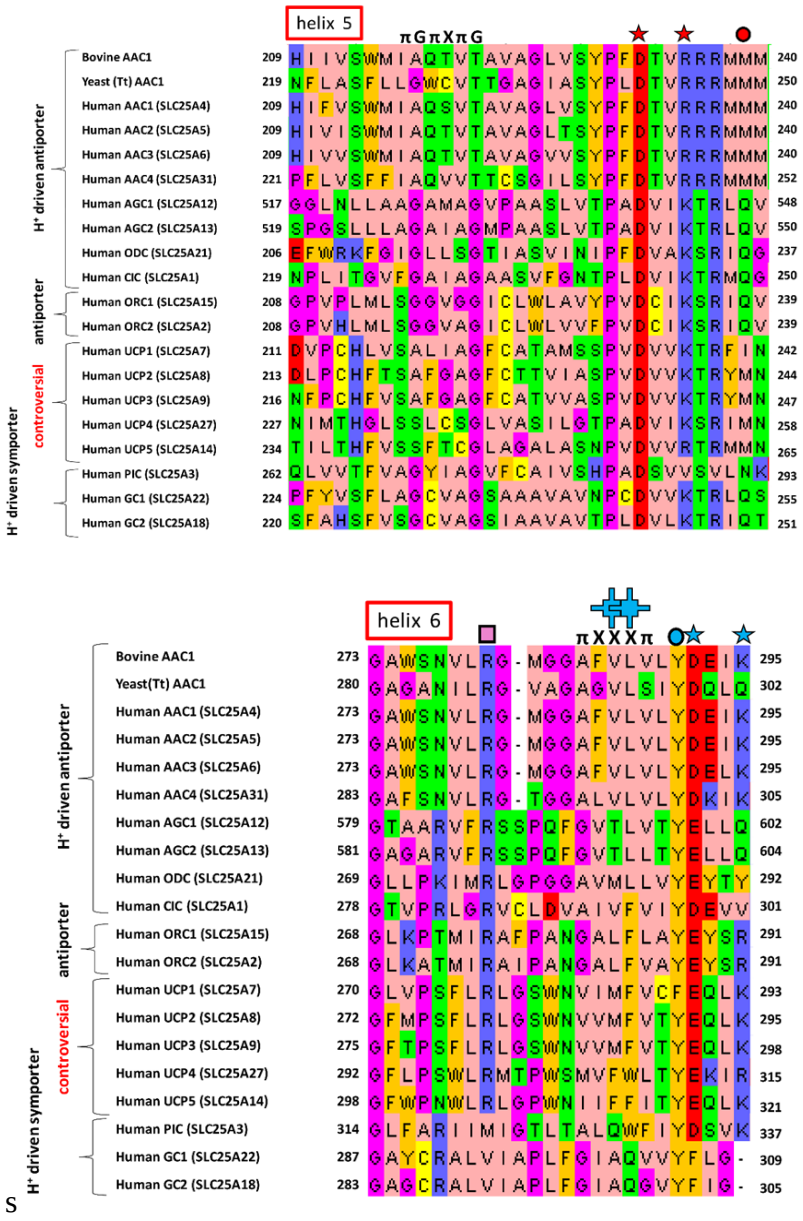

Figure A-1-1 Sequence alignment of selected proton transporters of the human MCF, with AAC1 from Bovine and yeast. Alignments were generated using Jalview. Amino acids are color coded as follow: hydrophobic (ILVAM) coral, aromatic (FWY) orange, positive (KHR) blue, negative (DE) red, hydrophilic (STNQ) green, conformationally special (PG) purple and cysteine (C) yellow. Residues involved in the matrix network (red star) and Q-brace (red circle), cytoplasmic network (blue star) and Y-brace (blue circle), bulky residues (blue cross), single binding site (purple square) and the small motifs can be distinguished by their relative signs on top of the columns. AAC: ADP/ATP carrier, AGC: aspartate/glutamate carrier, ODC: oxoadipate carrier, CIC: citrate carrier or tricarboxylate carrier, ORC: ornithine carrier, UCP: uncoupling protein, PIC: phosphate carrier, GC: glutamate carrier. Figure is generated by Jalview 2.11.0.

Appendix 2 (Chapter 2 appendix)

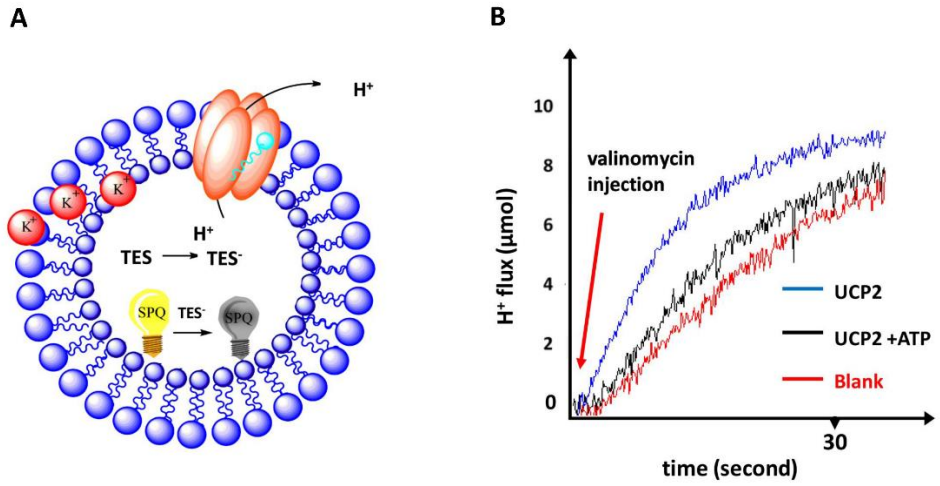

Figure A-2-1 Schematic view of an indirect fluorescence quenching assay used for measuring the rate of proton transport of UCPs in liposomes. A): The SPQ fluorescent dye trapped inside vesicles can be quenched by TES– anions. TES– anions are generated as a consequence of an increase in the internal pH. Valinomycin directs potassium ions into the liposomes resulting in an uneven charge distribution (inside positive) and osmotic imbalance across the lipid bilayer, which causes a fatty acid-dependent UCP-mediated proton efflux. Thus, the rate of proton transport is indirectly measured by the rate of quenching of the SPQ fluorescence signal. B): A typical result for measuring proton transport using the SPQ fluorescent quenching assay. UCP-mediated Proton transport in the absence and presence of its inhibitor ATP, and non-specific proton flux are shown for comparison. Figure generated by ChemBioDraw Ultra 14.0.

Appendix 3 (Chapter 3 appendix)

Table A-3-1 Salt-bridges formed in the oligomeric UCP2 systems. [a]

	Chain 1···Chain 2	
Dimer	K109	D202
	E112	K206
	K164	E46
	Chain 1···Chain 2	
Tetramer	K109	D202
	K164	E264
	Chain 3···Chain 4	
	K104	D202
	K164	E264

a) Chains 1, 2, 3 and 4 correspond to the blue, red, orange, and grey monomeric units shown in Figure A-3-7, respectively.

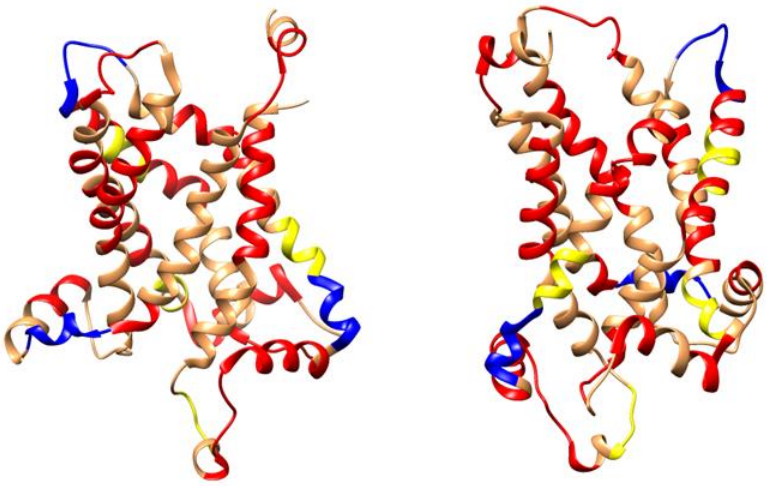

Figure A-3-1 The two interacting faces of UCP2 selected to form a dimer. The GXXXG, GXXXLXXG, and SmXXXSm (Sm = Gly, Ala, Ser, Thr) motifs, which promote oligomerization are shown in yellow, blue, and red, respectively. Figure generated by UCSF Chimera 1.13rc.

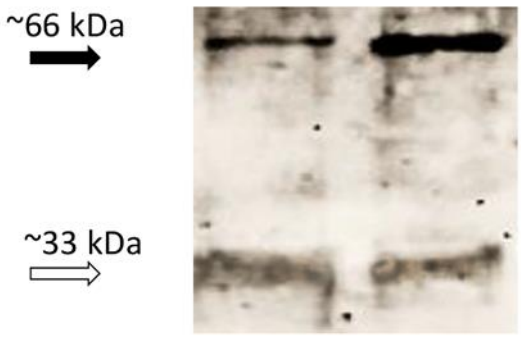

Figure A-3-2 Western blot analysis of AAC1 probed with α-AAC1 antibody confirms the co-presence of monomeric and dimeric states in OG.

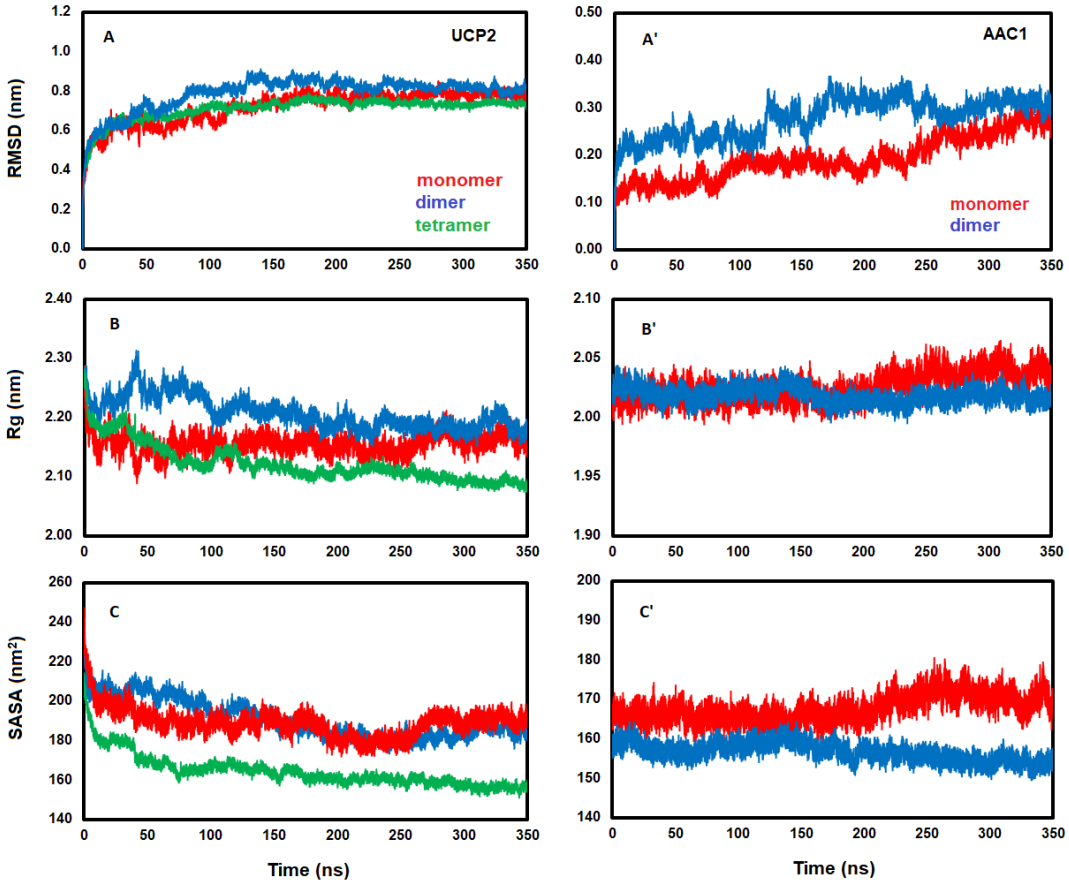

Figure A-3-3 (A – A′) Protein backbone RMSD, (B – B′) Rg, and (C – C′) SASA for UCP2 and AAC1 in phospholipid bilayer membrane over the course of MD simulation. Rg and SASA in oligomers are calculated per monomer.

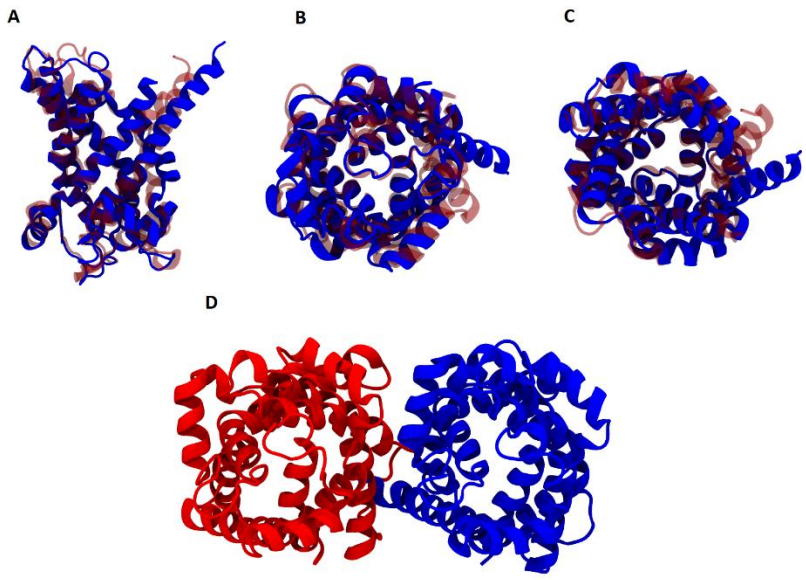

Figure A-3-4 Overlay of the AAC1 monomer (A-C) initial (PDB ID: 1OKC, red) and final (350 ns, blue) structures. (D) Final dimer structure. Figure generated by VMD 1.9.3.

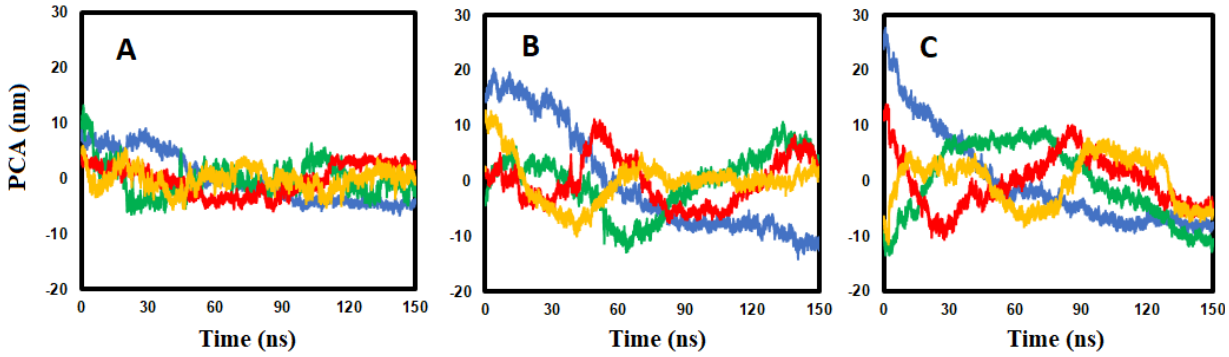

Figure A-3-5 PCA analyses for (A) monomeric, (B) dimeric, and (C) tetrameric UCP2 in POPC bilayer. Projection of the first 150 ns MD simulation trajectories on the first 4 eigenvectors [1st (blue), 2nd (green), 3rd (red), 4th (yellow)]

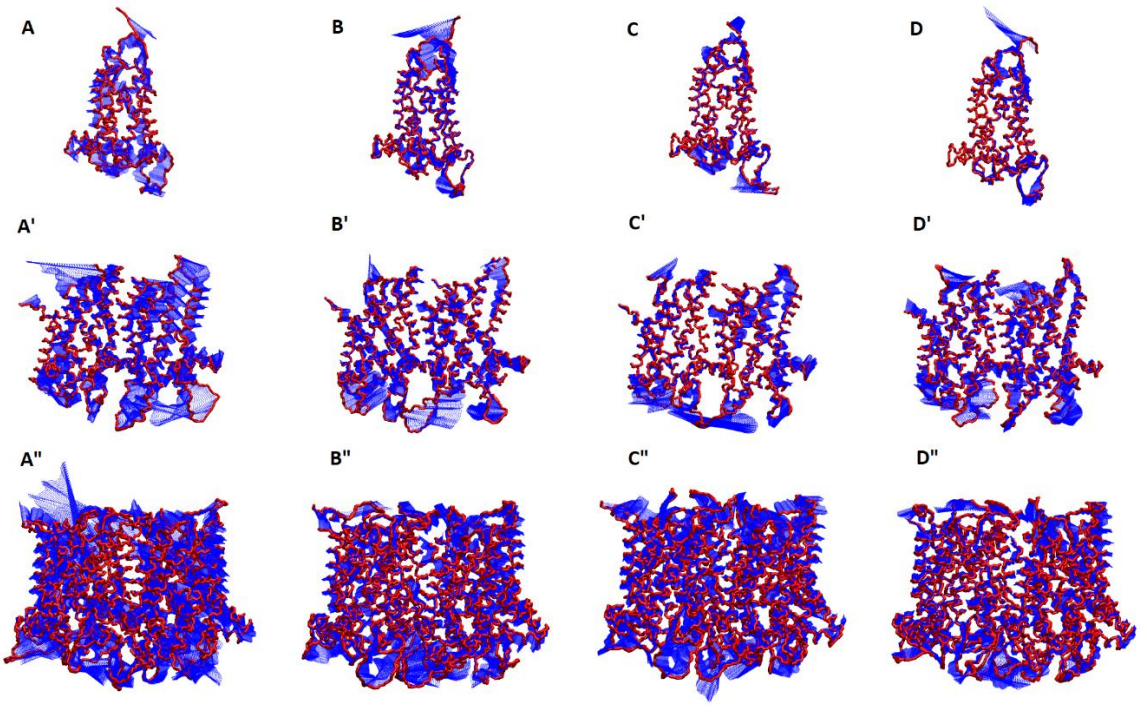

Figure A-3-6 Visualization of PCA: Projections of the first 150 ns MD simulations on the first four eigenvectors for the monomeric (A – D), dimeric (A′ – D′), and tetrameric (A″ – D″). Blue hatching represents the direction of motions. Figure generated by VMD 1.9.3.

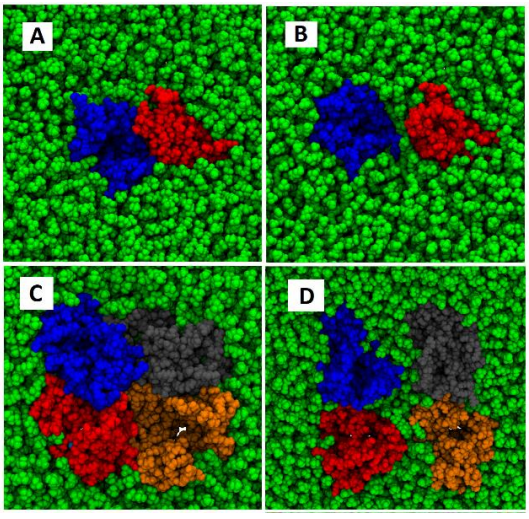

Figure A-3-7 Initial and final structures of the dimeric (A-B) and tetrameric (C-D) UCP2 used for the dissociation process. Dissociation of dimer to its constituting monomers needs higher energy (18.5 kcal more) than dissociation of tetramer to its constituting dimers, suggesting tighter packing of monomers within the dimer compared to the two dimers within the tetramer. Chains 1, 2, 3 and 4 are shown in blue, red, orange and grey, respectively. Figure generated by VMD 1.9.3.

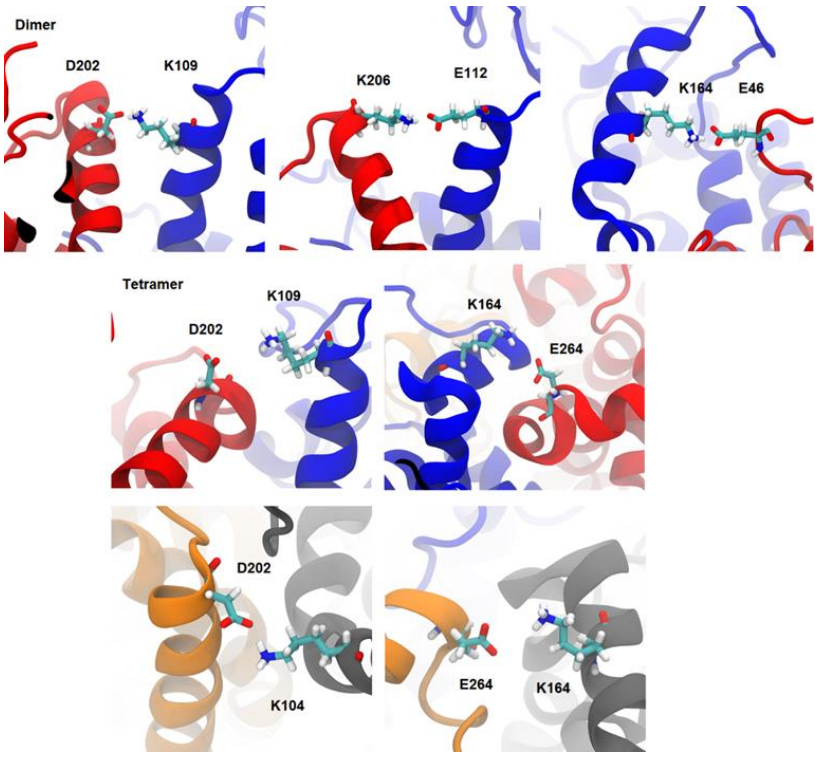

Figure A-3-8 Main salt-bridges between the neighboring UCP2 units in a dimer of UCP2 (top panel), and between chains 1 and 2 (middle panel), and chains 3 and 4 (bottom panel) in a tetrameric UCP2. Chains 1, 2, 3, and 4 are shown in blue, red, grey, and orange, respectively. Figure generated by VMD 1.9.3.

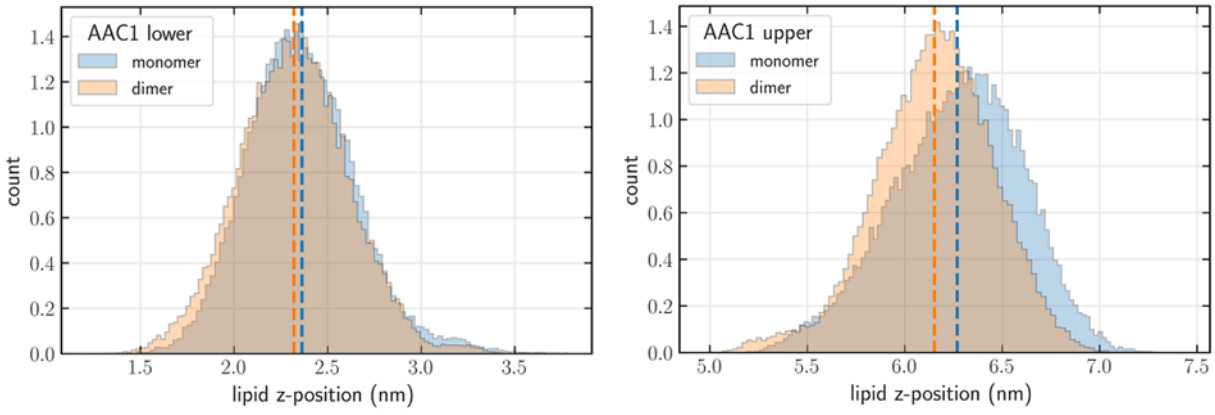

Figure A-3-9 Distribution of the lipid head groups (phosphate) in lower (left, matrix side) and upper (right; cytoplasmic side) leaflets for monomeric and dimeric AAC1. As is seen, the distribution is different depending on the leaflet and oligomerization state of the protein.

Appendix 4 (Chapter 4 appendix)

Table A-4-1 Proton transport rate of UCP2 and its mutants in the absence and presence of 500 µM ATP. All the units are in µmol of proton/min/mg protein

protein	proton transport rate (no ATP)	proton transport rate (500 µM ATP)
UCP2	5.24 ± 0.09	1.17 ± 0.09
D35N	10.43 ± 0.16	3.91 ± 0.01
K141Q	8.53 ± 0.12	3.25 ± 0.32
D138N	13.83 ± 1.06	5.64 ± 0.23
K239Q	11.38 ± 0.81	4.34 ± 0.20
D236N	10.62 ± 0.94	4.90 ± 0.28
K38Q	13.33 ± 0.70	6.03 ± 0.54
2DN	16.14 ± 0.93	7.67 ± 0.77
2KQ	12.41 ± 1.29	4.94 ± 0.35
3DN	31.26 ± 0.95	15.97 ± 0.55
3KQ	11.82 ± 0.48	5.21 ± 0.95
Hexamutant	6.21 ± 0.06	1.89 ± 0.11

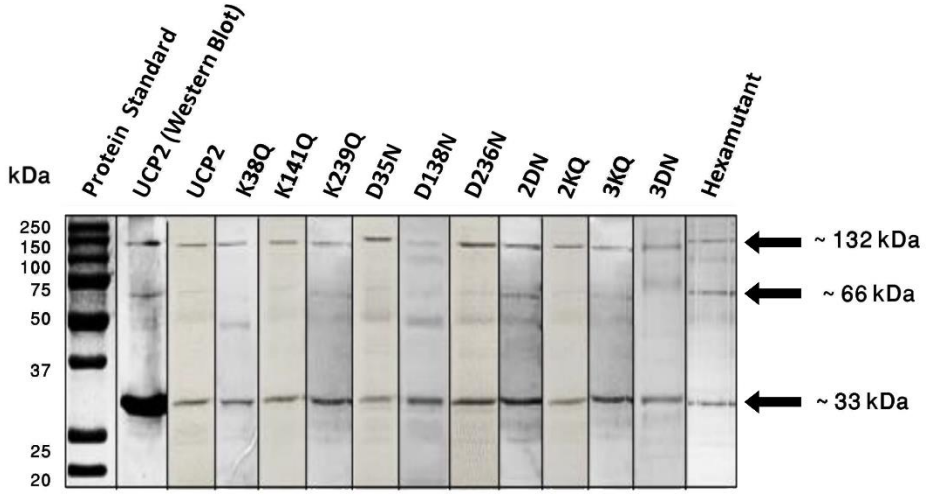

Figure A-4-1 Western Blot and Coomassie blue stained semi-native SDS-PAGE analysis of purified monomeric and oligomeric UCP2 and its mutants in 1% OG

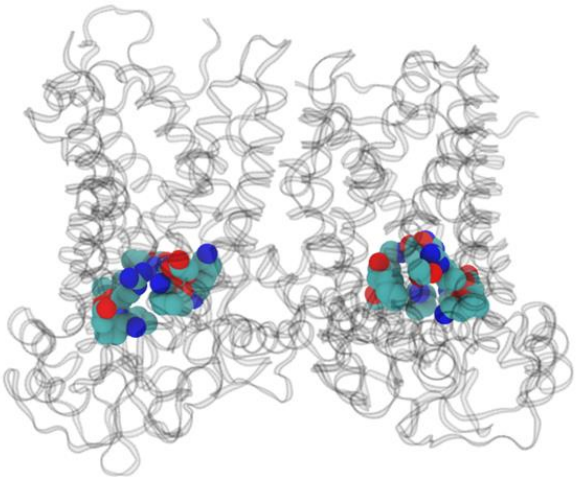

Figure A-4-2 Sideview of the overall structure of tetrameric UCP2 and relative position of matrix network residues. Carbon, nitrogen, and oxygen atoms are shown in cyan, blue, and red, respectively. Figure generated by VMD 1.9.3.

A

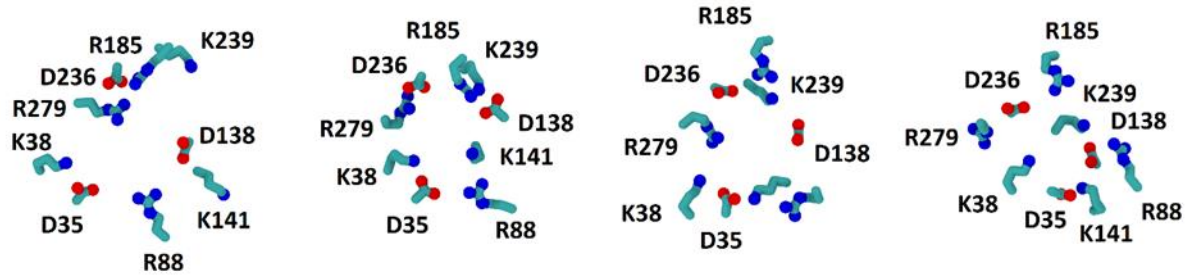

B

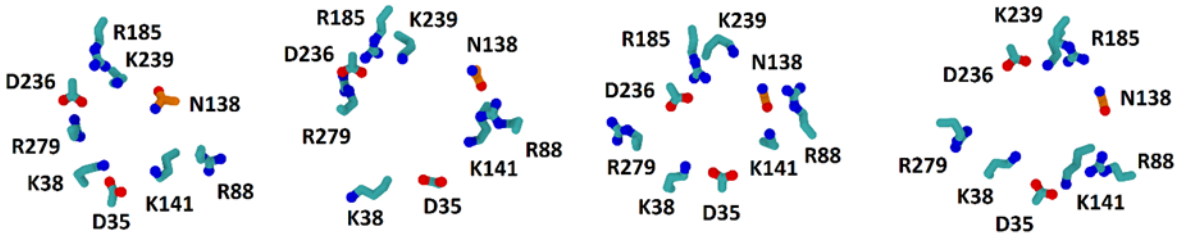

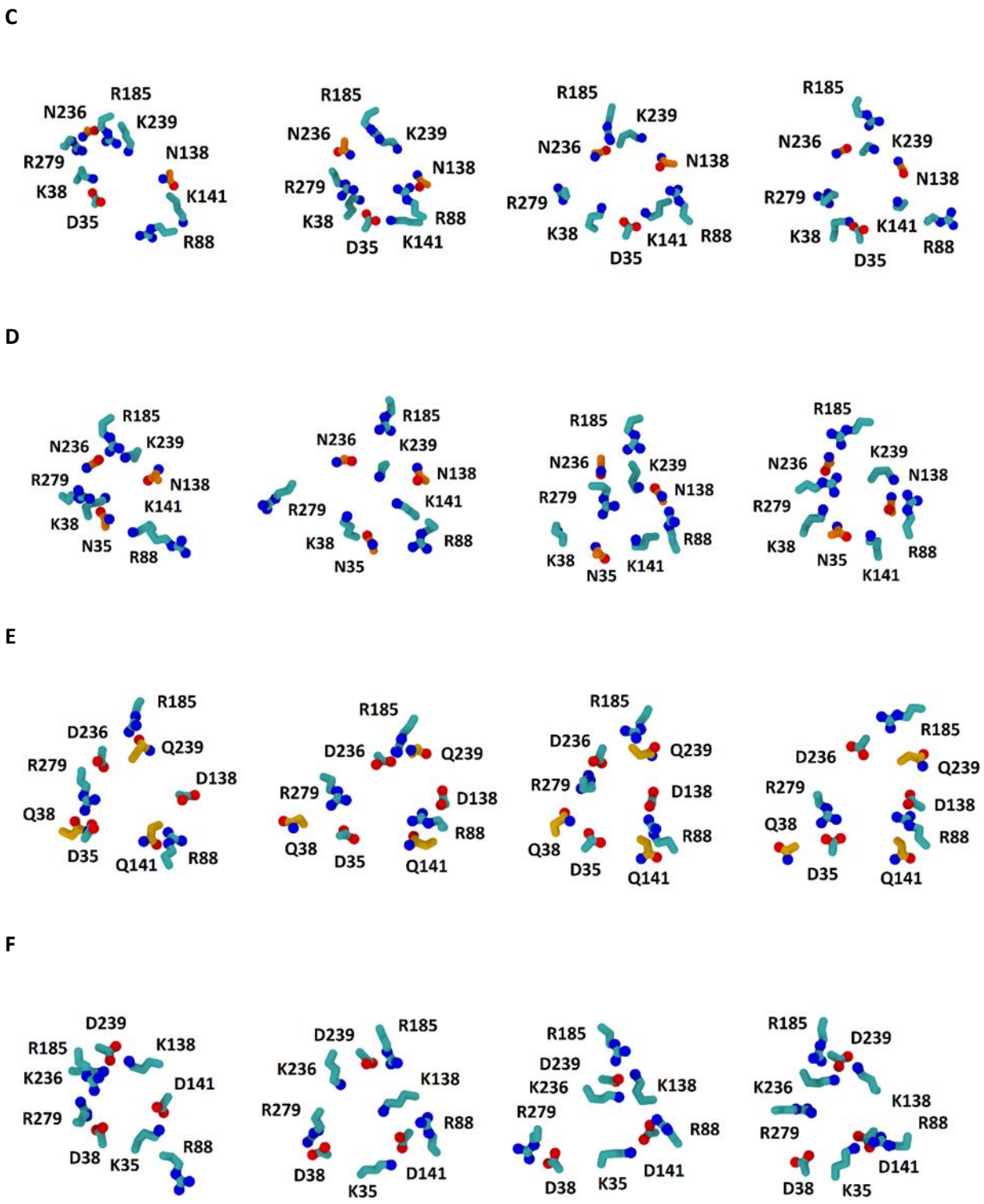

Figure A-4-3 Top view (from the cytoplasmic side), of the final structure of (A) UCP2, (B) DN, (C) 2DN, (D) 3DN, (E) 3KQ, and (F) Hexamutant subunits. D→N and K→Q mutations are shown in orange and yellow, respectively. Protein helices, backbone and hydrogen atoms omitted for clarity. Figure generated by VMD 1.9.3.

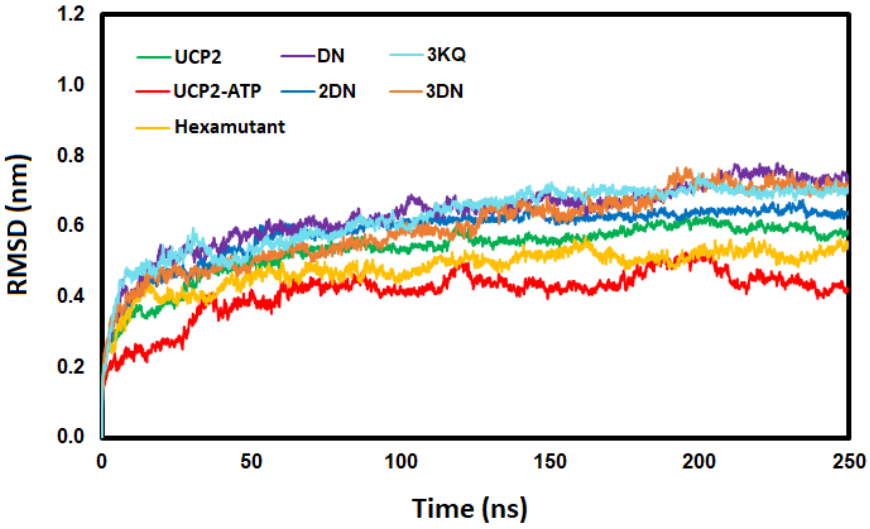

Figure A-4-4 RMSD of the backbone atoms for the tetrameric UCP2 systems in POPC bilayer.

REFERENCES

1. Vakifahmetoglu-Norberg, H., A.T. Ouchida, and E. Norberg, *The role of mitochondria in metabolism and cell death.* Biochemical and Biophysical Research Communications, 2017. **482**(3): p. 426
2. Kühlbrandt, W., *Structure and function of mitochondrial membrane protein complexes.* BMC Biology, 2015. **13**(1): p. 89
3. Llopis, J., et al., *Measurement of cytosolic, mitochondrial, and Golgi pH in single living cells with green fluorescent proteins.* Proceedings of the National Academy of Sciences, 1998. **95**(12): p. 6803
4. Jakobs, S., et al., *Light Microscopy of Mitochondria at the Nanoscale.* Annual Review of Biophysics, 2020. **49**: p.289
5. Kozjak-Pavlovic, V., *The MICOS complex of human mitochondria.* Cell and Tissue Research, 2017. **367**(1): p. 83
6. Wolf, D.M., et al., *Individual cristae within the same mitochondrion display different membrane potentials and are functionally independent.* The European Molecular Biology Organization journal, 2019. **38**(22): p. e101056
7. Krebs, H.A. and W.A. Johnson, *The role of citric acid in intermediate metabolism in animal tissues.* Enzymologia, 1937. **4**: p. 148
8. Osellame, L.D., T.S. Blacker, and M.R. Duchen, *Cellular and molecular mechanisms of mitochondrial function.* Best Practice & Research Clinical Endocrinology & Metabolism, 2012. **26**(6): p. 711
9. Krebs, H., *The tricarboxylic acid cycle,* Chemical Pathways of Metabolism, 1954. p. 109
10. Reid, R., J. Moyle, and P. Mitchell, *Synthesis of adenosine triphosphate by a protonmotive force in rat liver mitochondria.* nature, 1966. **212**(5059): p. 257
11. Vinothkumar, K.R., J. Zhu, and J. Hirst, *Architecture of mammalian respiratory complex I.* Nature, 2014. **515**(7525): p. 80
12. Cogliati, S., J.A. Enriquez, and L. Scorrano, *Mitochondrial cristae: where beauty meets functionality.* Trends in Biochemical Sciences, 2016. **41**(3): p. 261
13. Gu, J., et al., *The architecture of the mammalian respirasome.* Nature, 2016. **537**(7622): p. 639
14. Reyes-Galindo, M., et al., *Mitochondrial respirasome works as a single unit and the cross-talk between complexes I, III2 and IV stimulates NADH dehydrogenase activity.* Biochimica et Biophysica Acta - Bioenergetics, 2019. **1860**(8): p. 618
15. Boyer, P.D., *Energy, life, and ATP (Nobel lecture).* Angewandte Chemie International Edition, 1998. **37**(17): p. 2296
16. Davies, K.M., et al., *Structure of the yeast F1Fo-ATP synthase dimer and its role in shaping the mitochondrial cristae.* Proceedings of the National Academy of Sciences, 2012. **109**(34): p. 13602
17. Sena, L.A. and N.S. Chandel, *Physiological roles of mitochondrial reactive oxygen species.* Molecular Cell, 2012. **48**(2): p. 158
18. Ott, M., et al., *Mitochondria, oxidative stress and cell death.* Apoptosis : An International Journal on Programmed Cell Death, 2007. **12**(5): p. 913
19. Echtay, K.S., et al., *Uncoupling proteins: Martin Klingenberg's contributions for 40 years.* Archives of Biochemistry and Biophysics, 2018. **657**: p. 41

20. Busiello, R.A., S. Savarese, and A. Lombardi, *Mitochondrial uncoupling proteins and energy metabolism.* Frontiers in Physiology, 2015. **6**: p. 36
21. Jastroch, M., et al., *Mitochondrial proton and electron leaks.* Essays in Biochemistry, 2010. **47**: p. 53
22. Heaton, G.M., et al., *Brown-adipose-tissue mitochondria: photoaffinity labelling of the regulatory site of energy dissipation.* European Journal of Biochemistry, 1978. **82**(2): p. 515
23. Lin, C. and M. Klingenberg, *Isolation of the uncoupling protein from brown adipose tissue mitochondria.* Federation of European Biochemical Societies Letters, 1980. **113**(2): p. 299
24. Fleury, C., et al., *Uncoupling protein-2: a novel gene linked to obesity and hyperinsulinemia.* Nature Genetics, 1997. **15**(3): p. 269
25. Gimeno, R.E., et al., *Cloning and characterization of an uncoupling protein homolog: a potential molecular mediator of human thermogenesis.* Diabetes, 1997. **46**(5): p. 900
26. Boss, O., et al., *Uncoupling protein-3: a new member of the mitochondrial carrier family with tissue-specific expression.* Federation of European Biochemical Societies Letters, 1997. **408**(1): p. 39
27. Vidal-Puig, A., et al., *UCP3: an uncoupling protein homologue expressed preferentially and abundantly in skeletal muscle and brown adipose tissue.* Biochemical and Biophysical Research Communications, 1997. **235**(1): p. 79
28. Mao, W., et al., *UCP4, a novel brain-specific mitochondrial protein that reduces membrane potential in mammalian cells.* Federation of European Biochemical Societies Letters, 1999. **443**(3): p. 326
29. Sanchis, D., et al., *BMCP1, a novel mitochondrial carrier with high expression in the central nervous system of humans and rodents, and respiration uncoupling activity in recombinant yeast.* The Journal of Biological Chemistry, 1998. **273**(51): p. 34611
30. Hoang, T., et al., *A biophysical study on molecular physiology of the uncoupling proteins of the central nervous system.* Bioscience Reports, 2015. **35**(4).
31. Nicholls, D.G., *Brown adipose tissue mitochondria.* Biochimica et Biophysica Acta - Reviews on Bioenergetics, 1979. **549**(1): p. 1
32. Hoang, T., et al., *Role of positively charged residues of the second transmembrane domain in the ion transport activity and conformation of human uncoupling protein-2.* Biochemistry, 2015. **54**(14): p. 2303
33. Jezek, P. and K. Garlid, *New substrates and competitive inhibitors of the Cl-translocating pathway of the uncoupling protein of brown adipose tissue mitochondria.* The Journal of Biological Chemistry, 1990. **265**(31): p. 19303
34. Vozza, A., et al., *UCP2 transports C4 metabolites out of mitochondria, regulating glucose and glutamine oxidation.* Proceedings of the National Academy of Sciences, 2014. **111**(3): p. 960
35. Baffy, G., *Mitochondrial uncoupling in cancer cells: Liabilities and opportunities.* Biochimica et Biophysica Acta, 2017. **1858**(8): p. 655
36. Ruiz-Ramirez, A., et al., *Cell Death and Heart Failure in Obesity: Role of Uncoupling Proteins.* Oxidative Medicine and Cellular Longevity, 2016. 9340654.
37. Jia, P., et al., *Uncoupling protein 1 inhibits mitochondrial reactive oxygen species generation and alleviates acute kidney injury.* EBioMedicine, 2019. **49**: p. 331
38. Cadenas, S., *Mitochondrial uncoupling, ROS generation and cardioprotection.* Biochimica et Biophysica Acta - Bioenergetics, 2018. **1859**(9): p. 940

39. Andrews, Z.B., S. Diano, and T.L. Horvath, *Mitochondrial uncoupling proteins in the cns: in support of function and survival.* Nature Reviews Neuroscience, 2005. **6**(11): p. 829
40. Horvath, T.L., et al., *Brain uncoupling protein 2: uncoupled neuronal mitochondria predict thermal synapses in homeostatic centers.* Journal of Neuroscience, 1999. **19**(23): p. 10417
41. Waldeck-Weiermair, M., et al., *The contribution of UCP2 and UCP3 to mitochondrial Ca(2+) uptake is differentially determined by the source of supplied Ca(2+).* Cell Calcium, 2010. **47**(5): p. 433
42. Trenker, M., et al., *Uncoupling proteins 2 and 3 are fundamental for mitochondrial Ca2+ uniport.* Nature Cell Biology, 2007. **9**(4): p. 445
43. Trenker, M., et al., *UCP2/3—likely to be fundamental for mitochondrial Ca2+ uniport.* Nature Cell Biology, 2008. **10**(11): p. 1237
44. Brookes, P.S., et al., *UCPs--unlikely calcium porters.* Nature Cell Biology, 2008. **10**(11): p. 1235
45. Schumann, T., et al., *Solute Carrier Transporters as Potential Targets for the Treatment of Metabolic Disease.* Pharmacological Reviews, 2020. **72**(1): p. 343
46. Ruprecht, J.J. and E.R. Kunji, *The SLC25 Mitochondrial Carrier Family: Structure and Mechanism.* Trends in Biochemical Sciences, 2019. **45**(3): p. 244
47. Aquila, H., T.A. Link, and M. Klingenberg, *The uncoupling protein from brown fat mitochondria is related to the mitochondrial ADP/ATP carrier. Analysis of sequence homologies and of folding of the protein in the membrane.* The European Molecular Biology Organization Journal, 1985. **4**(9): p. 2369
48. Kunji, E.R. and A.J. Robinson, *The conserved substrate binding site of mitochondrial carriers.* Biochimica et Biophysica Acta - Bioenergetics, 2006. **1757**(9-10): p. 1237
49. Pebay-Peyroula, E., et al., *Structure of mitochondrial ADP/ATP carrier in complex with carboxyatractyloside.* Nature, 2003. **426**(6962): p. 39
50. Ruprecht, J.J., et al., *The molecular mechanism of transport by the mitochondrial ADP/ATP carrier.* Cell, 2019. **176**(3): p. 435
51. Robinson, A.J., C. Overy, and E.R. Kunji, *The mechanism of transport by mitochondrial carriers based on analysis of symmetry.* Proceedings of the National Academy of Sciences, 2008. **105**(46): p. 17766
52. Robinson, A.J. and E.R. Kunji, *Mitochondrial carriers in the cytoplasmic state have a common substrate binding site.* Proceedings of the National Academy of Sciences, 2006. **103**(8): p. 2617
53. Klingenberg, M., *The ADP, ATP shuttle of the mitochondrion.* Trends in Biochemical Sciences, 1979. **4**(11): p. 249
54. Jardetzky, O., *Simple allosteric model for membrane pumps.* Nature, 1966. **211**(5052): p. 969
55. Ruprecht, J.J., et al., *Structures of yeast mitochondrial ADP/ATP carriers support a domain-based alternating-access transport mechanism.* Proceedings of the National Academy of Sciences, 2014. **111**(4): p. E426
56. Ruprecht, J.J. and E.R. Kunji, *Structural changes in the transport cycle of the mitochondrial ADP/ATP carrier.* Current Opinion in Structural Biology, 2019. **57**: p. 135
57. Kunji, E.R. and A.J. Robinson, *Coupling of proton and substrate translocation in the transport cycle of mitochondrial carriers.* Current Opinion in Structural Biology, 2010. **20**(4): p. 440

58. Clamp, M., et al., *The jalview java alignment editor.* Bioinformatics, 2004. **20**(3): p. 426
59. Chipot, C., et al., *Perturbations of native membrane protein structure in alkyl phosphocholine detergents: a critical assessment of NMR and biophysical studies.* Chemical Reviews, 2018. **118**(7): p. 3559
60. Krauss, S., C.-Y. Zhang, and B.B. Lowell, *The mitochondrial uncoupling-protein homologues.* Nature Reviews Molecular Cell Biology, 2005. **6**(3): p. 248
61. Ježek, P., et al., *Fatty acid cycling mechanism and mitochondrial uncoupling proteins.* Biochimica et Biophysica Acta - Bioenergetics, 1998. **1365**(1-2): p. 319
62. Winkler, E. and M. Klingenberg, *Effect of fatty acids on H+ transport activity of the reconstituted uncoupling protein.* The Journal of Biological Chemistry, 1994. **269**(4): p. 2508
63. Berardi, M.J. and J.J. Chou, *Fatty acid flippase activity of UCP2 is essential for its proton transport in mitochondria.* Cell Metabolism, 2014. **20**(3): p. 541
64. Zoonens, M., et al., *Dangerous liaisons between detergents and membrane proteins. The case of mitochondrial uncoupling protein 2.* Journal of the American Chemical Society, 2013. **135**(40): p. 15174
65. Lin, C., H. Hackenberg, and E. Klingenberg, *The uncoupling protein from brown adipose tissue mitochondria is a dimer. A hydrodynamic study.* Federation of European Biochemical Societies Letters, 1980. **113**(2): p. 304
66. Klingenberg, M. and M. Appel, *The uncoupling protein dimer can form a disulfide cross-link between the mobile C-terminal SH groups.* European Journal of Biochemistry, 1989. **180**(1): p. 123
67. Crichton, P.G., et al., *Lipid, detergent, and Coomassie Blue G-250 affect the migration of small membrane proteins in blue native gels: mitochondrial carriers migrate as monomers not dimers.* The Journal of Biological Chemistry, 2013. **288**(30): p. 22163
68. Hoang, T., M.D. Smith, and M. Jelokhani-Niaraki, *Expression, folding, and proton transport activity of human uncoupling protein-1 (UCP1) in lipid membranes: evidence for associated functional forms.* The Journal of Biological Chemistry, 2013. **288**(51): p. 36244
69. Zhao, L., et al., *Specific Interaction of the Human Mitochondrial Uncoupling Protein 1 with Free Long-Chain Fatty Acid.* Structure, 2017. **25**(9): p. 1371
70. Berardi, M.J., et al., *Mitochondrial uncoupling protein 2 structure determined by NMR molecular fragment searching.* Nature, 2011. **476**(7358): p. 109
71. Jabůrek, M., et al., *Transport function and regulation of mitochondrial uncoupling proteins 2 and 3.* The Journal of Biological Chemistry, 1999. **274**(37): p. 26003
72. Bertholet, A.M. and Y. Kirichok, *UCP1: A transporter for H(+) and fatty acid anions.* Biochimie, 2017. **134**: p. 28
73. Fedorenko, A., P.V. Lishko, and Y. Kirichok, *Mechanism of fatty-acid-dependent UCP1 uncoupling in brown fat mitochondria.* Cell, 2012. **151**(2): p. 400
74. Modrianský, M., et al., *Identification by site-directed mutagenesis of three arginines in uncoupling protein that are essential for nucleotide binding and inhibition.* The Journal of Biological Chemistry, 1997. **272**(40): p. 24759
75. Echtay, K.S., et al., *Site-directed mutagenesis identifies residues in uncoupling protein (UCP1) involved in three different functions.* Biochemistry, 2000. **39**(12): p. 3311
76. Klingenberg, M and K.S. Echtay, *Uncoupling proteins: the issues from a biochemist point of view.* Biochimica et Biophysica Acta 1504 2001. **1504**: p. 128

77. Esteves, T.C. and M.D. Brand, *The reactions catalysed by the mitochondrial uncoupling proteins UCP2 and UCP3.* Biochimica et Biophysica Acta, 2005. **1709**(1): p. 35
78. Echtay, K.S., *Mitochondrial uncoupling proteins--what is their physiological role?* Free Radical Biology & Medicine, 2007. **43**(10): p. 1351
79. Rial, E., A. Poustie, and D.G. Nicholls, *Brown-adipose-tissue mitochondria: the regulation of the 32 000-Mr uncoupling protein by fatty acids and purine nucleotides.* European Journal of Biochemistry, 1983. **137**(1-2): p. 197
80. Hoang, T., M.D. Smith, and M. Jelokhani-Niaraki, *Toward understanding the mechanism of ion transport activity of neuronal uncoupling proteins UCP2, UCP4, and UCP5.* Biochemistry, 2012. **51**(19): p. 4004
81. Rebuffet, E., et al., *Cell-free production and characterisation of human uncoupling protein 1-3.* Biochemistry and Biophysics Reports, 2017. **10**: p. 276
82. Ye, Y., et al., *Labeling strategy and signal broadening mechanism of Protein NMR spectroscopy in Xenopus laevis oocytes.* Chemistry, 2015. **21**(24): p. 8686
83. Lee, Y., et al., *Uncoupling protein 1 binds one nucleotide per monomer and is stabilized by tightly bound cardiolipin.* Proceedings of the National Academy of Sciences, 2015. **112**(22): p. 6973
84. Ricquier, D., *UCP1, the mitochondrial uncoupling protein of brown adipocyte: A personal contribution and a historical perspective.* Biochimie, 2017. **134**: p. 3
85. Vignais, P.V., P.M. Vignais, and G. Defaye, *Adenosine diphosphate translocation in mitochondria. Nature of the receptor site for carboxyatractyloside (gummiferin).* Biochemistry, 1973. **12**(8): p. 1508
86. Henderson, P.J. and H.A. Lardy, *Bongkrekic acid an inhibitor of the adenine nucleotide translocase of mitochondria.* The Journal of Biological Chemistry, 1970. **245**(6): p. 1319
87. Erdelt, H., et al., *Some principle effects of bongkrekic acid on the binding of adenine nucleotides to mitochondrial membranes.* European Journal of Biochemistry, 1972. **30**(1): p. 107
88. Brustovetsky, N. and M. Klingenberg, *The reconstituted ADP/ATP carrier can mediate H+ transport by free fatty acids, which is further stimulated by mersalyl.* The Journal of Biological Chemistry, 1994. **269**(44): p. 27329
89. Skulachev, V.P., *Fatty acid circuit as a physiological mechanism of uncoupling of oxidative phosphorylation.* Federation of European Biochemical Societies Letters, 1991. **294**(3): p. 158
90. Bertholet, A.M., et al., *H+ transport is an integral function of the mitochondrial ADP/ATP carrier.* Nature, 2019. **571**(7766): p. 515
91. Wohlrab, H., *Molecular aspects of inorganic phosphate transport in mitochondria.* Biochimica et Biophysica Acta - Reviews on Bioenergetics, 1986. **853**(2): p. 115
92. Stappen, R. and R. Krämer, *Functional properties of the reconstituted phosphate carrier from bovine heart mitochondria: evidence for asymmetric orientation and characterization of three different transport modes.* Biochimica et Biophysica Acta - Biomembranes, 1993. **1149**(1): p. 40
93. Žáčková, M., R. Krämer, and P. Ježek, *Interaction of mitochondrial phosphate carrier with fatty acids and hydrophobic phosphate analogs.* The International Journal of Biochemistry & Cell Biology, 2000. **32**(5): p. 499

94. Thangaratnarajah, C., J.J. Ruprecht, and E.R. Kunji, *Calcium-induced conformational changes of the regulatory domain of human mitochondrial aspartate/glutamate carriers.* Nature Communications, 2014. **5**(1): p. 1
95. Palmieri, L., et al., *Citrin and aralar1 are Ca2+-stimulated aspartate/glutamate transporters in mitochondria.* The European Molecular Biology Organization Journal, 2001. **20**(18): p. 5060
96. Amoedo, N., et al., *AGC1/2, the mitochondrial aspartate-glutamate carriers.* Biochimica et Biophysica Acta - Molecular Cell Research, 2016. **1863**(10): p. 2394
97. Quinlan, C.L., et al., *Native rates of superoxide production from multiple sites in isolated mitochondria measured using endogenous reporters.* Free Radical Biology and Medicine, 2012. **53**(9): p. 1807
98. Indiveri, C., et al., *The purified and reconstituted ornithine/citrulline carrier from rat liver mitochondria: electrical nature and coupling of the exchange reaction with H+ translocation.* Biochemical Journal, 1997. **327**(2): p. 349
99. Krebs, H.A. and K. Henseleit, *Untersuchungen uber die Harnstoffbildung im Tierkörper.* Hoppe-Seyler s Zeitschrift für physiologische Chemie, 1932. **210**(1-2): p. 33
100. Kunji, E.R., *The role and structure of mitochondrial carriers.* Federation of European Biochemical Societies Letters, 2004. **564**(3): p. 239
101. Fiermonte, G., et al., *The mitochondrial ornithine transporter bacterial expression, reconstitution, functional characterization, and tissue distribution of two human isoforms.* The Journal of Biological Chemistry, 2003. **278**(35): p. 32778
102. Monné, M., et al., *Substrate specificity of the two mitochondrial ornithine carriers can be swapped by single mutation in substrate binding site.* The Journal of Biological Chemistry, 2012. **287**(11): p. 7925
103. Palmieri, F., *The mitochondrial transporter family (SLC25): physiological and pathological implications.* Pflügers Archiv, 2004. **447**(5): p. 689
104. Oxenoid, K., et al., *Architecture of the mitochondrial calcium uniporter.* Nature, 2016. **533**(7602): p. 269
105. Gunter, T.E. and D.R. Pfeiffer, *Mechanisms by which mitochondria transport calcium.* American Journal of Physiology-Cell Physiology, 1990. **258**(5): p. C755
106. Boyman, L., et al., *NCLX: the mitochondrial sodium calcium exchanger.* Journal of Molecular and Cellular Cardiology, 2013. **59**: p. 205
107. Garlid, K.D., *On the mechanism of regulation of the mitochondrial K+/H+ exchanger.* The Journal of Biological Chemistry, 1980. **255**(23): p. 11273
108. Numata, M., et al., *Identification of a mitochondrial Na+/H+ exchanger.* The Journal of Biological Chemistry, 1998. **273**(12): p. 6951
109. Nicholls, D.G., *Bioenergetics*. 2013: Academic Press.
110. Brett, C.L., M. Donowitz, and R. Rao, *Evolutionary origins of eukaryotic sodium/proton exchangers.* American Journal of Physiology-Cell Physiology, 2005. **288**(2): p. C223
111. Álvarez, B.V. and M.C. Villa Abrille, *Mitochondrial NHE1: a newly identified target to prevent heart disease.* Frontiers in Physiology, 2013. **4**: p. 152
112. Paulino, C., et al., *Structure and transport mechanism of the sodium/proton antiporter MjNhaP1.* Elife, 2014. **3**: p. e03583
113. Lee, C., et al., *A two-domain elevator mechanism for sodium/proton antiport.* Nature, 2013. **501**(7468): p. 573

114. Gupta, K., et al., *The role of interfacial lipids in stabilizing membrane protein oligomers.* Nature, 2017. **541**(7637): p. 421
115. Bolla, J.R., et al., *Membrane protein–lipid interactions probed using mass spectrometry.* Annual Review of Biochemistry, 2019. **88**: p. 85-111.
116. Kunji, E.R. and P.G. Crichton, *Mitochondrial carriers function as monomers.* Biochimica et Biophysica Acta, 2010. **1797**(6-7): p. 817
117. Wohlrab, H., *Homodimeric intrinsic membrane proteins. Identification and modulation of interactions between mitochondrial transporter (carrier) subunits.* Biochemical and Biophysical Research Communications, 2010. **393**(4): p. 746
118. Klingenberg, M., *Cardiolipin and mitochondrial carriers.* Biochimica et Biophysica Acta - Biomembranes, 2009. **1788**(10): p. 2048
119. Trézéguet, V., et al., *A covalent tandem dimer of the mitochondrial ADP/ATP carrier is functional in vivo.* Biochimica et Biophysica Acta - Bioenergetics, 2000. **1457**(1-2): p. 81
120. Wohlrab, H., *Novel inter-and intrasubunit contacts between transport-relevant residues of the homodimeric mitochondrial phosphate transport protein.* Biochemical and Biophysical Research Communications, 2004. **320**(3): p. 685
121. Moiseeva, V., et al., *On the mechanism and functional significance of the ADP/ATP carrier (AAC) dimerization.* Biochemistry (Moscow), Supplement Series A: Membrane and Cell Biology, 2017. **11**(4): p. 321
122. Echtay, K.S., et al., *A signalling role for 4-hydroxy-2-nonenal in regulation of mitochondrial uncoupling.* The European Molecular Biology Organization Journal, 2003. **22**(16): p. 4103
123. Ahnert, S.E., et al., *Principles of assembly reveal a periodic table of protein complexes.* Science, 2015. **350**(6266): p. aaa2245.
124. Li, E., W.C. Wimley, and K. Hristova, *Transmembrane helix dimerization: beyond the search for sequence motifs.* Biochimica et Biophysica Acta, 2012. **1818**(2): p. 183
125. Lemmon, M.A., et al., *Sequence specificity in the dimerization of transmembrane. alpha.-helixes.* Biochemistry, 1992. **31**(51): p. 12719
126. MacKenzie, K.R., J.H. Prestegard, and D.M. Engelman, *A transmembrane helix dimer: structure and implications.* Science, 1997. **276**(5309): p. 131
127. Russ, W.P. and D.M. Engelman, *The GxxxG motif: A framework for transmembrane helix-helix association1.* The Journal of Molecular Biology, 2000. **296**(3): p. 911
128. Sreedhar, A. and Y. Zhao, *Uncoupling protein 2 and metabolic diseases.* Mitochondrion, 2017. **34**: p. 135
129. Deng, S., et al., *UCP2 inhibits ROS-mediated apoptosis in A549 under hypoxic conditions.* Public Library of Science One, 2012. **7**(1): p. e30714
130. Horvath, S.E. and G. Daum, *Lipids of mitochondria.* Progress in Lipid Research, 2013. **52**(4): p. 590
131. Daum, G. and J.E. Vance, *Import of lipids into mitochondria.* Progress in Lipid Research, 1997. **36**(2-3): p. 103
132. Miles, A.J. and B. Wallace, *Circular dichroism spectroscopy of membrane proteins.* Chemical Society Reviews, 2016. **45**(18): p. 4859
133. Orosz, D.E. and K.D. Garlid, *A sensitive new fluorescence assay for measuring proton transport across liposomal membranes.* Analytical Biochemistry, 1993. **210**(1): p. 7
134. Hospital, A., et al., *Molecular dynamics simulations: advances and applications.* Advances and Applications in Bioinformatics and Chemistry, 2015. **8**: p. 37.

135. Schlegel, S., et al., *Optimizing membrane protein overexpression in the Escherichia coli strain Lemo21 (DE3).* The Journal of Molecular Biology, 2012. **423**(4): p. 648
136. Schlegel, S., et al., *Revolutionizing membrane protein overexpression in bacteria.* Microbial Biotechnology, 2010. **3**(4): p. 403
137. Wagner, S., et al., *Tuning Escherichia coli for membrane protein overexpression.* Proceedings of the National Academy of Sciences, 2008. **105**(38): p. 14371
138. Miroux, B. and J.E. Walker, *Over-production of proteins in Escherichia coli: mutant hosts that allow synthesis of some membrane proteins and globular proteins at high levels.* Journal of Molecular Biology, 1996. **260**(3): p. 289
139. Chen, Y., et al., *DnaK and DnaJ facilitated the folding process and reduced inclusion body formation of magnesium transporter CorA overexpressed in Escherichia coli.* Protein Expression and Purification, 2003. **32**(2): p. 221
140. Kanonenberg, K., et al., *Shaping the lipid composition of bacterial membranes for membrane protein production.* Microbial Cell Factories, 2019. **18**(1): p. 131
141. Monné, M., et al., *Functional expression of eukaryotic membrane proteins in Lactococcus lactis.* Protein Science, 2005. **14**(12): p. 3048
142. Molina, D.M., et al., *Engineering membrane protein overproduction in Escherichia coli.* Protein Science, 2008. **17**(4): p. 673-680.
143. Young, C.L., Z.T. Britton, and A.S. Robinson, *Recombinant protein expression and purification: a comprehensive review of affinity tags and microbial applications.* Biotechnology Journal, 2012. **7**(5): p. 620
144. Zuo, X., et al., *Enhanced expression and purification of membrane proteins by SUMO fusion in Escherichia coli.* Journal of Structural and Functional Genomics, 2005. **6**(2-3): p. 103
145. Deb, A., et al., *Bacterial expression, correct membrane targeting and functional folding of the HIV-1 membrane protein Vpu using a periplasmic signal peptide.* Public Library of Science One, 2017. **12**(2) e0172529
146. Lei, S.-P., et al., *Characterization of the Erwinia carotovora pelB gene and its product pectate lyase.* Journal of Bacteriology, 1987. **169**(9): p. 4379
147. Hilf, R.J. and R. Dutzler, *X-ray structure of a prokaryotic pentameric ligand-gated ion channel.* Nature, 2008. **452**(7185): p. 375
148. Matoba, N., et al., *Transcytosis-blocking abs elicited by an oligomeric immunogen based on the membrane proximal region of HIV-1 gp41 target non-neutralizing epitopes.* Current HIV Research, 2008. **6**(3): p. 218
149. Dörr, J.M., et al., *The styrene–maleic acid copolymer: a versatile tool in membrane research.* European Biophysics Journal, 2016. **45**(1): p. 3
150. Wittig, I., H.-P. Braun, and H. Schägger, *Blue native PAGE.* Nature Protocols, 2006. **1**(1): p. 418
151. Tribet, C., R. Audebert, and J.-L. Popot, *Amphipols: polymers that keep membrane proteins soluble in aqueous solutions.* Proceedings of the National Academy of Sciences, 1996. **93**(26): p. 15047
152. Popot, J.-L., et al., *Amphipols from A to Z.* Annual Review of Biophysics, 2011. **40**: p. 379
153. Rigaud, J.-L. and D. Lévy, *Reconstitution of membrane proteins into liposomes.* Methods in Enzymology, 2003, **372** p. 65

154. Knowles, T.J., et al., *Membrane proteins solubilized intact in lipid containing nanoparticles bounded by styrene maleic acid copolymer.* Journal of the American Chemical Society, 2009. **131**(22): p. 7484
155. Whitmore, L. and B. Wallace, *DICHROWEB, an online server for protein secondary structure analyses from circular dichroism spectroscopic data.* Nucleic Acids Research, 2004. **32**(suppl_2): p. W668
156. Madreiter-Sokolowski, C.T., et al., *Tracking intra-and inter-organelle signaling of mitochondria.* The Federation of European Biochemical Societies Journal, 2019. **286**(22): p. 4378
157. Winkler, E. and M. Klingenberg, *An improved procedure for reconstitution of the uncoupling protein and in-depth analysis of H+/OH− transport.* European Journal of Biochemistry, 1992. **207**(1): p. 135
158. Neher, E. and B. Sakmann, *The patch clamp technique.* Scientific American, 1992. **266**(3): p. 44
159. Luckey, M., *Membrane structural biology: with biochemical and biophysical foundations.* 2014: Cambridge University Press.
160. Strickholm, A., *A single electrode voltage, current-and patch-clamp amplifier with complete stable series resistance compensation.* Journal of Neuroscience Methods, 1995. **61**(1-2): p. 53
161. Yamaguchi, H., M. Jelokhani-Niaraki, and H. Kodama, *Second transmembrane domain of human uncoupling protein 2 is essential for its anion channel formation.* Federation of European Biochemical Societies Letters, 2004. **577**(1-2): p. 299
162. Mozo, J., et al., *Assessment of a high-throughput screening methodology for the measurement of purified UCP1 uncoupling activity.* Analytical Biochemistry, 2006. **351**(2): p. 201
163. Alder, B.J. and T.E. Wainwright, *Phase transition for a hard sphere system.* The Journal of Chemical Physics, 1957. **27**(5): p. 1208
164. Alder, B.J. and T.E. Wainwright, *Studies in molecular dynamics. I. General method.* The Journal of Chemical Physics, 1959. **31**(2): p. 459
165. Kukol, A., *Molecular modeling of proteins*. Vol. 443. 2008: Springer.
166. McCammon, J.A., B.R. Gelin, and M. Karplus, *Dynamics of folded proteins.* Nature, 1977. **267**(5612): p. 585
167. Chavent, M., A.L. Duncan, and M.S. Sansom, *Molecular dynamics simulations of membrane proteins and their interactions: from nanoscale to mesoscale.* Current Opinion in Structural Biology, 2016. **40**: p. 8
168. Polo, S.E. and G. Almouzni, *Chromatin dynamics after DNA damage: the legacy of the access–repair–restore model.* DNA Repair, 2015. **36**: p. 114
169. Lopes, P.E., O. Guvench, and A.D. MacKerell, *Current status of protein force fields for molecular dynamics simulations*. Molecular Modeling of Proteins, 2015. **1215:** p. 47
170. Jensen, F., *Introduction to computational chemistry*. 2017: John wiley & sons.
171. Case, D.A., et al., *AMBER 9.* University of California, San Francisco, 2006. **45**.
172. Brooks, B.R., et al., *CHARMM: a program for macromolecular energy, minimization, and dynamics calculations.* Journal of Computational Chemistry, 1983. **4**(2): p. 187
173. Kunz, A.P.E., et al., *New functionalities in the GROMOS biomolecular simulation software.* Journal of Computational Chemistry, 2012. **33**(3): p. 340

174. Damm, W., et al., *OPLS all-atom force field for carbohydrates.* Journal of Computational Chemistry, 1997. **18**(16): p. 1955
175. Kästner, J., *Umbrella sampling.* Wiley Interdisciplinary Reviews: Computational Molecular Science, 2011. **1**(6): p. 932
176. Case, D., et al., *AMBER 9.0 Software package*. 2006, University of California: San Francisco.
177. Brooks, B.R., et al., *CHARMM: the biomolecular simulation program.* Journal of Computational Chemistry, 2009. **30**(10): p. 1545
178. Hess, B., et al., *GROMACS 4: algorithms for highly efficient, load-balanced, and scalable molecular simulation.* Journal of Chemical Theory and Computation, 2008. **4**(3): p. 435
179. Nelson, M.T., et al., *NAMD: a parallel, object-oriented molecular dynamics program.* The International Journal of Supercomputer Applications and High Performance Computing, 1996. **10**(4): p. 251
180. Ježek, P., et al., *Mitochondrial uncoupling proteins: subtle regulators of cellular redox signaling.* Antioxidants & Redox Signaling, 2018. **29**(7): p. 667
181. Zackova, M., et al., *Activating omega-6 polyunsaturated fatty acids and inhibitory purine nucleotides are high affinity ligands for novel mitochondrial uncoupling proteins UCP2 and UCP3.* The Journal of Biological Chemistry, 2003. **278**(23): p. 20761
182. Donadelli, M., et al., *UCP2, a mitochondrial protein regulated at multiple levels.* Cellular and Molecular Life Sciences, 2014. **71**(7): p. 1171
183. Echtay, K.S., et al., *Superoxide activates mitochondrial uncoupling proteins.* Nature, 2002. **415**(6867): p. 96
184. Brand, M.D., et al., *Mitochondrial superoxide: production, biological effects, and activation of uncoupling proteins.* Free Radical Biology & Medicine, 2004. **37**(6): p. 755
185. Li, N., M. Karaca, and P. Maechler, *Upregulation of UCP2 in beta-cells confers partial protection against both oxidative stress and glucotoxicity.* Redox Biology, 2017. **13**: p. 541
186. Lytovchenko, O. and E.R.S. Kunji, *Expression and putative role of mitochondrial transport proteins in cancer.* Biochimica et Biophysica Acta, 2017. **1858**(8): p. 641
187. Ayyasamy, V., et al., *Cellular model of Warburg effect identifies tumor promoting function of UCP2 in breast cancer and its suppression by genipin.* Public Library of Science One, 2011. **6**(9): p. e24792
188. Li, W., et al., *Mitochondrial uncoupling protein 2 is up-regulated in human head and neck, skin, pancreatic, and prostate tumors.* Cancer Biomarkers, 2013. **13**(5): p. 377
189. Cheng, W. C., et al., *Uncoupling protein 2 reprograms the tumor microenvironment to support the anti-tumor immune cycle.* Nature Immunology, 2019. **20**(2): p. 206
190. Kuai, X. Y., Z. Y. Ji, and H. J. Zhang, *Mitochondrial uncoupling protein 2 expression in colon cancer and its clinical significance.* World Journal of Gastroenterology, 2010. **16**(45): p. 5773
191. Jekabsons, M.B., et al., *Molecular properties of purified human uncoupling protein 2 refolded from bacterial inclusion bodies.* Journal of Bioenergetics and Biomembranes, 2003. **35**(5): p. 409
192. Lin, C.S. and M. Klingenberg, *Characteristics of the isolated purine nucleotide binding protein from brown fat mitochondria.* Biochemistry, 1982. **21**(12): p. 2950
193. Govaerts, C., *Lipids can make them stick together.* Trends in Biochemical Sciences, 2017. **42**(5): p. 329

194. Marianayagam, N.J., M. Sunde, and J.M. Matthews, *The power of two: protein dimerization in biology.* Trends in Biochemical Sciences, 2004. **29**(11): p. 618
195. Agre, P. and D. Kozono, *Aquaporin water channels: molecular mechanisms for human diseases1.* Federation of European Biochemical Societies Letters, 2003. **555**(1): p. 72
196. Stroud, R.M., et al., *Selectivity and conductance among the glycerol and water conducting aquaporin family of channels.* Federation of European Biochemical Societies Letters, 2003. **555**(1): p. 79
197. Ando, M., et al., *Liposome chaperon in cell-free membrane protein synthesis: one-step preparation of KcsA-integrated liposomes and electrophysiological analysis by the planar bilayer method.* Biomaterials Science, 2016. **4**(2): p. 258
198. MacKinnon, R., *Potassium channels.* Federation of European Biochemical Societies Letters, 2003. **555**(1): p. 62
199. Tajkhorshid, E., et al., *Control of the selectivity of the aquaporin water channel family by global orientational tuning.* Science, 2002. **296**(5567): p. 525
200. Morrison, L.J. and J.S. Brodbelt, *193 nm Ultraviolet photodissociation mass spectrometry of tetrameric protein complexes provides insight into quaternary and secondary protein topology.* Journal of the American Chemical Society, 2016. **138**(34): p. 10849
201. Lee, A.G., *Lipid–protein interactions in biological membranes: a structural perspective.* Biochimica et Biophysica Acta - Biomembranes, 2003. **1612**(1): p. 1
202. Rigaud, J.-L., B. Pitard, and D. Levy, *Reconstitution of membrane proteins into liposomes: application to energy-transducing membrane proteins.* Biochimica et Biophysica Acta - Bioenergetics, 1995. **1231**(3): p. 223
203. Ohtsuka, T., et al., *Synthesis and in situ insertion of a site-specific fluorescently labeled membrane protein into cell-sized liposomes.* Analytical Biochemistry, 2011. **418**(1): p. 97
204. Moritani, Y., et al., *Direct integration of cell-free-synthesized connexin-43 into liposomes and hemichannel formation.* The Federation of European Biochemical Societies Journal, 2010. **277**(16): p. 3343
205. Saliba, A. E., I. Vonkova, and A.-C. Gavin, *The systematic analysis of protein–lipid interactions comes of age.* Nature Reviews Molecular Cell Biology, 2015. **16**(12): p. 753
206. Barrera, N.P., M. Zhou, and C.V. Robinson, *The role of lipids in defining membrane protein interactions: insights from mass spectrometry.* Trends in Cell Biology, 2013. **23**(1): p. 1
207. Pebay-Peyroula, E., et al., *Structure of mitochondrial ADP/ATP carrier in complex with carboxyatractyloside.* Nature, 2003. **426**(6962): p. 39
208. Studier, F.W., *Protein production by auto-induction in high-density shaking cultures.* Protein Expression and Purification, 2005. **41**(1): p. 207
209. Peterson, G.L., *A simplification of the protein assay method of Lowry et al. which is more generally applicable.* Analytical Biochemistry, 1977. **83**(2): p. 346
210. Smith, M.D., et al., *atToc159 is a selective transit peptide receptor for the import of nucleus-encoded chloroplast proteins.* The Journal of Cell Biology, 2004. **165**(3): p. 323
211. Gaidukov, L., et al., *Glycine dimerization motif in the N-terminal transmembrane domain of the HDL receptor SR-BI required for normal receptor oligomerization and lipid transport.* The Journal of Biological Chemistry, 2011. **286** (21): p. 18452
212. Senes, A., M. Gerstein, and D.M. Engelman, *Statistical analysis of amino acid patterns in transmembrane helices: the GxxxG motif occurs frequently and in association with β-*

branched residues at neighboring positions1. Journal of Molecular Biology, 2000. **296**(3): p. 921
213. Lee, J., et al., *CHARMM-GUI input generator for NAMD, GROMACS, AMBER, OpenMM, and CHARMM/OpenMM simulations using the CHARMM36 additive force field.* Journal of Chemical Theory and Computation, 2015. **12**(1): p. 405
214. Kiebish, M.A., et al., *Lipidomic analysis and electron transport chain activities in C57BL/6J mouse brain mitochondria.* Journal of Neurochemistry, 2008. **106**(1): p. 299
215. Jorgensen, W.L., et al., *Comparison of simple potential functions for simulating liquid water.* The Journal of Chemical Physics, 1983. **79**(2): p. 926
216. Huang, J., et al., *CHARMM36m: an improved force field for folded and intrinsically disordered proteins.* Nature Methods, 2016. **14**(1): p. 71
217. Lee, S., et al., *CHARMM36 united atom chain model for lipids and surfactants.* The Journal of Physical Chemistry B, 2014. **118**(2): p. 547
218. Abraham, M.J., et al., *GROMACS: High performance molecular simulations through multi-level parallelism from laptops to supercomputers.* SoftwareX, 2015. **1**: p. 19
219. Hess, B., *P-Lincs: A parallel linear constraint solver for molecular simulation.* Journal of Chemical Theory and Computation, 2008. **4**(1): p. 116
220. Nosé, S., *A unified formulation of the constant temperature molecular dynamics methods.* The Journal of Chemical Physics, 1984. **81**(1): p. 511
221. Hoover, W.G., *Canonical dynamics: equilibrium phase-space distributions.* Physical Review A, 1985. **31**(3): p. 1695
222. Parrinello, M. and A. Rahman, *Polymorphic transitions in single crystals: a new molecular dynamics method.* Journal of Applied Physics, 1981. **52**(12): p. 7182
223. Darden, T., D. York, and L. Pedersen, *Particle mesh Ewald: An N· log (N) method for Ewald sums in large systems.* The Journal of Chemical Physics, 1993. **98**(12): p. 10089
224. Essmann, U., et al., *A smooth particle mesh Ewald method.* The Journal of Chemical Physics, 1995. **103**(19): p. 8577
225. Wong-ekkabut, J. and M. Karttunen, *Assessment of common simulation protocols for simulations of nanopores, membrane proteins, and channels.* Journal of Chemical Theory and Computation, 2012. **8**(8): p. 2905
226. Wong-ekkabut, J. and M. Karttunen, *The good, the bad and the user in soft matter simulations.* Biochimica et Biophysica Acta - Biomembranes, 2016. **1858**(10): p. 2529
227. Göddeke, H., et al., *Atomistic mechanism of large-scale conformational transition in a heterodimeric ABC exporter.* Journal of the American Chemical Society, 2018. **140**(13): p. 4543
228. Torrie, G.M. and J.P. Valleau, *Nonphysical sampling distributions in Monte Carlo free-energy estimation: Umbrella sampling.* Journal of Computational Physics, 1977. **23**(2): p. 187
229. Kumar, S., et al., *The weighted histogram analysis method for free-energy calculations on biomolecules. I. The method.* Journal of Computational Chemistry, 1992. **13**(8): p. 1011
230. Efron, B., *Bootstrap methods: another look at the jackknife annals of statistics 7: 1–26,* 1979.
231. Bienengraeber, M., K.S. Echtay, and M. Klingenberg, *H+ transport by uncoupling protein (UCP-1) is dependent on a histidine pair, absent in UCP-2 and UCP-3.* Biochemistry, 1998. **37**(1): p. 3

232. Greenfield, N.J. and G.D. Fasman, *Computed circular dichroism spectra for the evaluation of protein conformation.* Biochemistry, 1969. **8**(10): p. 4108
233. Cooper, T.M. and R.W. Woody, *The effect of conformation on the CD of interacting helices: a theoretical study of tropomyosin.* Biopolymers, 1990. **30**(7-8): p. 657
234. Salom, D., et al., *pH-dependent tetramerization and amantadine binding of the transmembrane helix of M2 from the influenza A virus.* Biochemistry, 2000. **39**(46): p. 14160
235. Sala, F.A., et al., *Heterotypic coiled-coil formation is essential for the correct assembly of the septin heterofilament.* Biophysical Journal, 2016. **111**(12): p. 2608
236. Popot, J.-L. and D.M. Engelman, *Membrane protein folding and oligomerization: the two-stage model.* Biochemistry, 1990. **29**(17): p. 4031
237. Faham, S., et al., *Side-chain contributions to membrane protein structure and stability.* Journal of Molecular Biology, 2004. **335**(1): p. 297
238. Hong, H. and L.K. Tamm, *Elastic coupling of integral membrane protein stability to lipid bilayer forces.* Proceedings of the National Academy of Sciences, 2004. **101**(12): p. 4065
239. Ollila, O.S., et al., *Role of sterol type on lateral pressure profiles of lipid membranes affecting membrane protein functionality: comparison between cholesterol, desmosterol, 7-dehydrocholesterol and ketosterol.* Journal of Structural Biology, 2007. **159**(2): p. 311
240. Endres, N.F., et al., *Conformational coupling across the plasma membrane in activation of the EGF receptor.* Cell, 2013. **152**(3): p. 543
241. Róg, T., et al., *Role of cardiolipins in the inner mitochondrial membrane: insight gained through atom-scale simulations.* The Journal of Physical Chemistry B, 2009. **113**(11): p. 3413
242. Bond, P.J. and M.S. Sansom, *Membrane protein dynamics versus environment: simulations of OmpA in a micelle and in a bilayer.* Journal of Molecular Biology, 2003. **329**(5): p. 1035
243. Yaacob, N., et al., *The Role of Solvent-Accessible Leu-208 of Cold-Active Pseudomonas fluorescens Strain AMS8 Lipase in Interfacial Activation, Substrate Accessibility and Low-Molecular Weight Esterification in the Presence of Toluene.* Molecules, 2017. **22**(8): p. 1312.
244. Lopes-Rodrigues, M., et al., *Influence of the surrounding environment in re-naturalized β-barrel membrane proteins.* Biophysical Chemistry, 2018. **234**: p. 6
245. Pravda, L., et al., *MOLEonline: a web-based tool for analyzing channels, tunnels and pores (2018 update).* Nucleic Acids Research, 2018. **46**(W1): p. W368
246. Jurcik, A., et al., *CAVER Analyst 2.0: analysis and visualization of channels and tunnels in protein structures and molecular dynamics trajectories.* Bioinformatics, 2018. **34**(20): p. 3586
247. Corradi, V., et al., *Lipid–protein interactions are unique fingerprints for membrane proteins.* American Chemical Society Central Science, 2018. **4**(6): p. 709
248. Dey, S., G.A. Grant, and J.C. Sacchettini, *Crystal structure of mycobacterium tuberculosis D-3-phosphoglycerate dehydrogenase extreme asymmetry in a tetramer of identical subunits.* The Journal of Biological Chemistry, 2005. **280**(15): p. 14892
249. Nagradova, N.K., *Interdomain interactions in oligomeric enzymes: creation of asymmetry in homo-oligomers and role in metabolite channeling between active centers of hetero-oligomers.* Federation of European Biochemical Societies Letters, 2001. **487**(3): p. 327

250. Immadisetty, K., J. Hettige, and M. Moradi, *Lipid-Dependent Alternating Access Mechanism of a Bacterial Multidrug ABC Exporter.* American Chemical Society Central Science, 2019. **5**(1): p. 43
251. Hutter, C.A., et al., *The extracellular gate shapes the energy profile of an ABC exporter.* Nature Communications, 2019. **10**(1): p. 1
252. St-Pierre, J.-F.o., et al., *Molecular dynamics simulations of the bacterial ABC transporter SAV1866 in the closed form.* The Journal of Physical Chemistry B, 2012. **116**(9): p. 2934
253. Jezek, P., et al., *Mitochondrial Uncoupling Proteins: Subtle Regulators of Cellular Redox Signaling.* Antioxidants & Redox Signaling, 2018. **29**(7): p. 667
254. Li, J., et al., *UCP 2 gene polymorphisms in obesity and diabetes, and the role of UCP 2 in cancer.* Federation of European Biochemical Societies Letters, 2019. **593**(18): p. 2525
255. Crichton, P.G., Y. Lee, and E.R. Kunji, *The molecular features of uncoupling protein 1 support a conventional mitochondrial carrier-like mechanism.* Biochimie, 2017. **134**: p. 35
256. Heckman, K.L. and L.R. Pease, *Gene splicing and mutagenesis by PCR-driven overlap extension.* Nature Protocols, 2007. **2**(4): p. 924
257. Richardson, L.G., M. Jelokhani-Niaraki, and M.D. Smith, *The acidic domains of the Toc159 chloroplast preprotein receptor family are intrinsically disordered protein domains.* BMC Biochemistry, 2009. **10**(1): p. 1
258. Schrödinger, L., *The PyMOL Molecular Graphics System, Version 1.8* .
259. Pettersen, E.F., et al., *UCSF Chimera—a visualization system for exploratory research and analysis.* Journal of Computational Chemistry, 2004. **25**(13): p. 1605
260. Humphrey, W., A. Dalke, and K. Schulten, *VMD: visual molecular dynamics.* Journal of Molecular Graphics, 1996. **14**(1): p. 33
261. Toniolo, C., et al., *Circular dichroism spectrum of a peptide 310-helix.* Journal of the American Chemical Society, 1996. **118**(11): p. 2744
262. King, M.S., et al., *Formation of a cytoplasmic salt bridge network in the matrix state is a fundamental step in the transport mechanism of the mitochondrial ADP/ATP carrier.* Biochimica et Biophysica Acta - Bioenergetics, 2016. **1857**(1): p. 14
263. Klingenberg, M., *Wanderings in bioenergetics and biomembranes.* Biochimica et Biophysica Acta, 2010. **1797**(6-7): p. 579
264. Kumar, S. and R. Nussinov, *Close-range electrostatic interactions in proteins.* ChemBioChem, 2002. **3**(7): p. 604
265. Yi, Q., et al., *Molecular dynamics simulations on apo ADP/ATP carrier shed new lights on the featured motif of the mitochondrial carriers.* Mitochondrion, 2019. **47**: p. 94
266. https://www.scopus.com/.
267. Mailloux, R.J. and M.-E. Harper, *Uncoupling proteins and the control of mitochondrial reactive oxygen species production.* Free Radical Biology and Medicine, 2011. **51**(6): p. 1106
268. Bouillaud, F., M.-C. Alves-Guerra, and D. Ricquier, *UCPs, at the interface between bioenergetics and metabolism.* Biochimica et Biophysica Acta - Molecular Cell Research, 2016. **1863**(10): p. 2443
269. Pleshakova, T.O., et al., *Atomic force microscopy for protein detection and their physicochemical characterization.* International Journal of Molecular Sciences, 2018. **19**(4): p. 1142
270. Möller, C., et al., *Determining molecular forces that stabilize human aquaporin-1.* Journal of Structural Biology, 2003. **142**(3): p. 369

271. Echtay, K.S., M. Bienengraeber, and M. Klingenberg, *Role of intrahelical arginine residues in functional properties of uncoupling protein (UCP1).* Biochemistry, 2001. **40**(17): p. 5243
272. Botta, J., et al., *Design and development of stapled transmembrane peptides that disrupt the activity of G-protein–coupled receptor oligomers.* The Journal of Biological Chemistry, 2019. **294**(45): p. 16587